INVESTIGATION AND SIMULATION OF RESISTANCE SPOT WELDING USING DP600 STEEL IN AUTOMOTIVE INDUSTRY

A THESIS SUBMITTED TO
THE INSTITUTE OF GRADUTE PROGRAMS OF
KARABUK UNIVERSITY

BY

ABDULKARIM R. OMER ALZAHOUGI

IN PARTIAL FULFILLMENT OF THE REQUIREMENTS FOR
THE DEGREE OF DOCTOR OF PHILOSOPHY IN
DEPARTMENT OF
MANUFACTURING ENGINEERING

January 2020

I certify that in my opinion the thesis submitted by Abdulkarim R. Omer ALZAHOUGI "INVESTIGATION AND SIMULATION OF RESISTANCE SPOT WELDING USING DP600 STEEL IN AUTOMOTIVE INDUSTRY" is fully adequate in scope and in quality as a thesis for the degree of Doctor of Philosophy.

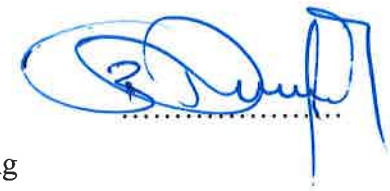

Prof. Dr. Bilge DEMİR
Thesis Advisor, Department of Manufacturing Engineering

This thesis is accepted by the examining committee with a unanimous vote in the Department of Manufacturing Engineering as a Ph.D thesis. January 15, 2020

Examining Committee Members (Institutions)	Signature
Chairman: Prof. Dr. Mustafa ACARER (SÜ)	
Member : Prof. Dr. Bilge DEMİR (KBÜ)	
Member : Prof. Dr. Ahmet DURGUTLU (GÜ)	
Member : Prof. Dr. Yavuz SUN (KBÜ)	
Member : Assoc. Prof. Dr. Yakup KAYA (KBÜ)	

The degree of Doctor of Philosophy the thesis submitted is approved by the Administrative Board of the Institute of Graduate Programs, Karabük University.

Prof. Dr. Hasan SOLMAZ
Head of Institute of Graduate Programs

"I declare that all the information within this thesis has been gathered and presented in accordance with academic regulations and ethical principles and I have according to the requirements of these regulations and principles cited all those which do not originate in this work as well."

Abdulkarim R. Omer ALZAHOUGI

ABSTRACT

Ph.D. Thesis

INVESTIGATION AND SIMULATION OF RESISTANCE SPOT WELDING USING DP600 STEEL IN AUTOMOTIVE INDUSTRY

ABDULKARIM R. OMER ALZAHOUGI

Karabük University
Institute of Graduate Programs
Department of Manufacturing Engineering

Thesis Advisor:
Prof. Dr. Bilge DEMİR
January 2020, 156 pages

The aim of this study is to investigate the weldability and quality of spot resistance welded joints of advanced strength steels in DP 600 sheet steel by theoretical and experimental methods. Today, spot resistance welding is a predominantly manufacturing process in automotive body manufacturing, which necessary strict monitoring of welding quality. Destructive and non-destructive material inspection techniques are used extensively in the determination and development of welding quality and world standards on welding quality are being developed and applied to provides the best weldability. According to the general acceptance the most important result for welding quality and validity is the nugget geometry. Since many different welding parameters can be used in spot resistance welding processes, it is very useful to create a welding map of welded joint materials and the most suitable welding parameters according to their thickness and the welding properties it can provide.

In this study, commercial DP600 automotive sheet steel pairs were examined experimentally; Different welding time, different welding current and different welding electrode pressure parameters are combined with resistance spot welding. Tensile shear test was applied to determine the effect of welding parameters on the tensile load carrying capacity of resistance spot welded joints. In addition, according to optical microscopic images and the Scanning Electron microscope (SEM), were investigations used as the material characterization technique. the phase of base metal contains of a certain amount of hard martensite phase in a soft ferrite matrix, which is changed to a certain amount of ferrite in martensite phase in HAZ while in FZ the phase is almost of lath martensite lath Martensite is thought to form and contains very thin Lath or retained austenite between laths.

Theoretically, SIMUFACT, TAQUCHI and ANOVA programs and software were used for analysis and optimization. Experimental and theoretical study results showed that welding mechanical properties improved with increasing welding time and welding current but decreased with increasing electrode pressure. Both studies showed that welding current and electrode pressure was very effective. The optimum value of tensile shear and Nugget diameter development was determined and compared with the experimental studies it was at welding current 8 kA and clamping load 3.5 bar. To identify the type of failure mode, macroscopic inspection was made on the spot-welding samples, which passed the tensile shear strength. The PF is generally always preferred to the failure mode. The failure mode in this thesis occurs at HAZ and BM.

The results showed in Minitab software Taquchi (DOE) and analysis of Anova the effect of welding current is more effect of clamping load. At the welding current increase the tensile shear load bearing capacity of RSW samples and Nugget formation increase at constant the time whereas increase the clamping load lead to decrease the tensile shear load bearing capacity and nugget formation.

Keywords **:** Resistance Spot Welding, Dual-Phase Steel, Mechanical Properties, Microstructure, Finite Element Method, Optimization.

Science Code : 91415

ÖZET

Doktora Tezi

OTOMOTİV DP600 ÇELİĞİ KULLANILARAK NOKTA DİRENÇ KAYNAĞININ SİMÜLASYONU VE İNCELENMESİ

ABDULKARIM RAMADAN OMER ALZAHOUGI

Karabük Üniversitesi
Lisansüstü Eğitim Enstitüsü
İmalat Mühendisliği Anabilim Dalı

Tez Danışmanı:
Prof. Dr. Bilge DEMİR
Ocak 2020, 156 sayfa

Bu çalışmanın amacı, DP 600 sac çeliği özelinde ileri dayanımlı çeliklerin Nokta direnç kaynaklı birleştirmelerinin kaynak kabiliyeti ve kalitesinin teorik ve deney yolu ile incelenmesidir. Günümüzde otomotiv gövde imalatında Nokta direnç kaynağı ağırlıklı bir imalat olması kaynak kalitesinin sıkı olarak takibe dilmesi ihtiyacını doğurmaktadır. Kaynak kalitesinin belirlenmesi ve geliştirilmesinde tahribatlı ve tahribatsız malzeme muayene teknikleri yoğun olarak kullanılmakta ve kaynak kalitesi üzerine dünya standartları her geçen gün daha geliştirilerek uygulanmaktadır. Genel kabule göre Kaynak kalitesi ve geçerliliği için en önemli sonuç ve gösterge esasında NDK düğme geometrisidir. Nokta direnç kaynak işlemlerinde çok farklı kaynak parametreleri kullanılabildiği için kaynaklı birleştirme malzemeleri ve kalınlığına göre en uygun kaynak parametre ve sağlayabildiği kaynak özelliklerinin kaynak haritasının oluşturulması oldukça faydalıdır.

Bu çalışmada deneysel olarak inceleme için ticari DP600 otomotiv sac çelik çiftleri; farklı kaynak zamanı, farklı kaynak akımı ve farklı kaynak elektrot basıncı parametrelerinin kombinasyonu kullanılarak nokta direnç kaynağı ile birleştirilmiştir. Nokta direnç kaynaklı birleştirmelerin çekme yük taşıma kapasitesine kaynak parametrelerinin etkisini belirlemek amacıyla çekme makaslama testi uygulanmıştır. Ayrıca malzeme karakterizasyon tekniği olarak detaylı optik ve stereo metalografi, SEM-EDS incelemeleri kullanılmıştır. Teorik olarak analiz ve optimizasyon için SIMUFACT, TAQUCHI ve ANOVA program ve yazılımları kullanılmıştır. Deney ve teorik çalışma sonuçları kaynak zamanı ve kaynak akımının artması ile kaynak mekanik özelliklerinin geliştiğini fakat elektrot basıncının artması ile azaldığını göstermiştir. Her iki çalışmada da kaynak elektrot basıncının çok etkili olduğu görülmektedir. Teorik çalışmalar ile optimum düğme çapı gelişimi belirlenmiş ve deney çalışmaları ile kıyaslanmıştır ve optimum kaynak parametresi olarak 8 kA ve 3.5 bar elektrot basıncı belirlenmiştir. Kırılmış numunelerin makro ve mikro incelenmesinde yırtılma ile kırılmaların ana malzemeden, fakat pull out-düğme çıkması kırılmalar söz konusu olduğunda kırılmanın ITAB ve kaynak metalinden olabildiği gözlemlenmiştir. Minitab software Taquchi (DOE) and analysis of Anova analiz sonuçları kaynak akımının kaynak baskı kuvvetinden çok daha etkili olduğunu göstermektedir. Kaynak akımının artması ile NDK kaynak düğme çapı ve NDK kaynaklı birleştirme çekme makaslama maksimum taşıma kuvveti artarken, NDK kaynak baskı kuvvetinin artması ile çekme makaslama maksimum taşıma kuvveti ve düğme çapı azalmaktadır.

Anahtar Kelimeler : Nokta Direnç kaynağı, çift fazlı çelik, mekanik özellikler, mikroyapı, Sonlu elemanlar analizi, optimizasyon.

Bilim Kodu : 91415

ACKNOWLEDGMENT

The name of Almighty Allah, the praise is to the God. The work was carried out in the Faculty of Technology at Karabük University, between September 2016 and December 2019 under the supervision of Prof. Dr. Bilge DEMIR, whom I would like to thank sincerely for his encouragement, guidance and advice throughout experimental work and for his constructive criticism during the preparation of this thesis.

I am also particularly grateful to Dr. Muhammed Elitas and Mustafa Göktaş for carrying out some experiment, and for their advice and support. I would like to thank also all staff in the department for their help.

I am thankful to my Mother, my Sister and my wife, for their patience and commendable support during the preparation of this thesis. I cannot forget my children, whose have been a great motivating force during these tense moments. I would like to extent my thanks also to my brothers and for their kind support. I would like also to extent my thanks to my friendship of Ali Kheiry for his help.

CONTENTS

Page

Page

Page

Page

Page

LIST OF FIGURES

Page

Page

Page

Page

Page

LIST OF TABLES

Page

LIST OF SYMBOLS AND ABBREVITIONS INDEX

SYMBOLS

d_n	: weld nugget diameter
h_n	: weld nugget height
$e_{i,}$	: electrode indentation
h_n/d_n	: weld nugget size ratio

ABBREVIATIONS

AHSS	: Advanced High Strength Steel
HSS	: High. Strength Steel
TRIP	: Transformation Induced Plasticity
DP	: Dual Phase Steel
TWIP	: Twin Induced Plasticity
Ac_1	: Temperature of austenite formation on heating
Ac_3	: Temperature at which transformation of ferrite into austenite is completed on heating
RSW	: Resistance Spot Welding
TS	: Tensile Strength
UTS	: Ultimate Tensile Strength
YS	: Yield Strength
MPa	: Mega Pascal, the unit for tensile strength
TSS	: Tensile Shear Strength
CTS	: Cross Tensile Strength
SEM	: Scanning Electron Microscope
EDS	: Energy Dispersive X-Ray Spectroscopy
HV	: Vickers Hardness
HAZ	: Heat Affected Zone

FZ	: Fusion Zone
PF	: Pullout Failure
PIF	: Partial Interfacial Failure
IF	: Interfacial Failure
CP	: Complex Phase
MS	: Martensitic Steel
FB	: Ferritic Bainitic

PART 1

INTRODUCTION

The increase in the level of production competition obviously has higher and more advanced quality; advanced, lighter, safer, more environmentally friendly, and ultimately more affordable, cheaper materials for the development of modern cars that improve the environment, protection and vehicle performance, thereby inspire all possible standard improvements to new steel grades. Because like traditional low, carbon steel; ultra-deep drawing (EDD), deep drawing (DD), baking hardening (BH), gap free (IF) steel and technically high strength steel (HSS), for example; carbon-manganese steel and high-strength low-alloy (HSLA) steel is now more than ever, and because of the better mixture of ductility and strength. It is even being increasingly replaced by advanced high-strength steel (AHSS). It has now been noted and recognized that the increased strength of metallic materials technically leads to reduce the formability [1].

Conventional HSLA steel with high tensile strength seems to have moderate formability but retains its functional applications in the automotive industry [2]. Recently, phase-induced plasticity (TRIP) steel, dual-phase (DP) steel, and their galvanized products have been extensively used to produce and industrialize the automotive parts including bumper reinforcements, lists and bumper beams. Be one. Together, DP steel and TRIP steel offer great possibility for higher combinations of formability and strength [3-5]. Then, these steels were characterized and subjected to their high work hardening rate, high tensile formability, incessant yield behavior, high tensile strength, high elongation, baking hardening ability (DP), and low yield stress. Grouping high yield strength (TRIP), Tensile stress ratio (DP) and high uniform elongation (TRIP), excellent resistance of corrosion (galvanized products) [6]. In addition, in recent years, steels characterized by twin induced plasticity (TWIP) have attracted attention and are built on such steels. In combination with

high strength under cold deformation conditions, many alloying concepts are provided for TWIP steel to achieve excellent plasticity and ductility [7]. It is well known that TWIP materials are highly alloyed, and in all relevant standards, it is important to note that they have a complete austenitic structure at any given room temperature under processing conditions. TRIP steel is a low alloy steel with a predominant ferrite microstructure. As a part of low alloy steel, the soft ferrite phase combination and hard martensite phase in DP steel brings superior ductility and is work hardened with given tensile strength.

In contrast, the microstructure of TRIP steel involves of bainite, ferrite and retained austenite phases. During the strain process, the metastable residual austenite is transformed into martensite, resulting in transformation-induced plasticity that is considered the main reason for improving durability and plasticity.

The most commonly used method and technique of welding is the Resistance Spot Welding (RSW) by which metal adhesion can be generated and produced on the joint surface. The resistance of the workpiece to the current generates heat at the joint. The principle of resistance spot welding operation includes extrusion time, pre-heating time, welding time, cooling time, post-heating time and final holding time.

Functional operation includes the corresponding application of mechanical pressure and current of appropriate size and duration. Not surprisingly; the welding current should pass from the electrode over the workpiece. The welding current continuity is achieved by applying a load and by applying a load. Shaped electrodes offer the essential pressure and current density. Therefore, sufficient heat is generated to increase the limited metal volume to a molten state. Later, this metal is cooled under pressure until it has the sufficient strength in order to hold the parts together. The welding current and electrode force should form nuggets but not very high as to allow molten metal to escape from the welding area. The welding time should be short enough to inhibit the electrode surface from overheating to avoid shortening the life [8].

A comprehensive study through the literature survey showed and proposed that the number of this study was very limited and related to the resistance spot weldability of AHSS. It is significant to recognize that research on TRIP and resistance spot welding of DP steels has greatly targeted.

1.1. PREFACE

Technology through welding is the most popularly, and universally used method of remaking or making a metal structure that is used to link and assemble different kinds of structures connecting them with surfaces through heat and or pressure on materials such as metals, polymers and even composite. During welding, the melting point of the pieces of work to be connected at the interface to give a good welding joint and solidification. In the late 19th century, France and Germany implemented the blueprint for modern cars [9]. In addition, the revolution of Americans in the early 20th century automotive industry has brought a great advantage to our daily life and the towns have become more compact. But with the side effects of lasting innovation in the automotive industry including the fossil fuel consumption, environmental pollution, and climate change new challenges have been emerged [10].

The main aim in the automotive industry is also that cars and other vehicles have saved fuel from the beginning. Saving the energy every time important energy, this reality took place strongly and strongly during the economic crisis. In the 1970s, there was a serious economic crisis in the world, especially in the United States. Therefore, there has been a huge dispute between the company and the researchers, why should we find energy-saving bodies in white materials, especially automobile body steel. This was mainly done through a speech by and researchers, before the story began, but first it was strongly targeted.

In order to accomplish these goals, the use of lighter materials and light construction are of a high requirement and demand. The car has the same average size in 1908 Figure 1.1. a) And the concept of today, such as a four-wheel starter engine. But compared to modern models, design and efficiency are very different Figure 1.1. b)

Low-cost manufacturing in the automotive industry is one of the key objectives of ever-increasing global competition. Low cost production is often linked to the term light manufacturing term although light technologies may increase production costs in many cases due to the need for new processes and equipment. Also increasing progressively to meet higher safety requirements. Therefore, the development of a new, low-cost, innovative manufacturing process is one of the key objectives in the formation of metal metals: new light production principles are of major importance in these new processes. The two main trends to produce light automotive parts are the application of high-level steels or light materials. There is an important point, what accompanying to that, is manufacturing processes of auto body. These parts are made of formed sheet and conjected via welding particularly spot welding which don't need to filler metal and extra metals therefore auto body weight does not increase due to spot welding.

Figure 1.1. a) Ford Model T from 1908, b) Mercedes-Benz concept style coupe (preview 2013 CLA-Class) at 2012 Paris Auto Show [11].

1.2. BACKGROUND

Resistant spot welding (RSW) is an effective and binding process that is extensively used to make metal sheet assemblies. The RSW was created by Elihu Thomson in the 1880s, when he revealed the concept to connect metals through resistance spot welding [12]. Currently, RSW that used now depends on the same basic principles. Nowadays, RSW operates mainly in the automotive industry. Nevertheless, RSW is used in many products including the circuit elements, appliances, aerospace industry and small-scale furniture [13]. The spot-resistance welding is the most suitable

binding process that is widely practiced in the automotive industry. RSW has been used extensively in order to joint sheet metal because of its ease of operation, high production efficiency and high speed and low cost. A modern white body usually has thousands of spots. Advanced High-Strength Steels (AHSS) were viewed as a Dual phase steel (DP) is considered a new solution for fuel proficiency, vehicle safety and cost savings in the automotive industry [14].

RSW is recorded to be one of the oldest forms of welding processes. It is one type of resistance welding, an approach of combining two or more sheets of metal through the application of pressure and heat in the welding area. (RSW) is widely used as junction metal sheets of automotive industry, through heat and pressure to use, also sheets, aluminum is subject to spot-welding, but more use of steels in spot-welding and seam welding which is very important to use automotive industry, for good technique, light weight, low environments and less processing time. RSW, seam and Friction Stir welding are different to other welding process is simple to use, suitable for cars, For example, 7000 to 12,000 spots of welding, of greater speed, no extra (filler) material, less weight and environment according to new assembly automatic. So, spot welding is a significant process in an automatic body assembly [15].

There are some parameters to consider in the spot welding. These parameters will effect on the quality of tests. The suitable combination of the spot-welded parameter creates a robust connection and will be highly visible. Welding parameters include: Electrode force, electrode diameter, squeeze time, Weld time, thickness of sheets and Welding current. Size and number of the welding structure of the welding determines the strength of the component in this process. The size of the spot diameter ranges between 3-12.5 mm [16].

In order to study the strength of spot welds in terms of the welding parameter, base metal strength, welding schedule, specimen geometry, testing speed and testing formation of the tensile test approach can also be used to study the spot-welding strength. To create the thesis framework, the RSW process is offered and described in detail at the following chapters. RSW is a type of resistance welding with its discrete self-characterized areas. Resistant spot welding is dissimilar to arc welding

where RSW consists of a metal binding method in which the materials are connected using an electrical resistance spot welding instead the electric arc [17]. The principle behind the connection approach is passing a current through two or more sheets as a pair of electrodes press them together. In addition, the following situations, advantages, disadvantages and welding devices are described in the following chapters.

1.3. THE OBJECTIVE OF THE THESIS

The objectives of this study can be illustrated as follows :

- The main goal of this thesis is to study the RSW of AHSS by examining the process, properties of sheet steel material used in the automotive industry.
- Characterization of spot welded AHSS microstructure.
- Usability and weldability of DP 600 steel in weld structures of automotive industry.
- Optimize tensile shear strength, Nugget Formation, indentation depth of the electrode force and mechanical properties (microhardness test) for all of WM, HAZ and BM.
- Investigate and choosing the right and optimal control of the parameters including welding current, welding time and electrode force to get on the best weldability.
- Also compare and optimize the experimental results with simulation results such as Taguchi (Minitab 17 software) and Anova, Also Simufact software.

PART 2

ADVANCED HIGH STRENGTH STEEL (AHSS)

Advanced high strength steels (AHSS) are engineering materials that combine higher strength (performance), good ductility (formability) and excellent energy absorption (crashworthiness). Global demand for energy saving and increasing concern for environmental pollution and global warming affect the scientific community and relevant studies are on the rise. The improvement of strength, capacity and properties of materials, most importantly metals, reduces material cross section, the reduction of part weight and the resultant decrease in fuel consumption, has made possible to reduce greenhouse gas emissions. For various functional requirements of current vehicles, advanced high strength steel is the ideal solution [18].

In the 1980s, automotive faced many challenges to enhance safety, reducing fuel and weight consumption. Advanced High Strength Steel (AHSS) levels contribute significantly to safety, exhaust gas pollution, good formability, viability, fuel efficacy, durability, environmental policy and quality requirements at relatively low cost [19]. Consistent with steel makers, AHSS is a new generation of steel that offers very high strength and other beneficial mechanical features whereas preserving high capacity. Advanced High Strength steels (AHSSs) combine between ductility and strength by phase transformation and solution reinforcement and accomplish a strength-to-weight rate of light applications in the automotive industry [20,21]. The content of carbon and use classify the steels [22]. Carbon steels (0 – 0,30 wt% C) are the most significant for the integrity of structure for the automotive vehicle as they structure the Body in White (BIW). The plain carbon steels features depend mainly on their microstructure and carbon content.

The main beneficial effect of these alloying elements is increasing toughness and strength in addition to the material hardenability. Practically, the stiffness is not effected [9]. The plain carbon steels by quality of their microstructural homogeneousness and low carbon content, generally present good formability and weldability and both of them provide great significance in automotive industry. Nevertheless, increasing strength is required in automotive industry for the purpose of performance. It is possible to increase the strength by the cold working. However, this is limited because of the chemical composition of the steel. Increasing level of alloying will increase the cost and have positive impact on weldability. High Strength Low Alloyed (HSLA) steels have been developed to enhance toughness and strength of steels at the same time retaining good weldability [23]. In general, low alloyed steels contain silicon and manganese and may show both good formability and high strength, if they are first heat preserved to create a matrix of ferrite with islands of martensite [24]. The Advanced High strength steels (AHSS) combine between ductility and strength through phase transformation and solution strengthening and accomplish a strength-to-weight rate for light applications in the automotive industry [20,21].

2.1. WELDING OF ADVANCED HIGH STRENGTH STEELS

The industry witnessed the emergence of many joining techniques and methods for advanced high strength steel. Since TRIP and DP steels have been selected for the automobiles industry, spot welding is considered one of the most significant joining methods of these types of steels [3,25]. The study of RSW for TRIP and DP steels is directed to steels with tensile strengths under 980 MPa, equal mixture and simple welding processes [26-28]. Thus, at the next section, we will provide information about RSW.

2.2. CLASSIFICATION OF ADVANCED HIGH STRENGH STEEL (AHSS)

Advanced high strength steel (AHSS), reached much higher tensile strength than the conventional high strength steel (HSS). One of the most important and valuable features of high strength steel is its excellent strength-ductility relationship. There are

several types of advanced high strength steels (AHSS) which can be categorized according to the processing, and mechanical features of the material. Nowadays, the most frequently used types include High strength low alloy (HSLA), dual-phase (DP), complex phase (CP), martensitic steel (MS), transformation induced plasticity (TRIP), ferritic bainitic (FB) and martensite (MART) twinning-induced plasticity (TWIP) [29], Among the characteristics associated with the equipped 590R, there are enhanced formability together with high strength has met ample range of applications in the automobile industry. this new steel has been developed based on a stable weldable alloy with low levels of carbon and alloying elements [30].

High Definition Path and Types of AHSSs are families of steels that are stronger and have higher formability or ductility than conventional high strength steels (HSSs), reported by Bouaziz et al. 2013, keeler et al. 2014 and Kuziak et al. 2008 [31,32]. It is possible to distinguish between the AHSS family and the strength levels that can be roughly defined: product yield strength> 300 Mpa and ultimate tensile> 600 Mpa. The fuel economy is a key factor and therefore a weight reduction for the automotive industry [33-37]. Light vehicles were developed with high passive quality using high level steels, such as multiphase steels. These include an excellent choice of dual-phase steels (DP) which its microstructure is composed mostly of ferrite and martensite, for applications with low yield strength, high tensile strength, continuous result and uniform elongation required the main materials of AHSS are TRIP and DP steels.

Other types of AHSS were developed and all of them have a microstructure involving two or more different phases, of which (at least) one adds hardness and strength to the materials while the others deliver more formability as shown in Table 2.1.

Table 2.1. Advanced High Strength Steels [38].

AHSS		Microstructure Composition
DP	Dual Phase steel	ferrite, martensite [LLewellyn & Hudd 2000]
TRIP	Transformation Induced Plasticity steel	ferrite, bainite, retained austenite [LLewellyn & Hudd 2000]
CP	Complex Phase steel	martensite, pearlite, retained austenite [IISI, 2006]
FB	Ferritic Bainitic steel	ferrite, bainite [IISI, 2006]
MS	Martensitic Steel	martensite, bainite, ferrite [IISI, 2006]
Q&P	Quenching & Partitioning steel	martensite, ferrite, retained austenite. [Wang & Weijun, 2011

Since Hot Forming (HF) steels and Twinning-Induced Plasticity (TWIP) steels are sometimes showed enhanced formability and strength, they grouped under heading AHSS [38] Nevertheless, they do not include complex microstructural composition which sets AHSS apart from HSLA steels. In addition, while the chemical composition of TWIP steels include high content of manganese (17 - 24 %), it does not categorize them as carbon-steels. The microstructural composition is not only the feature through which the Advanced High Strength Steels can be classified but depending on the application, they can be categorized according to the thickness of the material, the chemical composition and the mechanical properties. The main criteria of AHSS in Europe is so called the Euro norm [22].

2.3. DUAL PHASE STEELS (DP)

The Dual phase steels term can be defined to mean; a class of high- strength steels composed of two phases; the first phase is a ferrite matrix and second phase is usually dispersed martensite kept austenite and / or ferrite. DP steels have been developed in the 1970s. Dual phase steel is considered as one of the advanced high strength steels used for automobile industry. It has a ferrite and martensite. It contains of 10 - 25 % hard martensite phase in a soft ferrite matrix and, in some cases, small additions of retained austenite, bainite and/or pearlite [29]. But now days

contains of up to 80%. It has good ductility and formability at high strength steels. In-service benefits like weight reduction (gas consumption) are realized when using DP steel, and because of the inherent mechanical properties; DP steel has become an attractive material for applications in the autobody construction. An increased number of automotive parts such as rails, bumpers, pillars, panels, etc. made with traditional high strength low alloy steel (HSLA) have been gradually changed by DP steel [29].

2.3.1. Classification of DP Steels

DP steels are existed with many types such as DP 600, DP 1000 and so forth in accordance with the ultimate tensile strength. DP steels have tensile strength above 1000 MPa for DP 1000 and 600 MPa for DP 600 compared with traditional high strength steels in the 400 - 440 MPa range. However, they have the same production strength and they are considered a good section for light weight vehicles [39,40]. Consequently, it is possible to use more thin DP sheets that reduce the car weight without losing their strength. Also, they enjoy by similar or higher energy accident absorption. Industrialists agree, that the design of high-level steel-based parts (AHSS) offers an opportunity for vehicle decoration and lower production cost. Currently, TRIP and DP steels are well established similar to AHSS. In general, they reported weight decreases of about 30-40% for 1300-1500 MPa steels [41]. These features are at DP 600 steel and prefer today. Adding to it, it is significant that thermal properties of cars and other products including welding, formation etc. are obtained. By increasing the temperature, the mechanical properties of DP cold-forming steels change quickly that lead to loss the load bearing capacity of DP-shaped cold steels [40]. Therefore, design DP-shaped steel structures require good knowledge and understanding to the thermal properties of the mechanical properties with increasing temperatures. Thus, it is necessary to understand carefully the thermal properties associated with yield strength and DP 600 elastic module at high temperatures. An investigational study was therefore performed to study the mechanical properties of DP 600. Tensile tests have been conducted by the use of a fixed state test method for temperatures in the range 20 ^{o}C. Table 2.2 show the various types of DP steel. Table 2.3 and with different temperature.

Table 2.2. Reviews the product property requirements for many types of DP steels, according to ArcelorMittal standard 20×80 mm ISO tensile specimens (thickness: less than 3mm) [42].

Steed grade	Yield Strength (YS) [MPa]	Ultimate Strength (UTS) [MPa]	Total Elongation [%]	Direction
DP 450	280-340	450-530	% 27	Transversal
DP 500	300-380	500-600	% 25	Longitudinal
DP 600	330-410	600-700	% 21	Longitudinal
DP780 Y450	450-550	780-900	% 15	Longitudinal
DP780 Y500	500-600	780-900	% 13	Longitudinal
DP980 Y700	700-850	980-1100	% 8	Longitudinal
DP 1180	900-1100	1180	% 5	Longitudinal

Table 2.3. Mechanical properties of DP 600 Steel at different temperature [42].

Temp.	**E. Modulus**	**Yield strength**	**Ultimate strength**	**Total Strain**
	E	RP 0.2	Rm	A
°C	GPa	MPa	MPa	%
20	201.40	431	671	22.9
200	200.94	413	630	18.3
400	198.80	378	619	22.9
600	97.38	168	224	28.8
700	54.38	84	110	41.1
800	26.63	38	46	80.8

2.3.2. Microstructure of DP Steel

The conventional microstructures of the DP steels involve of the polygonal soft ferrite matrix and that of a 10–40% of the hard martensite island, Figure. 2.1 which gives ductility and strength to the steel respectively. This type of structure helps in

accomplishing the ultimate tensile strength ranging between 500–1200 MPa. When the volume fraction of the martensite surpasses the 20%, of DP steels which are often referred to as; the partial martensitic. In order to fulfill the customized requirements, the ferrite-bainite-martensite And the ferrite-bainite steels have been created to adjust the mechanical properties: bainite instead of martensite have revealed to enhance the formability with a little reduction to the strength and the advancement [43-45]. The impact of the martensite fraction, spreading and the martensite size of area, and the impact of the ferrite fraction and the grain size on the mechanical behavior of the DP steels which have been extensively researched [32,46].

A very clear example of the dual phase microstructure is clearly revealed and presented in the Figure 2.1. The hard martensite phase looks and is shown as the dark regions and the soft ferrite phase is in white in the microstructure.

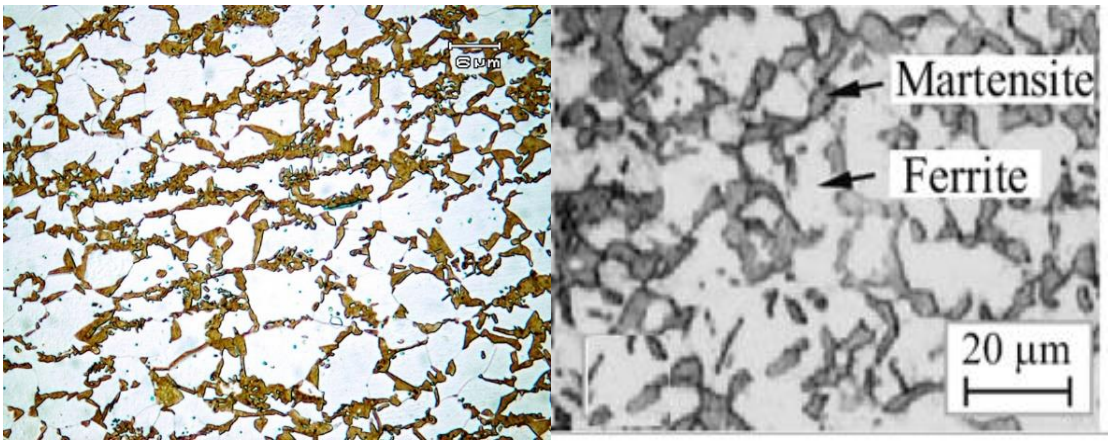

Figure 2.1. The microstructure of DP steel[42].

Technically, the DP steel begins as a low or a medium carbon steel and it is reduced from the temperature above the A_1 temperature, but under the A_3 temperature on a continuous cooling transformation scheme. However, this result is in the microstructure which consists of a soft ferrite matrix that include islands of martensite as the secondary phase (martensite increases the tensile strength). Furthermore, the carbon content, morphology, the grain size and volume fraction control the inclusive behavior of DP steel. In order to achieve these microstructures,

the DP steels normally contains a 0.06–0.15 % C thereby strengthening the martensite and the stabilizing austenite phases.

The percentage 1.5-3% Mn causes strengthening in the ferrite and the stabilizing of the austenite phases. It is believed that the formation of bainite or pearlite is retarded by the chrome and molybdenum. The Si promotes the transformation of ferrite. Elements of (V and Nb) are the reason behind the microstructure refinement and precipitation strengthening. Moreover, the mechanical behavior of DP steels is effected by the distribution of martensite [47-49]. The martensite areas present as separated regions inside the result of ferrite matrix in a more better mixture of the strength and that of the ductility than that of the martensite areas that form a chain-like network structure neighboring ferrite [47]. The areas of refinement of ferrite or/and martensite concurrently improves the ductility and strength [50-53].

2.3.3. Mechanical Properties

The automobile industry required steel grades with high tensile elongation in order to guarantee the viability and high tensile strength to establish crash resistance and fatigue, low alloy material in order to guarantee the weldability will not affect the cost production. The amount of martensite phase is an essential factor governing the mechanical properties of dual-phase steel; for example, DP steel has a number of particular properties like continuous yielding behavior (no yield point), low yield strength (i.e. 0.2 percent offset), high work-hardening ratio, high tensile strength (up to 1000 MPa) and usually high uniform and total elongation [54]. The demands on DP steels will continue for many years later. The materials which combine between good sustainability and high strength and therefore, they lead to reduce the weight of cars and other products have many economic and environmental benefits. As shown in Figure 2.2 that comparison between DP steels and other high-strength low alloy steels (HSLA), showed that DP steels present better properties than others. Increasing demand on higher fuel efficiency in cars motivated automotive industrialists to consider new materials to be considered among other strategies [55]. The new materials have been assessed for light or higher strength, with the target of decreasing the weight of the car, are estimated, resulting in a reduction in fuel

consumption. Technically, the TRIP steels have the required and needed capability in absorbing more energy through crashes because of the delayed transformation of reserved austenite to martensite up on deformation. The great combination between ductility, formability and strength of TRIP steels compared with traditional steels can be achieved through the careful design of the microstructure. The volume of fractions, size, chemical constituent and shape of the micro-structural constituents particularly retained austenite were important in the tailoring of the mechanical properties of the TRIP steels [56]. Because of their microstructure, the TRIP steels show a higher uniform and the total elongation with an equal strength level as dual phase (DP) and the traditional high strength low alloyed (HSLA) steels which are been illustrated and shown in Figure 2.2.

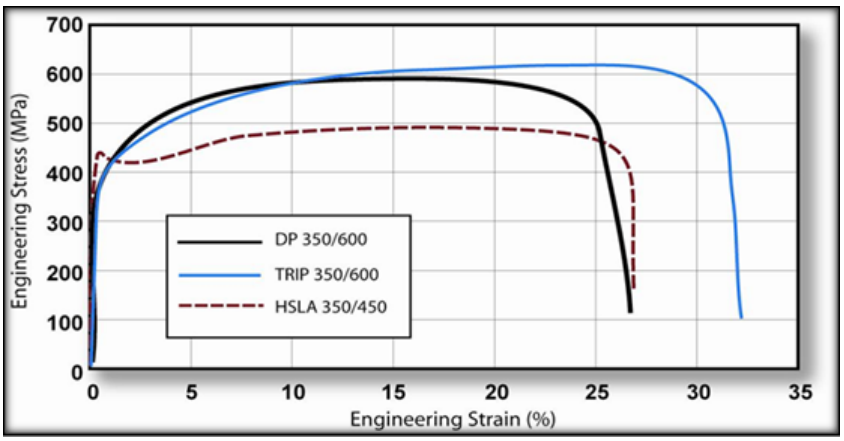

Figure 2.2. Tensile curves of HSLA, DP350/600,and TRIP350/600 steels[56].

Recent study has generally focused on the microstructure, Nugget formation and mechanical properties of the AHSS welded resistance especially on description of a single steel grade response. For instance, Marya et al [57]. tested the impacts of the RSW process parameters on the failure method through the tensile testing on DP steels. Likewise, Tong et al [58], tested the mechanical properties of DP-spotted steels and their impact on failure behavior. However, the existing literature fails to make a critical comparison between the mechanical properties and microstructure of spot occurrences in different AHSS ranks.

2.3.3.1. Tensile Properties

The experimentally determined uniaxial tensile characteristics 0.2% yield strength (YS), ultimate tensile strength (UTS), % elongation for longitudinal samples for the base metals of all DP steels are listed in Table2.4. The mechanical properties listed in Table 6-3 correlate well to the volume fraction of martensite; for example, DP steel with higher *fm* value corresponded to higher UTS and lower elongation.

Table 2. 4. Tensile Properties of the DP steels[64].

Steel	YS (MPa)	UTS (MPa)	Total Elongation %
DP600A	369	631	25
DP600B	380	612	28
DP780A	496	827	18
DP780B	480	834	18
DP800	524	820	18
DP980A	534	979	15
DP980B	674	1061	12

2.3.3.2. Relationship between Ultimate Tensile Strength and Uniform Elongation of Many Steels

The stress strain curves of TRIP and DP steels presents high tensile strength, low yield to tensile strength ratio, continuous yielding and a high uniform and aggregate elongation [59], as displayed in Figure 2.3. Through the DP steels, this behavior may be recognized by the martensite in the ferrite matrix. Since the martensite is shaped through the transformation from the austenite, it is convoyed by volume increase. The ferrite matrix is deformed because of the locally increased volume which lead to mobile displacements at the interface of the ferrite/martensite, accommodating continuous yielding. The ultimate tensile strength is increased by the hard martensite [60]. In TRIP steels distortion through the tensile loading causes the reserved austenite to convert to martensite. Moreover, this transformation includes volume expansion which result in a limited increase of the strain hardening factor.

This deferrals the emergence of necking and leads to total elongation and higher uniform [61].

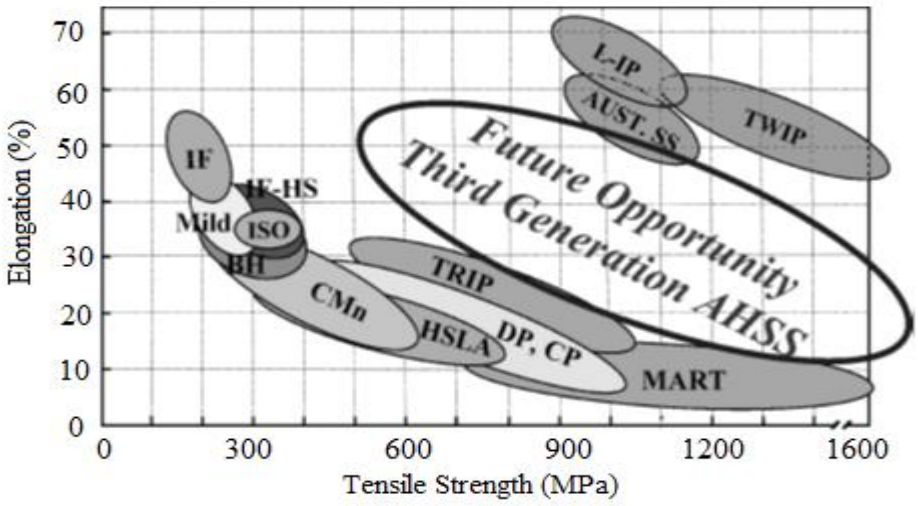

Figure 2.3. Summary of relationship of tensile strength (UTS) and tensile elongation (Uniform) for numerous members of tradational and advanced high - multi strength sheet steels (AHSS) [68].

Therefore, the excellent mechanical properties in automotive industry include the provision of decreasing the weight of the body, energy efficiency, better passive safety and good viability. In 2007, the regular vehicle had 11.6% of medium-sized and high-trust steel and the entire steel material was 57% [19]. Because of increasing the use of AHSS in different practical applications, the researches resulted in enhancing its mechanical performance in fewer amounts. Thus, engineers today face many challenges to select the suitable combination of intensity, ductility, strength and properties of Fatigue.

2.3.3.3. Relationship between Yield Strength and Ultimate Tensile Strength for Various Types of Steels (Yield Ratio)

It is important to notice that; the Martensitic MS steels are used in various industries and can be seen in many applications such as of harvesters, ground helmets, cranes, and more. The conventional HSSs including low-level alloy (HSLA) have been existed from more than thirty years and have experience to construct technological

base. The users of AHSS asked the quick accumulation of information and distribution because they apply these new types of steels. The strength of total yield and elongation axes present an important challenge. As shown in Figure 2.4, that the steels with high strength reduced elongation ratio. At present time, researchers and manufactures try to find methods to keep the percentage of total elongation with high strength steels.

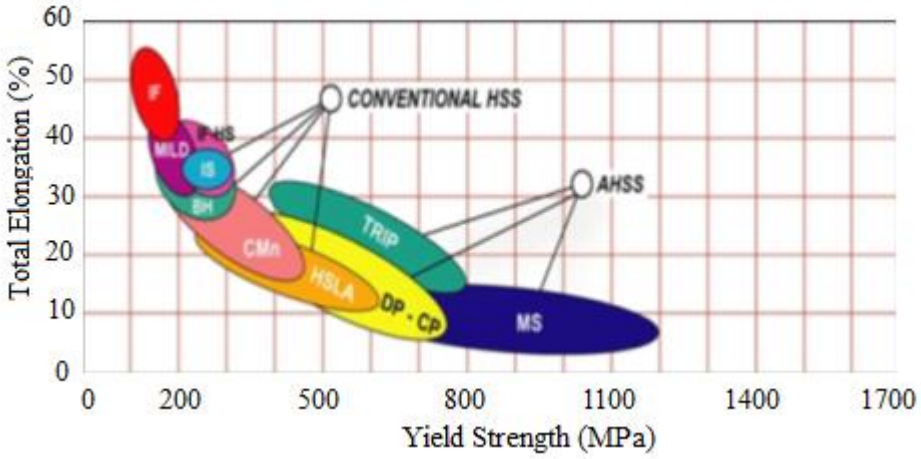

Figure 2.4. Relationship between yield strength and total elongation for many types of steels[19,38].

2.3.3.4. Evaluation of Macrostructure and Weld Nugget Geometry of Weldment

Therefore, the geometrical factors of nugget include the nugget height, the weld nugget diameter, the electrode indentation depth, the nugget size rate, the sheet thickness, and the specimen width, the list goes on. These factors together configure significant parameters to assess the spot weld quality that consist the physical weld properties, mechanical properties, and the failure mode. The geometry of weld nugget consisted the weld nugget diameter, (d_n) the weld nugget height (h_n) the weld nugget rate (nugget height/nugget diameter), (h_n/d_n) and electrode indentation, (e_i) of the spot welds for equal and unequal thickness TRIP800-DP600 steel couple are determined on the crosswise section of tensile shear test sample as shown in Figure 2.5. There are three different methods are used to conduct the quantitative measurements of the weld nugget as follows:

- Right from the diameter of weld button on peel coupons with a digital caliper.
- Right from the cross-section of the weld nugget as illustrated in Figure 2.5.
- Right from the section of weld nugget with a digital caliper.

In this research, nugget height (h_n), electrode indentation ($i_{e)}$ and the weld nugget diameter (d_n) were measured from the cross-section of the macrostructure and from the weldment. The popular criteria of the average weld nugget diameter must be larger than $4\sqrt{t}$ (t: material thickness in mm) for the preferred pullout failure (PF) mode for the steels. Nevertheless, it is observed that there is no information on the average weld nugget diameter, weld nugget height, and weld nugget size rate (h_n/d_n) the resistance of steel spot weldment for the production of the required (PF) mode.

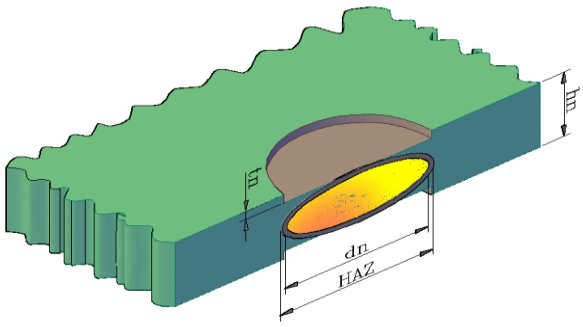

Figure 2. 5. Weld nugget diameter sections of weldment .

2.3.4. Processing of Dual Phase Steel (DP)

In recent years, DP steels development were witnessed great interest in automotive industry. Precisely, the DP steel is produced from a low or medium carbon steel (0.05-0.2 wt. %). This is resulted by the production of steel with potential weight reduction by the use of cheap alloying without losing the mechanical properties. Generally, |DP steel is made up of two phases which are ferrite and martensite. Nevertheless, in addition to the martensite, the DP steel microstructure consists small amounts of other phases including pearlite, retained austenite and new ferrite depending on the thermos-mechanical processing and cooling ratio. The DP steels have been generated by some authors by heating the steel in the area of austenite in the iron-carbon phase diagram, then direct quenching from temperature over Ac_1

temperature (i.e. inter-critical temperature). However, below the A_3 temperature on a constant cooling transformation diagram and is reserved to full austenitic microstructure as shown in Figure 2.6. Later, the steel will be cooled to the ferrite + austenite area and stay at that temperature degree and thus, the ferrite can be nucleated at the austenite boundaries. After nucleation, the ferrite produces to the austenite grains. Therefore, the microstructure will be decorated by the ferrite and martensite phases. Also, DP steel has been generated by other researchers based on and derived from the CCT diagram that covers slow cooling (air) up to the preferred ferrite transformation from austenite and then quenching for converting the continuing austenite to martensite [62,63]. It has been reported about limited works in order to produce the bainite/ferrite or martensite/ ferrite microstructure of dual phase steels by first performing laminar cooling then ultra-fast cooling up to coiling temperature and then by coil cooling until the room temperature of hot rolled strip strictly [46].

The dual phase steel melt is created by an oxygen top blowing process in the converter and they expose to an alloy treatment in the secondary metallurgy process [64]. DP steels are produced by many ways and the common way is by the cold rolling of the low alloy steels that is followed by inter-critical annealing in a continuous hardening line. The inter-critical denotes to the two-phase field of austenite/ferrite in the (Fe-C) diagram. The quenching determines the transformation of austenite phase to martensite and it is provided in appropriate hardenability. The results is the structure of a soft continuous of ferrite and entrenched hard elements of the martensite which has been detected in the study [65]. The martensite will configure lath or plates depending on the content of carbon in austenite before to quenching [66,67].

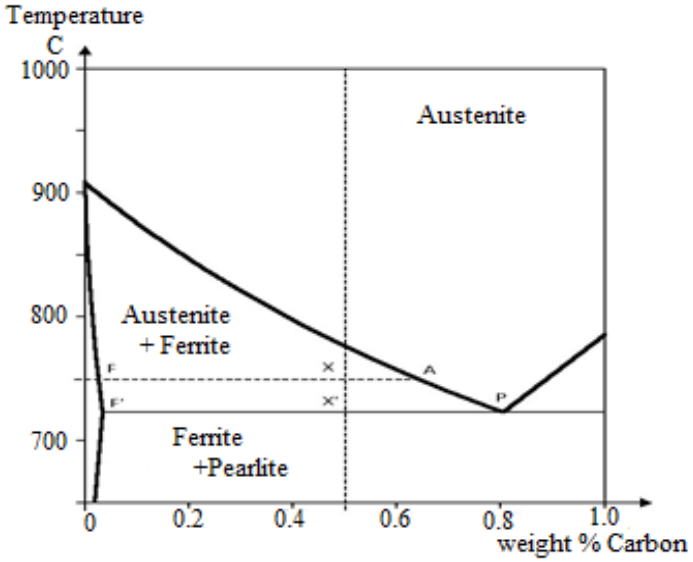

Figure 2.6. Illustration of the lever rule [74].

Many practical applications used the sequential quenching process such as suspension components, bumpers and wheels [68]. As shown in Figure 2.7 that the intercritical annealing process, is normally used to thin sheets. The primary of the microstructure of sheet comprises of a ferrite-pearlite mixture that is turned to cold with the preferred thickness. The sheet is heated to the ferrite-austenite area where the suspension of pearlite arises. This process is usually too fast be studied deeply [69]. Depending on the temperature of annealing, it is supposed that the dissolution of pearlite with most low carbon steels takes from fifteen seconds to two minutes. Increasing the temperature of intercritical annealing increases the size of austenitem decrease the carbon content of the austenite and the steel resistance.

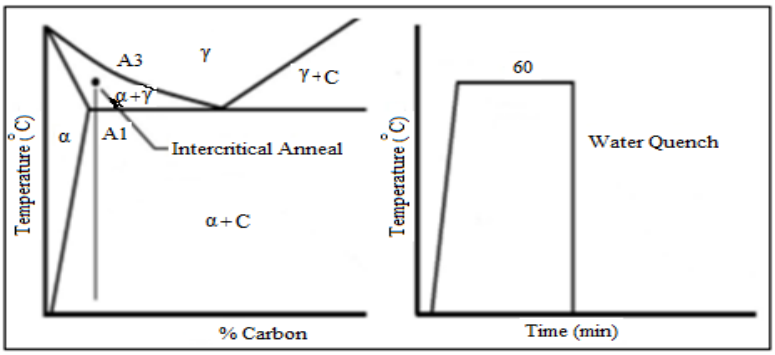

Figure 2.7. Intercritical annealing of DP steel [76,77].

Retained austenite is usually existed at the martensite islands edges because of some austenite regressive to ferrite through the cooling. Ferrite rejects carbon into the austenite as it cools that decreases the local martensite finish temperature to be under the temperature of room [70]. By comparing the two operations, in the intercritical annealing process austenite nucleates and grows at ferrite grain borders; in consecutive quenching, ferrite nucleates and grows at the austenite grain borders. The volume fraction is determined by the annealing time (holding time), accompanied by the temperature and cooling ratio. In the higher annealing temperature, the content of carbon in the austenite will be decreased but the volume fraction of austenite itself will be increased. The intermediate quenching is the third less familiar approach to produce DP steels. At this operation, the streel must be heated to the austenitic area and held for about thirty minutes to certify that the structure comprises of only austenite. Then, it is quenched to the room temperature that forms a wholly martensitic microstructure. The sample is heated for about sixty minutes in the ferritic/austenitic area to form ferrite at the grain borders. At the end, it is quenched in order to transform the austenite back to martensite islands to complete the structure of DP [71]. This operation associates DP steel with the content of higher martensite in mineral and mining parts that do not need welding operations.

2.3.5. Dual Phase Steel in Automotive Industry

Entering DP steels in automotive industry made the resistance spot welding the preferred process to join this steel. As we mentioned earlier, DP steel recently is commonly used in the automotive industry. Currently, this automation form is increasingly used by the automated people in order to increase the structural elements of HSLA. The most popular AHSS is the Dual-stage steel (DP) because of many features such as continuous yield and quick working increase, the good ductility and viability with comparatively high strength, low tensile yield rate and non-aging behavior at ambient temperature [72-74]. The most significant thing that must be taken into consideration when designing with DP steels as with other AHSS, is the pressure and increase of baking. DP steels can be developed with a high low tensile yield rate (YTS), allowing a widespread set of applications starting from a

crumple area to the structure of body. Occasionally DP steel is chosen to make the body structure and the visible parts including doors, hoods, front and rear railings. also, DP steel is used in more popular applications such as corrugated reinforcements, beams and cross-members, slab, and pillars; cowl inside and out; crush cans; shock towers, fasteners and wheels [75-77]. Figure 2.8. shows many DP grade applications which are used in automotive industry.

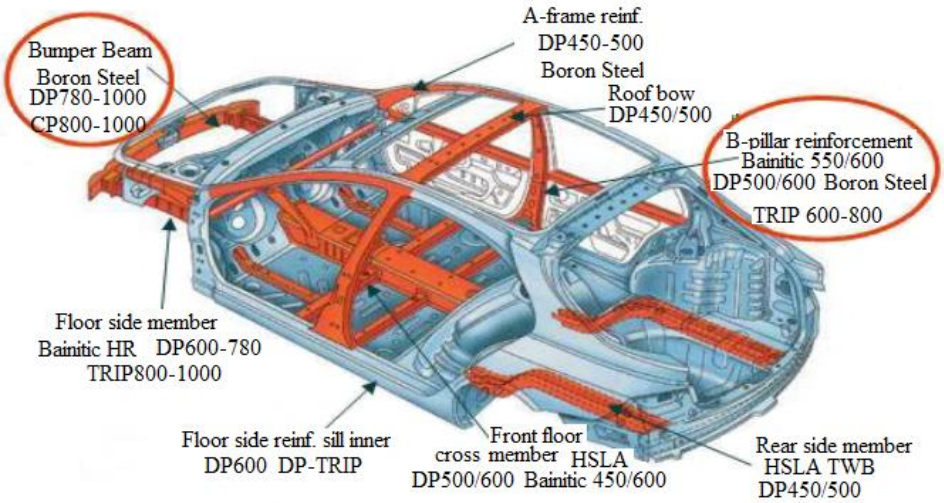

Figure 2.8. Applications of DP steels in automotive industry [88].

PART 3

RESISTANCE WELDING AND SPOT WELDING AND THEIR COMBINATION

In the previous years, iron and its applications have been used in many applications such as buildings, ships, bridges and vehicles because of many features iron enjoy including machining abilities, low price and mechanical properties. In manufacturing industries, many welding methods have been used such as flux core arc welding (FCAW), submerged arc welding (SAW), tungsten arc welding (GTAW), shielded metal arc metal welding (SMAW) and resistance spot welding (RSW). These consist the wide use of RSW in industries because of many reasons such as easily controlled process, repeatability and cheap equipment [79]. to join of metal sheets including titanium alloys [80], magnesium alloys [81], iron and steel [82] and aluminum alloys [83] .In addition, RSW is used due to numerous psychical and mechanical properties of different joint metals including iron-aluminum [84]. Through RSW approach, heat can be gotten by operate a large electric current in short period of time and overlapping sheets are gotten between two electrodes [85].

Therefore, electrical resistance spot welding within the metal interface leads to local heating to join and at the end, the spot resistance welded is generated by combining heat, pressure and processing time [86]. Stainless steel particularly with low grades of carbon were used extensively in many industrial applications including the manufacture of appliances because of its resistance to corrosion and correct decorative appearance in the ambient air. One of the most significant verities of austenitic stainless steels is the stainless-Steel grade 316L. It comprises of austenite and ferrite phases. Since its decorative appearance, high corrosion resistance [87] and outstanding weld ability [88], this grade has been used widely in many industrial applications.

3.1. CLASSIFICATION OF RW AND SW AND THEIR COMBINATION

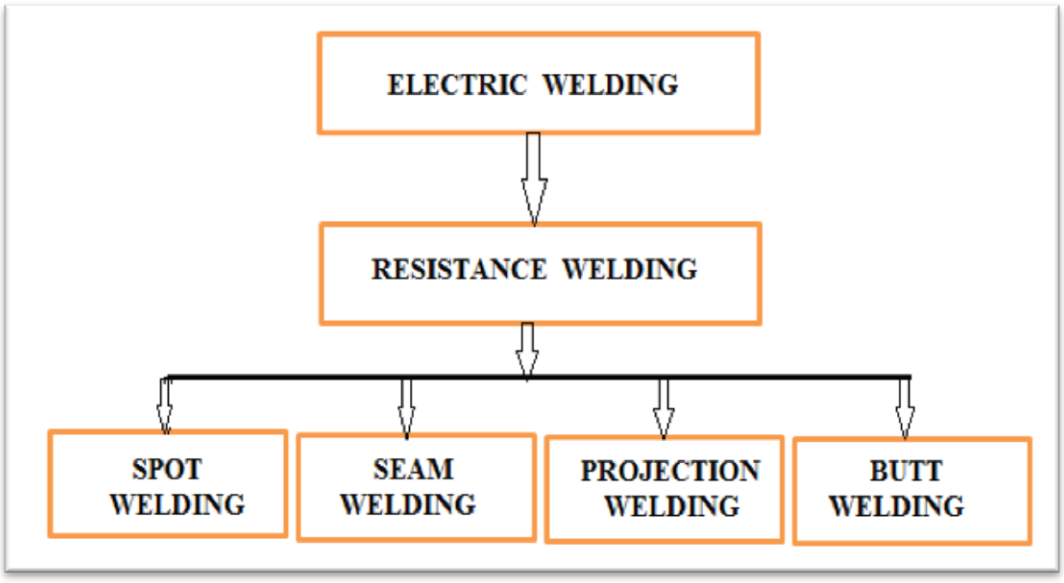

Figure 3.1. Classification of Resistance welding [96].

3.2. RESISTANCE WELDING

This type of welding is the joint of metals by applying pressure. The current is passed for a long period of time through the metal region that is to be joined. The main benefit of this type of welding is that no need to other materials to create the bond and this issue makes this process very cost effective. The resistance welding is a welding technique that commonly utilized in many industrial applications to join metal sheets and components. The weld is conducted by making strong current by combining the metal to heat up and finally melt the metals in predetermined localized points by the design of work piece to be welded or the electrodes. In general, the force is applied before, during and after the application of current in order to restrict the area of contact in the weld interface and in other applications to forge the work pieces [89].

3.2.1. Resistance Welding Processes

The resistance welding process is classified into many variants depending on the form of electrodes and work pieces. The most frequently used are seam welding,

projection welding, butt welding and spot welding. At the following steps, we will describe each one of them briefly.

3.2.1.1. Spot Welding

Elihu Thomson [Compton, 1939] has invented the Resistance Spot Welding (RSW). This development process has a long history and return back to 1890 when Thomson filed a patent on a "*Method for Electric Welding*" [Thomson, 1890]. The idea has been developed more and in 1909 Thomson filed a patent on "*Electric Welding of Sheet Metal*" [Thomson, 1909]. Currently, cars contain thousands of spot-welded joints. The number of spot-welded joints depend on the size of vehicle and the number of parts which need to be joined in the combination and the joining strategy that used by the manufacturer. This type of welding is a resistance welding process and used to join the metal sheets by directly applying opposite forces of electrodes with pointed tips. Figure 3.2. shows the resistance wedding process. Welding is created by using the heat generated from the resistance to the flow of welding current between the faying surfaces, in addition to the force in order to push the work pieces together, applied above the defined period. This type of welding applies the face geometrics of the welding electrodes themselves in order to focus the current of welding at the required location and applying the welding force on the work piece. The materials set down and combined when efficient resistance is generated, and a weld nugget is formed. The electrode tip contact area defines the size of weld nugget. The main joining process is the spot welding and it is used in many applications regarding the automotive industry and it is a key point to assemble large components in automobile bodies.

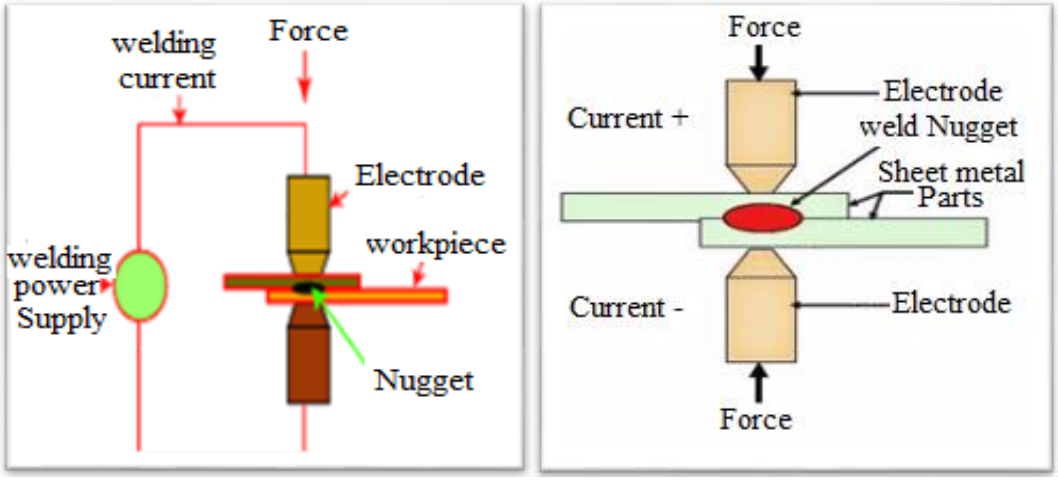

Figure 3.2. Resistance Spot Welding [97].

In addition, it is commonly used to manufacture domestic equipment and furniture. The Principle of Resistance Spot Welding During spot welding, (2 or 3) are overlying or stacked stamping plates that are welded together because of the heat generated by the resistors. This is offered though the work piece that held together under the pressure between the two electrodes. It is possible to perform the spot welding by several ways such as robotically, manually or through a dedicated spot welder [90], 91].

3.2.1.2. Resistance Seam Welding

This type of welding is a subset of Resistance Spot Welding process to join metal sheets in continuous, often leak tight, and seam joints by directly relating opposite forces with electrodes involving of rotary wheels. Resistance Seam Welding uses wheel-shaped electrodes in order to carry force and welding current to specific parts as clarified in Figure 3.3 and Figure 3.4. The welding here is performed on the work piece rolls between wheel-shaped electrodes while weld current is applied. Depending on settings of weld time and the particular weld current, the welds performed may be overlapping, creating complete welded seam or may just be individual spot weld at determined intervals. Resistance seam welding is used in many application such as heat exchangers, radiators and manufacturing of containers [92].

Figure 3.3. Seam welding machine [100].

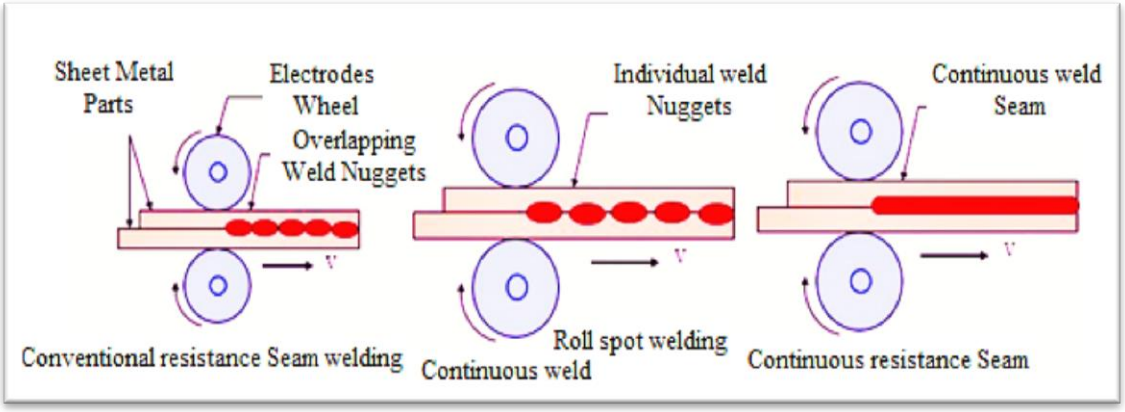

Figure 3.4. Seam welding [100].

3.2.1.3. Resistance Projection Welding

Figure 3.5 shows the projection welding process to join components or sheets of metal with embossments by directly applying opposing forces with electrodes which have been particularly designed in order to be a proper for the forms of the workpieces. Generation of heat and current are confined by the workpieces shape by

their natural shape or by the particularly designed projection. Collapse or large deformation will happen in the projection part of the workpiece. This refers to the implication of high process/machine dynamics [93]. When the weld current creates efficient resistance in the contact point, the weld nugget will be formed by the projection collapse. The solid projection is mainly used to weld the fasteners parts. Embossments are mainly used to join sheet or plate materials. Resistance projection welding is used in many applications including automotive and construction industries, electronics, electrical, and sensors manufacturing, pumps and valves etc.

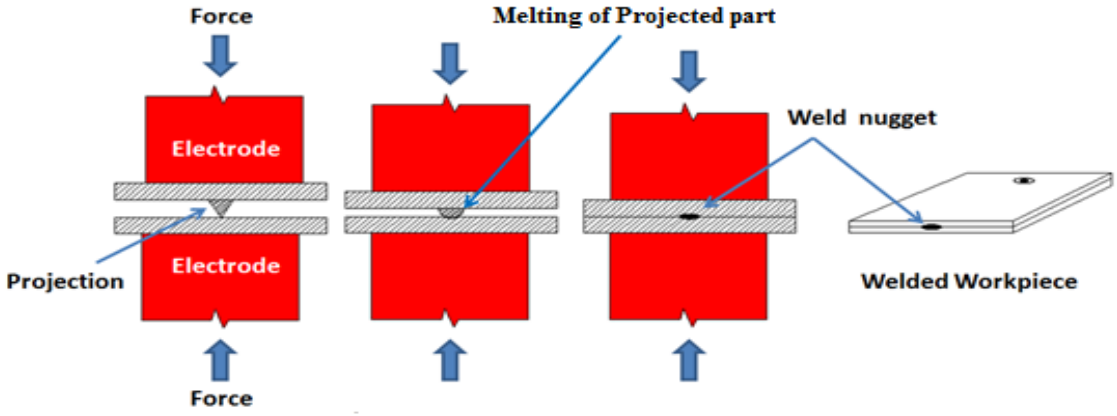

Figure 3.5. Projection welding [101].

3.2.1.4. Resistance Butt Welding

This type of welding is mainly used for joining bars or thick metal plates at the ends by directly applying opposing forces with electrodes clamping the workpieces [94]. After heating up the workpiece, the forging operation is applied. Frequently, no melt happens and thus, a solid-state weld can be gotten as shown in Figure 3.6. Butt welding is used in many applications such as railway track joints, wire joints and manufacturing of wheel rims etc.

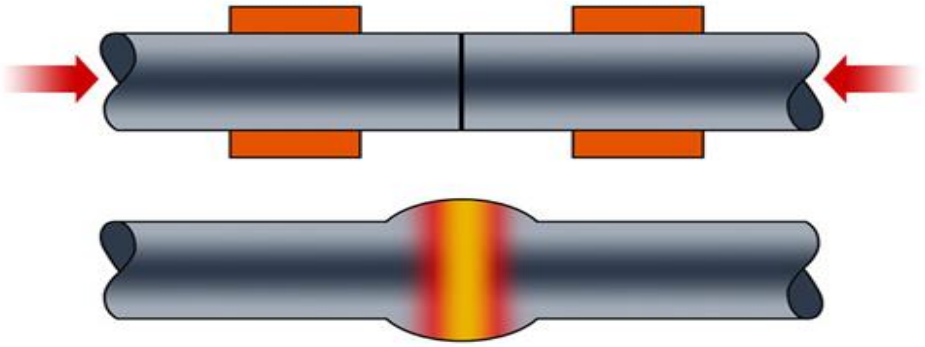

Figure 3.6. Butt welding [102].

3.3. SPOT WELDING (LASER WELDING, STIR WELDING)

3.3.1. Laser Welding

Laser welding is considered a significant industrial process due to many advantages such as the bonding process over the broadly used joining methods. This type of welding characterizes by high penetration, parallel-sided fusion area and narrow weld width. These characteristics due to the high-power density that make laser welding to be one of the keyhole welding processes [95]. The shape of laser weld-bead is determined by the parameters of laser welding input due to the combination of these elements control the heat input. It is necessary to select the combination of welding speed, output power, position, focal shielding gas and position accuracy correctly in order to get good weld quality [96]. Resistance Spot Melding is commonly used in the prediction of the weld bead geometry and mechanical properties in several welding process as showing in Figure 3.7.

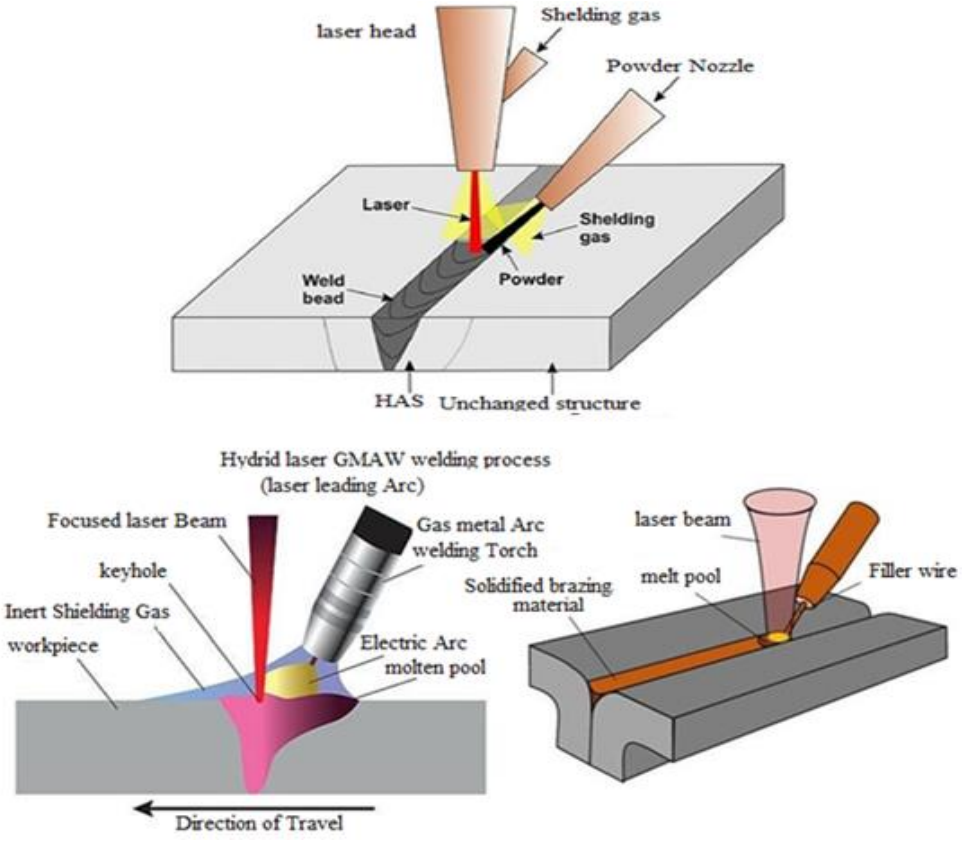

Figure 3.7. Laser welding [105].

3.3.2. Friction Stir Welding

Friction stir welding is considered a new technique and it is a solid-phase process giving. This type of welding is proven its quality butt and lap joints to create high quality welding in many materials such as those which difficult to be welded by using traditional fusion process [97]. Figure 3.8. illustrates the basic principle of friction stir welding. It operates on generating frictional heat between the rotating tools of harder material than the workpiece being welded, in such a way as to thermally state the abutting weld area in the softer material. The tool is shaped with a bigger diameter shoulder and a smaller diameter, particularly profiled probe. At the beginning, the probe creates a contact as it is plunged into the joint area. The initial plunging friction contact is heating a cylindrical column of metal around the probe in addition to a small area of material under the probe. The length of probe under the shoulder of the tool controls the penetration depth.

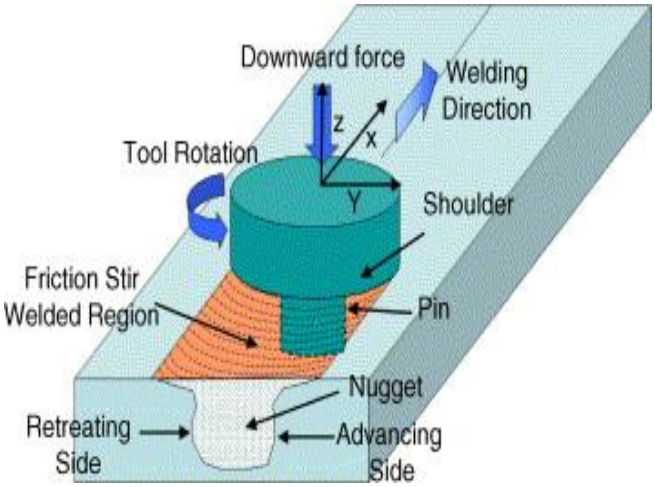

Figure 3.8. Friction stir welding [106].

3.4. RESISTANCE SPOT WELDING

Through this research, we can understand and conclude that resistance spot welding is a process for joining the surfaces of contacted metals together by the electrodes alleged together under pressure, and heat resulting from the welding current. Conservatively, the thickness of the sheet range of (0.5 to 3) mm. two large-shaped cooper alloy electrode are used in order to focus the welding current in a small “spot” and clamping the plates together simultaneously. Forcing a large current to be flowed through this point might melt the metal and form a weld nugget. The importance of spot welding is the ability of transferring a large amount of energy to spot welding in a short time (about 10-100 milliseconds).

This type of welding allows the welding process without overheating the remaining sheets [6]. In other word, resistance spot welding depends on heating by passing high current between the electrodes through the intersecting sheets to be joined. Schedule of spot welding includes the extrusion time, pre-heating time, welding time, cooling time, post-heating time and final holding time. Figure 3.9 shows the basic single pulse welding cycle. Mainly, the squeeze time through which force (squeeze force) is applied to the joint by the electrodes before the welding current flow. The resistance of contact R is generated on the joint interface. Later, the welding current (I) is

applied during the workpiece of time (t). The current flow during the resistance of contact between the metal sheets creates heating.

Technically, it is significant to realize that the contact area temperature among the metal sheets that quickly increasing the forming of a molten nugget on the joint interface. Later, the welding current is prevented, and the pressure is continuing (forging force) to combine the weld for a period (hold time) whereas the weld solidifies. The welding time and welding current are the most significant variables. They create heat and the applied electrode forces for the resistance spot welding method. Mainly, the squeeze force effects the contact resistance between the metal's sheets.

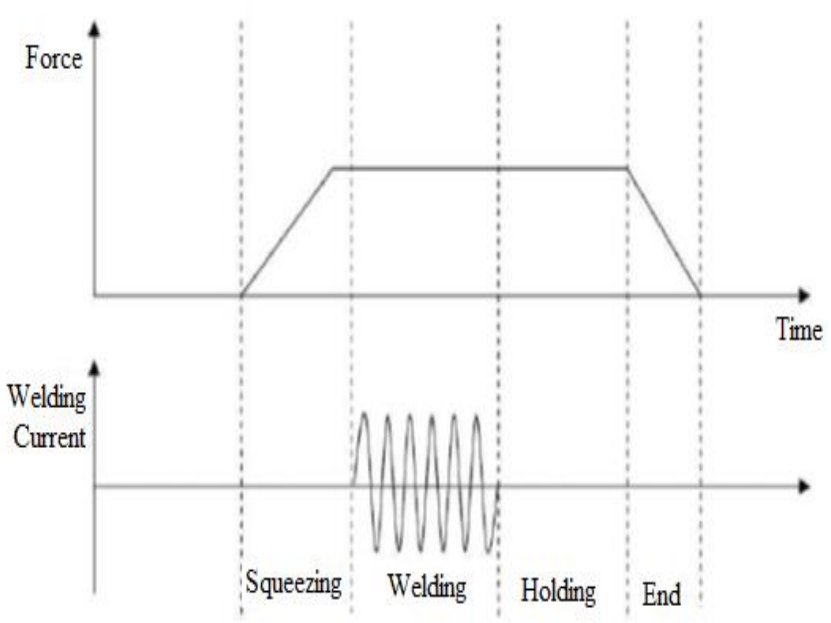

Figure 3.9. Basic single pulse welding cycle for resistance spot welding [112].

The clarifications in Figure 3.10 the workpiece (3 and 5) that are joined are cooperatively pushed together mechanically by the electrodes (1 and 7) and an electric current is conceded through the faying interfaces (2 and 6) in resistance spot welding. There are many factors affect the heat which is created in the interface including the current flow time, interface resistance and current. The metal parts around the interface are heated because of this generated heat resulted in melting and forming the weld pool. The temperature starts to reduce, the weld pool hardens and

weld nugget (4) is generated when the current flow is switched off. Through the welding process, the electrodes (1 and 7) are cooling down to decrease the heat created from the electrode-work piece interface and in order to avoid fusion at these interfaces [98, 99].

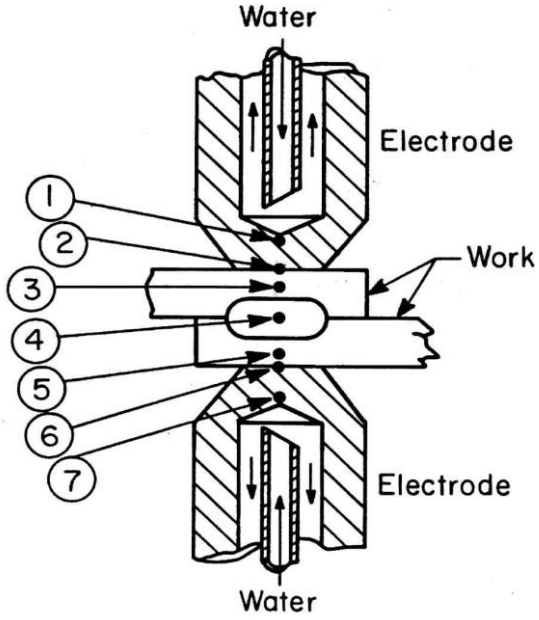

Figure 3.10. The schematic illustration of resistance spot welding processes [113,114].

3.4.1. Principle Working and Thermo Electrical Process of RSW

Whereas in terms of spot-welding process, (2 or 3) are overlapped or stacked stamped sheets that both are welded because of the heat generated by the electrical resistance. This is offered by the work piece because they are held both under the pressure between the two electrodes. Various ways are used to perform the spot welding such as robotically, manually, and by specific spot welding machine [90,91]. The equal spot welding which have the same feature can be gotten in high production speeds by governing weld time automatically, the welding current and electrode force [100,101]. Figure 3.11 shows and reveals a systematic illustration of resistance spot welding.

Four major sources have resistance, and therefore heat generation, typical values of materials used in RSW. (1) Resistance of the electrodes. (2, 6) The contact resistance

between the electrodes and the sheets. (3, 5) Bulk resistance of sheets. (4) The contact resistance between the sheets. For boys with more than two sheets, contact resistance and bubble resistance are applied accordingly.

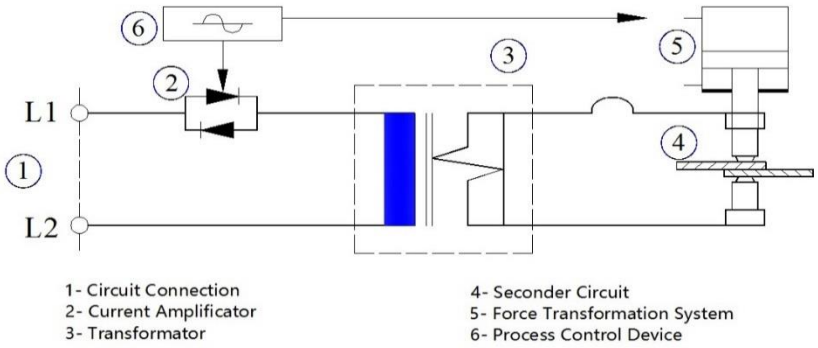

Figure 3.11. The schematic illustration of electrical RSW [117].

As mentioned and clarified that welding current should flow from the electrodes through the work piece. It's technically the continuity which is supplied through the forces that are applied to the electrodes. Hence, the sufficient heat generates for raising a confined volume of metal to the molten state. Later, this molten metal is permitted to cool while under pressure until it has sufficient strength in order to hold the parts together. The weld current and electrode force ought to be such that a nugget is configured, but not so high that molten metal is expelled from the weld area. The time period of the weld current should be adequately short in order to avoid the excessiveness of the heating of the electrode end tip. The heat that used for RSW processes is created from the resistance of the workpiece to the electric current that pass through the material. Due to the short electric current path in the workpiece and limited weld duration, reasonably the high welding current is necessary in order to develop the required welding heat. *Based on the; "*$Q = I^2 \times R \times t$" formula, the quantity of heat created relies on these three factors:

- The weld current
- The resistance of the conductor
- The duration of current [102].

The resistance (R) in the heat formula is influentially controlled by the welding pressure through its impact on contact resistance at the interface amongst the workpieces.

3.4.2. Resistance Spot Welding of DP Steel

Resistance spot welding is a joining technique which comprises the pressing of two or more overlapped metals together whereas the current is passed the localized contact area to heat the metal to a satisfactory temperature and form the weld nugget [103]. However, the resistance spot weld ability [104] of DP steel is tighter when compared to the typical HSLA steel due to the multiphase structure properties and the relatively higher alloying level in DP steel. For example, it is known that the tensile performance of spot welding depend highly on geometric properties of the weld nugget [105,106]; Nevertheless, phase transformations arising at the fusion zone (FZ) and/or heat affected zone (HAZ) have great effect on the tensile characteristics of resistance spot welded dual-phase (RSW-DP) steel [26]. Table 3.1 shows the number of spots welds that used in assemble of Automotive Body in white (BIW).

Table 3.1. Number of spot welds used to assemble the Body in White (B.I.W.) of several brands and models, as presented at conferences. If data is available for updated models (e.g. Ford Fiesta), the data of the latest model are presented here [107].

Model	**Number of spotwelds**	**[Reference]**
Audi A4 Avant	5061	[Rebele *et al.*, 2008]
Audi A6	5102	[Wilde *et al.*, 2004]
Audi Q5	5580	[Rebele *et al.*, 2008]
Citroën C4	4360	[Perrot *et al.*, 2004]
Citroën C5 Berline	4051	[Le Floch & Barbier, 2008]
Citroën C5 Tourer	4282	[Le Floch & Barbier, 2008]
Ford Fiesta 3-Door	3184	[Liesenfelder *et al.*, 2008]
Ford Fiesta 5-Door	3305	[Liesenfelder *et al.*, 2008]
Honda Jazz	2060	[Ito *et al.*, 2008]
Jaguar XJ Saloon	3185	[White, 2006]
Jaguar XK Convertible	2620	[White, 2006]
Jaguar XK Coupe	2620	[White, 2006]
Mercedes SLK	4840	[Trost *et al.*, 2004]
Mini Cabrio	4178	[Brunies *et al.*, 2004]
Mini Hatch	4475	[Brunies *et al.*, 2004]
Nissan Murano	4307	[Saito & Nakamura, 2004]
Nissan Teana	5821	[Michiura *et al.*, 2008]
Opel Insignia	6331	[Heim *et al.*, 2008]
Opel Vectra	4613	[Heim *et al.*, 2008]
Peugeot 307	4434	[Perrot *et al.* 2004]
Peugeot 307 Space Wagon	4764	[Perrot *et al.*, 2002]
Peugeot 407 Sedan	4335	[Bonte & Deren, 2004]
Peugeot 407 Station Wagon	4607	[Bonte & Deren, 2004]
Renault Clio	2916	[Delhommeau & Hoareau 2004]
Renault Laguna Coupe	4379	[Plaideau *et al.*, 2008]
Renault Laguna Hatchback	3998	[Plaideau *et al.*, 2008]
Renault Modus	3746	[Delhommeau & Hoareau 2004]
Renault Twingo	2213	[Delhommeau & Hoareau 2004]
Skoda Octavia 24	4333	[Sekyr, 2004]
Skoda Octavia 34	4771	[Sekyr, 2004]
Skoda Octavia 35	5011	[Sekyr, 2004]
Skoda Superb 451	5051	[Simon & Senkyr, 2008]
Skoda Superb 461	5157	[Simon & Senkyr, 2008]
Volvo V50	3779	[Jonsell *et al.*, 2004]
Volvo XC60	4337	[Lassl, 2008]

3.4.3. Resistance Spot Welding Processing

In spot-welding, two or more overlapping metals are pressed and joined together. It uses an alloy electrode to generate pressure for squeezing the metals. The leg pedal applies the weld force that moves the electrode and squeezes it on the work pieces. This results in heat resistance that welds the work pieces using the right pressure, which is quite important for obtaining the welding quality. Since the current passes through a local area of contact, which heats the metal until a certain adequate temperature, at which, weld nuggets are formed [103]. After completion, there is a need to lift the upper electrode that helps work pieces to move out, which makes them ready to initiate the next welding [108]. This material combines high electrical resistivity with low thermal conductivity as compared to the electrode that makes steel relatively easier-to-weld. Some metals, including aluminum and copper have close values for thermal conductivity and electrical resistivity but aluminum certainly has a lower melting point as compared to copper. Greater force of electrodes decreases the contact resistance on the interface that further decreases the expulsion at the Nugget and heat/temperature; so, it is possible to determine the maximum diameter with no expulsion when the electrode geometry is constant. The higher the electrode force is, the higher the current requirement will be, which damages electrodes, and increases the processing cost, indentation, and the surface penetration.

The pressure is maintained during the holding stage; so the current should be turned off, which allows the nugget to cool down under pressure (Figure 3.12). The concept behind the resistance spot welding has been developed on the basis of the first Joule's Law, which mathematically expresses the generated heat that takes place because of the current flows through a conductor. The heat, which is generated between the metal sheets with respect to time, is a product of the total resistance, the current squared intensity, and the welding duration. Certain factors have an impact on the generated heat, as the formula indicates [102]; it is given as follows $Q = I^2Rt$

Here *Q* represents the generated heat (J), *R* represents the conductor resistance (Ω), *I* imply current (A), which travels through a conductor and *t* shows the time of current application (s).

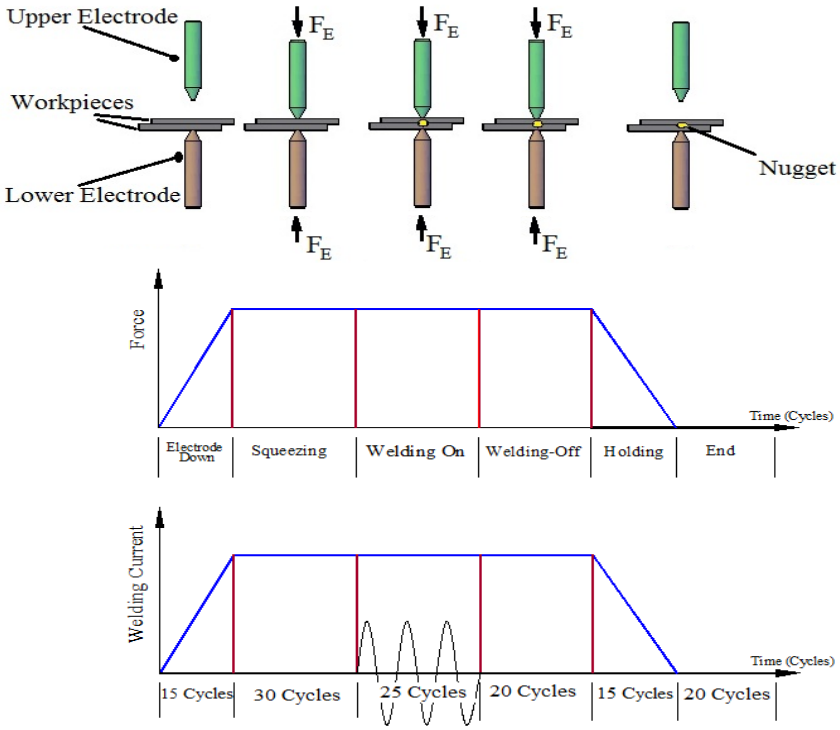

Figure 3.12. Resistance spot welding processing weld time parameters.

Four factors play a significant role during the spot-welding operations: 1. Passage of current through a work piece. 2. Electrodes' pressure on the work piece. 3. Time taken by current to flow in a work piece. 4. The electrode tip contact area of a work piece. The current study discusses the welding processes conducted on a series of DP600 steel sheets, which were welded together when the electrode form is fixed. When the electrode force is changed with the help of welding current, the sheets get exposed to the micro-hardness and tensile-shear tests [111]. The mentioned tests predict the strength of the joint. In case of variable current/resistance, the following will be the mathematical expression:

$$dQ = I(t)^2 R(t) dt \tag{3.1}$$

The welding current duration needs to be limited because it helps avoiding the electrode faces' excessive heating. The real-time control is provided by the power supply. Long-duration welding leads to heat up the metal sheet, but on the other hand, it softens the heat-affected zone, which reduces the joint. Cooling is the last stage, which holds the molten nugget on the work piece until the time it becomes cold, stable, strong and solid.

3.4.4. Resistance Spot Welding Parameters

The resistance welding works using the principle of the Law of Joule Heating, while Q represents generated heat that depends on three fundamental elements, which are expressed as: $Q = I^2Rt$ In this case, "I" represents the current in the metal combination while t implies the time taken, and R shows the base metals' and the contact interfaces' resistance. Several parameters describe the resistance spot welding process, while the time and the current force describe the welding process. The surfaces of the sheet metal and the size, shape and thickness of the electrodes substantially affect the welding quality. The next chapter discusses the details of machine parameters as well as their impact on the spot weld.

It is possible to assure the preferred nucleus diameter through excellent repositioning of welding time versus current intensity. The values of the parameter have been selected such that it allows at least $4*\sqrt{t}$ nugget diameter. Here, t stands for sheet thickness that can be accomplished after RSW. Spot-welding parameters are significant because even a small change in any of the parameters affects the remaining parameters. They determine the welding quality. In case of short welding time, there is decreased nugget diameter. Contrary to that, the molten metal quantity increases that makes the fused metal spurt out, which results in reducing the welding joint strength [102]. After conducing several experiments and tests, we have summarized the most significant parameters as follows.

3.4.4.1. Welding Current

Among all the welding parameters, welding current is a very important parameter that influences welding specific materials. Moreover, the NS determines the heat generation in resistance welding using the power of squares, which is clearly shown through the formula. The weld nugget size rapidly increases when the welding current increases; however, high current deteriorates the electrode and results in expulsions [109]. The welding current is technically linked with the heat generation, and the intensity of the AC power. The single-phase AC is commonly used in production (Figure 3.13), while the DC power is used to weld metals and alloys because it provides higher current densities. They generate the heat needed for the process of fusion [110]. A DC system reduces the power requirement in the AHSS welding, and makes RSW efficient [111]. The RSW current profiles are altered by adding upward and downward slopes and pulsing. According to Tawade et al. [112] adding the upward slope helps increasing the welding lobe window for AHSS.

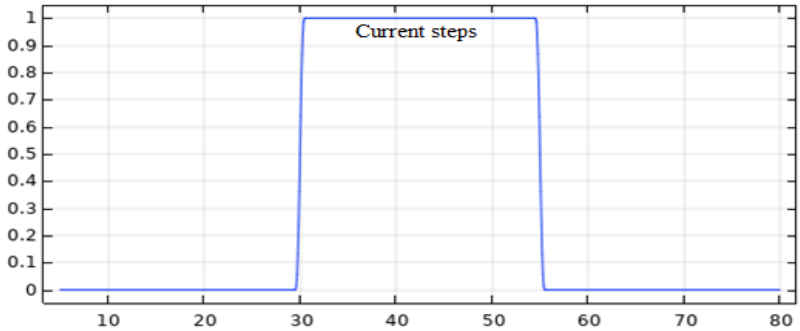

Figure 3.13. Welding current parameters.

Aslanlar [102] asserted that in RSW, two factors control the weld current: Transformer tap switch setting that determines the maximum weld current and the current control percentage, which help assessing the available current for welding. The currents for low percentage welds are generally not recommended because they might reduce the weld quality. The weld current needs to be minimized. When the welding current is determined, the intensity of the current slowly increases that causes weld spatter, which shows that the correct weld current is attained [102]. Several studies can be found in literature [9]. which show that low current cannot

provide sufficient heat for the formation of a nugget. In case of high welding current, the weld nugget size increases when the welding time increases and becomes similar to the area of the electrode tip. Very high current leads to higher-than-boiling-point temperature and expulsion of the nugget [16]. In case of expulsion, the nugget size reduces, which might negatively affect the surrounding parts and equipment [113]. We used 4, 6, and 8kA welding currents for this research.

3.4.4.2. Welding Time

It is an important parameter, which implies the duration when the welding current comes in contact with the metal sheets. It is calculated and adjusted in line voltage cycles. A cycle means fiftieth part of a second with 50Hz power; so every cycle equals 0.02 seconds. Since the welding time is linked with the weld spot, optimum weld time is difficult to evaluate. Technically, an RSW process has four durations, which are mentioned in Figure 3.14. They include squeeze, weld, hold and final release. The duration of welding depends on the type of material, quality, and productivity. In squeeze intervals, the metal sheets are positioned and clamped with the help of electrodes. As soon as the electrode force reaches its required level, the current is applied to begin with welding. When it happens, it leads to melting and joining [114]. Here, squeeze duration implies the time between the electrode force and its initial application on a work piece. The weld current should be delayed until assuring the attainment of electrode force to the required level; so, the time/duration of the welding process is calculated and adjusted in the line voltage cycles like the case of all the timing functions. If it continues for a long time, the molten metal quantity increases that results in the spurting out fused metal that creates peaks and valleys, which are obvious if the surface of the metal is observed with a microscope; so, the crystalline structure changes. If electrodes are suddenly disconnected, dissipation of heat occurs that darkens the contact surface. When a welding operation ends, the weld is chilled using electrodes. The holding time is essential for electrode because it solidifies the weld nugget; however, it shouldn’t be too long because it spreads the heat on a weld spot. For instance, long duration of holding electrode is only recommended when galvanized carbon steel is welded [102].

The time speed shows current flows to a component, which is predicted/measured in terms of size, material thickness, changes in the current and cross-sectional areas on contact surfaces of the welding tips [102]. The spot-welding procedure takes place during a short time period. In case of short time, the diameter of the nucleus reduces. Contrary to that, when the time period is longer, the molten metal quantity improves; so, spurting of fused metal takes place, which reduces the welding joint strength decreases [102].

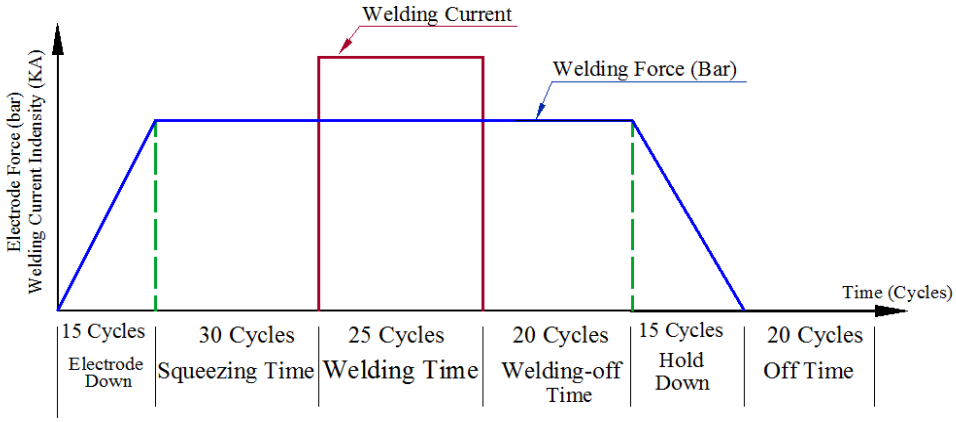

Figure 3.14. Weld time parameters [111].

3.4.4.3. Welding Force

The electrode clamping affects resistance welding because it has contact resistance effect on the contact area and the interfaces because it results in material deformation. When the electrode force is high, it leads to low resistance and improved interfacial contact, which further result in reduced heat generation while welding. It should be compensated either through increased welding time or current input [115]. Furthermore, force of an excessive electrode causes higher work piece indentation [110].

The basic purpose behind the electrode force is joining the metal sheets through constraining them together. It needs greater electrode force; otherwise, the weld quality cannot be considerable. In addition, increasing electrode force reduces heat energy, which means that it will require higher electrode force. Higher weld current results in spatter between the sheets and electrodes. It causes electrodes to stick with

sheets. The electrode force is 700kg/cm^2, which is the adequate target value [8,102]. Another problem is increasing the contact surface during the welding process. For maintaining similar conditions; gradually the electrode force should be increased. Since it is difficult to change the electrode force because of "mushrooming" electrodes; so average value is selected [102]. In case of too low welding force, it leads to immediate expulsion when the welding current is applied because of high contact resistance, which ultimately results in immediate heat generation [116].

When there is high clamping force, large contact area leads to low contact resistance and current density, which reduce generation of heat and limits the weld nugget size. In case of too high pressure, the sheet material softens [Kearns, 1980] [117]. In case high indentation isn't needed due to cosmetic considerations, or it might generate stress on concentration points when deformation of the sheet material takes place. The increasing electrode force ultimately reduces the contact resistance. The contact resistance becomes uniform after certain pressure [Kearns, 1980] [117]. The heat energy reduces, if the electrode force is enhanced; so, high pressure on a weld joint reduces resistance between the tips of electrode and the surface of the parts where the point of contact exists [102]. It implies that high electrode force should accompany high welding current. It is most likely to result in weld spatter because of too low pressure on the tips. It also happens when there is too high weld current [118]. When the pressure is too high, it results in a small spot weld. It means that increasing pressure transfers the heat and electrical current to a wide area, but it will reduce the weld area and penetration [119]. According to Figure 3.15, the electrode forces' pressures have been used for the current thesis, which are 3.5, 4.5 and 5.5bars.

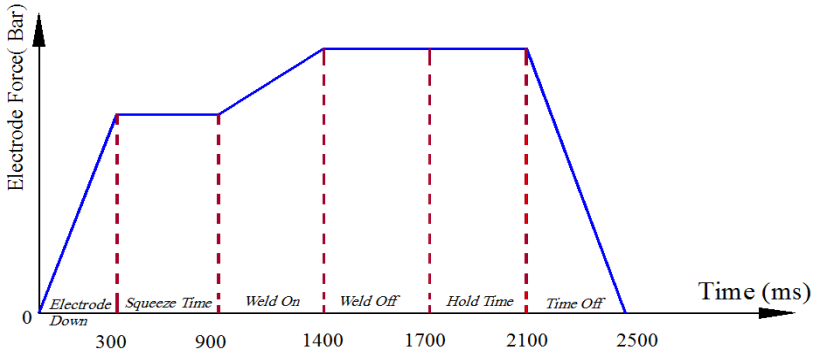

Figure 3.15. Welding force parameters [128].

3.4.4.4. Geometry and Dimensions

The geometry and dimensions of workpieces and electrodes are significant because they affect the distribution of current density and therefore, the resistance welding results. In spot welding, the geometry of electrodes controls the current density and the resulting weld nugget size. Different metal sheets thickness needs different welding current and other settings of process parameter. In projection welding, the local projection geometry design is important and must be considered together with the properties of materials particularly when joining different metals. The projection or embossment must be inserted on the material with low resistance to obtain a good heat balance on the weld interface [129].

3.4.4.5. Electrode Degradation and Tip Dressing

The resistance welding process can be described as a high current pass through the welded materials between the electrodes under the pressure in order to generate focused heat to form a weld.

3.4.4.6. Mechanisms of Electrode Degradation

The electrodes tips are exposed to high risk of degradation because of the sever conditions of high current and pressure through the resistance welding. The right side of Figure 3.16 shows a comparison of the new and used electrode tips in spot welding of galvanized steel sheets. Figure 3.16 also shows that increasing number of welds will lead to two main changes in the electrode tips.

- Geometric changes: The wear and deformation such as pitting, mushrooming or local material removal by picking up will cause increase in the diameter of the electrode tip.
- Metallurgical changes: The properties of the material around the tip surface will change through the resistance welding including coating materials and alloying with sheet and softening and recrystallization by overheating.

Figure 3.16. Electrodes tip [131].

3.4.4.7. Effects of Electrode Degradation

Increasing the tip diameter causes a larger contact zone between the electrode and sheet and thus, decreasing the current density which pass through the weld interface. Simultaneously, alloying the material of electrode with sheet and coating materials at the tip surface will decrease the conductivity of electrode tip and therefore drag the concentration of heat away from the weld interface. These effects together cause increasingly the reduction of the weld nugget sizes. Number of achievable welds until the obtained weld nugget sizes releasing to the weld quality limit is called the "electrode life". Number of degradation mechanisms which have been identified are five namely; alloy formation, softening, tip diameter growth, pitting and recrystallization [120]. The increased temperature of the electrode repeatedly through the spot-welding resistance cause the cropper breading.

Therefore, deformation of softer metal will increase and the tip diameter after much welding will be increased too. Re-crystallization denotes to the metallurgical operation that lead to higher temperature of the electrode through the welding process. Moreover, contact with zinc through the welding coated steels will cause some alloys by the electrode tip to create brass.

The uneven tip will decrease the sight conditions and raise the elimination dangerous by the semi-electrode interface. The expressively degraded electrode top is shown in

Figure 3.17. Different measures can be applied in order to extend the life of electrode. The use of electrodes is the most important issue. Moreover, electrode degradation can be enhanced by improving the welding parameters by keeping electrode forces low. Tip dressings avoidance will display a concave top. In similar serious cases, only the tip outline is contacting the sheet. Thus, no heat will be created in the center of the electrode and the resulted welding has a ring shape and occasionally called a donut bridge.

Figure 3.17. Example of a severely pitted electrode [100].

3.4.4.8. Diameter of the Electrode Contact Surface

Resistance spot welding have one main standard is that the weld will have a nugget diameter of 5×t1/2, “t” being the thickness of the steel sheet [118]. Therefore, the spot weld created in two sheets, each 1 mm in thickness may create a nugget 5 mm in diameter according to the 5×t1/2, “t”-rules. Diameter of the electrode contact surface must be somewhat larger than the diameter of nugget [121]. The electrode diameter used in the work in 8mm.

3.4.5. Electrode Geometry

In production, the result of welding is affected by the size and shape of electrodes. Figure 3.18 explains the geometry of different electrodes geometry. The contact zone between the electrodes and metal sheet is considered the most significant area in the

electrode geometry. Typically, the electrode tip diameter must be equal to the thickness of the sheet [122]. The contact will influence the current density of welding and the pressure of contact. It may be necessary to use different electrode on each side of the stack in order to enhance the welding parameters. The top curvature of the electrode is a measure against the degradation of the electrode tip. As the electrode degrades the preliminary curvature will be a flat surface. After continues welding process, a concave surface may initially cause a concave top. The most properly used electrode geometry is defined in the ISO standard - 5821: 2009 [123].

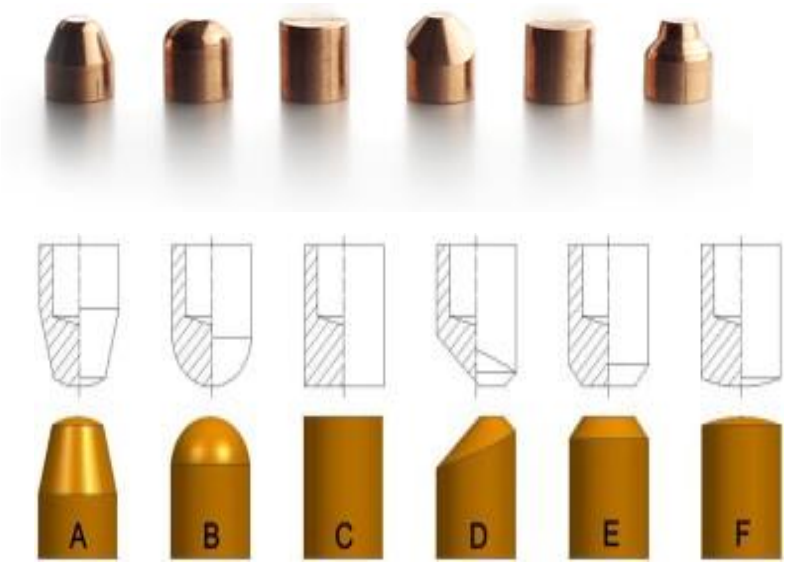

Figure 3.18. Electrode geometry types [133].

3.4.5. Electrode Materials

The most appropriate and most effective functions of the electrodes are to send an electric current and squeezing the sheets together. Thus, the most significant factors in welding the suitable electrons are hardness, compressions strength and electrical conductivity. The material is right to the best copper-based alloys and copper demands, as illustrated in the standard ISO 5182: 2008 [124]. The most proper electrode materials are higher resistance alloys of nickel, alloy of chopium-chromium, beryllium and / or cobalt can be used for higher strength steels and stainless steels.

3.5. WELD GEOMETRY (NUGGET GEOMETRY)

The weld nugget or FZ size D that can be defined as the width of the weld nugget at the interface of the sheet in the longitudinal direction is considered the most significant element to determine the quality of spot welds [125,126]. The fusion area size that controls the total bonding zone of the joint is governed by the heat input that in turn controlled by the welding elements generally electrode force, welding time and welding current. Penetration depth can be defined as the width of melted area through the thickness direction void in FZ. Void formation in weld nugget have two sources which are expulsion and solidification shrinkage [127]. The explosion leads to the lack of materials in order to fill the weld nugget upon solidification. The electrode force determines the formation of void after the cooling. If the electrode force is adequately high, there will not be cavities or pores left after the cooling.

The clamping load impact on the growth of nugget are observed in the range of the loading from 1.5 kN to 5.5 kN. Figure 3.19 shows the relationship of the nugget diameter and penetration rate related to the loading magnitude. There are two conflicting effects are cause when increase the clamping load: increasing the heated contact region and spreading the current density. The greatest value of the nugget diameter is specified at the clamping load 3.5 kN. In the same figure (Figure 3.19), it is found that the nugget penetration rate tends to decrease through an inflection point at the clamping load of 3.5 kN. The magnitude of the current density may be a prevailing element of the nugget penetration at the vertical direction. Whereas the melting area is governed to inside the sheet thickness by the cooling of the electrode [128].

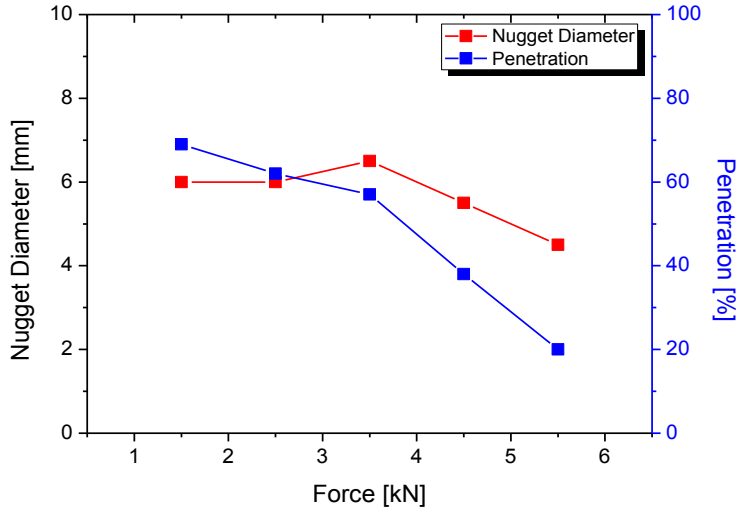

Figure 3.19. Effect of the clamping load on the nugget formation [172].

The effect of the input current on the growth of nugget are observed in the range of current from 5kA to 7 kA. Figure 3.20 shows the relationship between the nugget diameter and the penetration rate related to the input current. Increasing the input current offers monotonic increase to both nugget diameter and penetration rate. Nevertheless, softening of the steel sheet is the reason behind the expansion of the contact region and the decrease of the current density. Thus, nugget size increase is saturated in the area of the input current of more than 6kA [128].

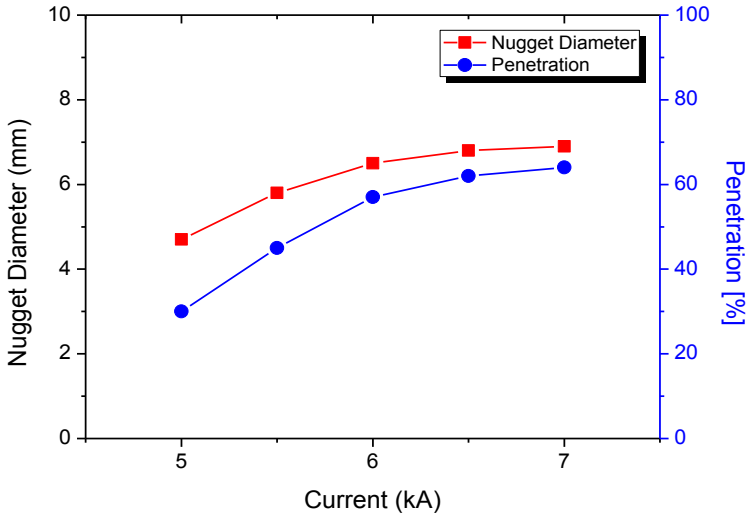

Figure 3.20. Effect of the input current on the nugget formation [172].

3.5.1. Penetration and Indentation in RSW of DP Steel

The depth of penetration can be defined as the melted area width through the thickness direction. The penetration is considered the other side of weld quality where it describes the degree of thickness melting through the welding process. The small penetration may point to inadequate heating and refer to the cold weld. Generally, the great penetration is desired. However, since the amount of heating determines the penetration, the large penetration cause softening of the materials and possible large indentation by the electrodes. In general, the penetrating requirements are loose, but the huge penetration will be accepted if it will not generate huge deformation [22].

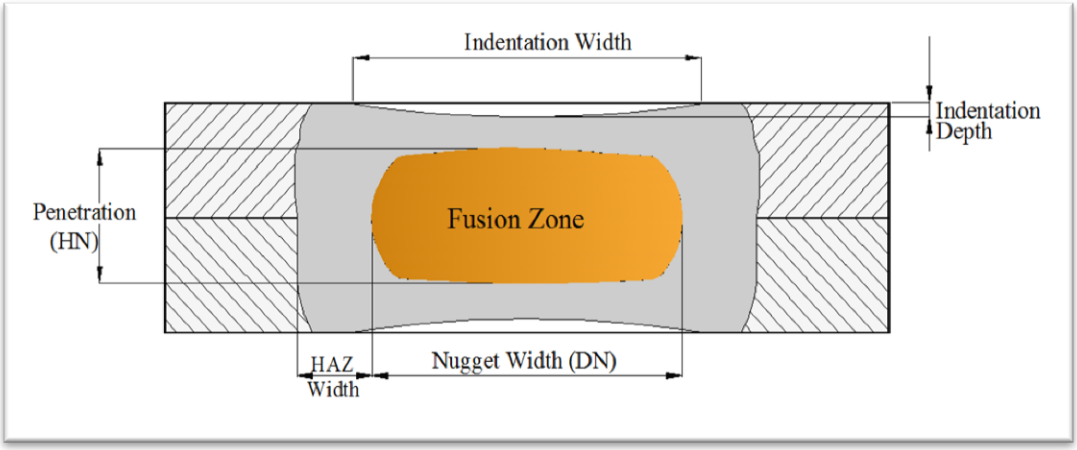

Figure 3.21. Penetration in the RSW [151, 152].

As we stated earlier, the most significant factor of weld ability is the lifetime of electrode which means the number of welds that can be created within the set margins. Nucleus diameters (DN) effect, height of the nucleus (HN) electrode indentation were measured and the nucleus size ratios, (HN / ND) were measured too. The specimens size of an impact and effect nucleus size on tensile shear strength and micro hardness have been researched by placing and employing the results gotten in the associated diagram Figure 3.21 [102,129]. The diameter of the nucleus, dn or height of nuclear, hn is not adequate to simplify the impact of the weld core on the tensile shear strength of the joint. Thus, the Nucleus ratio, hn / dn can be adjusted for this reason [131,132]. An example of table with least nugget diameter for ranges of sheet thickness and for various applications is clarified in Table 3.2. The

indentation depth of electrode indentation (see Figure 3.22), that make and impact on the mechanical properties of the spot welds, depends on the temperature of electrode/ sheet interface and pressure of electrode. The temperature of electrode/sheet interface is increased when increase the heat input which in turn increasing the degree of plastic deformation that can happen in the sheet surface under the pressure of electrode [133]. It is necessary to control the welding parameters and electrode geometry in order to keep the indentation depth at the least level. Hardness and material properties of FZ and HAZ: the weld thermal cycle interaction, the initial microstructure of the BM and chemical composition control the Hardness and material properties of FZ and HAZ. HAZ size: the heat transfer from FZ into the surrounds determines the size of HAZ.

Many researchers mentioned that size of HAZ can make an impact on the ductility of the spot welded joints [106]. The preliminary microstructure of the BM, chemical composition and interaction of weld thermal cycle control the hardness and material properties of FZ and HAZ.

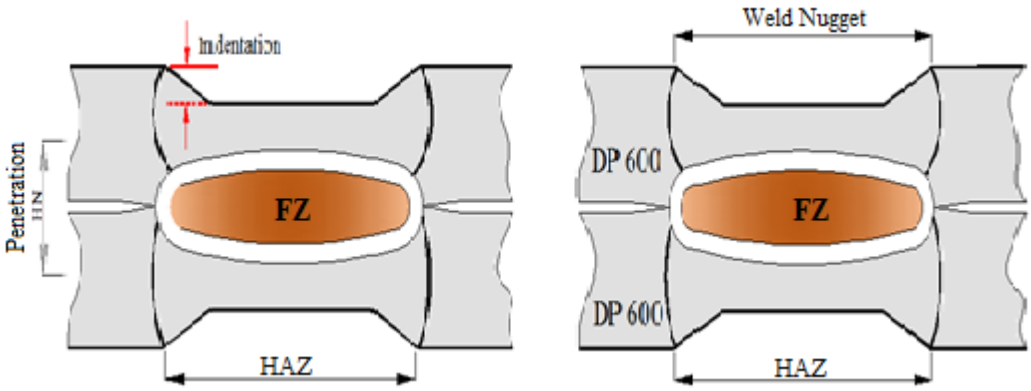

Figure 3. 22. Indentation in The Rsw [115].

Table 3.2. The minimum Nugget Diameter at different sheet thickness [115].

	Minimum nugget diameter [mm]	
Sheet thickness [mm]	**Category A & B**	**Category C**
≥ 0.50 < 0.60	2.5	2.2
≥ 0,60 < 0,70	2.8	2.4
≥ 0,70 < 0,85	3.0	2.7
≥ 0,85 < 1,10	3.5	3.0
≥ 1,10 < 1,25	3,9	3,3
≥ 1,25 < 1,50	4,1	3,5
≥ 1,50 < 1,60	4,3	3,7
≥ 1,60 < 1,75	4,4	3,8
≥ 1,75 ≤ 1,80	4,7	4,0
> 1,80 ≤ 2,00	5,0	4,2
> 2,00 ≤ 2,25	5,3	4,5
> 2,25 ≤ 2,50	5,5	4,8
> 2,50 ≤ 3,00	6,0	5,2

3.6. MICROSTRUCTURE

Through the resistance spot welding, many changes occur in the metallurgical and mechanical properties of the weld metal and the heat affected zone (HAZ). Study these change are significant for strength, safety and protection to the welded joints [134].

The microstructure of the metal after welding is different than the microstructure of the metal before the welding process and this is the key point to determine the formability and strength of the materials. After the welding, three areas are identified and the original microstructure is destroyed as shown in Figure 3.23 [135].

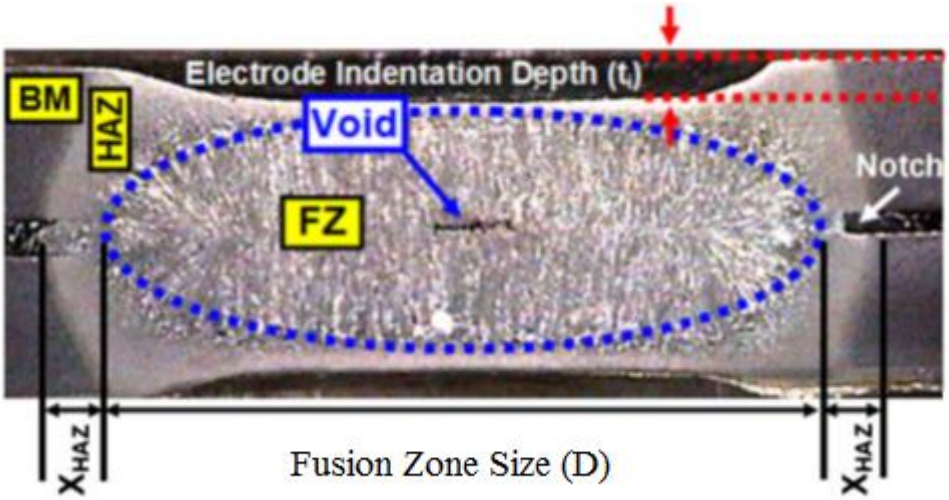

Figure 3.23. Typical macrostructure of resistance spot welds showing the weld physical attributes including FZ size D, electrode indentation depth ti and the width of HAZ XHAZ. The presence of a natural notch at the sheet/sheet interface significantly affects the m behaviour of resistance spot welds [3].

- The weld nugget,
- The heat affected zone (HAZ),
- Unaffected base material.

The weld nugget comprises of the materials which has been melted through the welding. After the welding, the material will be solidified and then undergoes phase transformations. According to the chemical composition of the material, two routes can be recognized [136,137]:

- Liquid, delta ferrite, austenite, martensite and/or bainite,
- Liquid, austenite, martensite and/or bainite.

The chemical composition and cooling rate determine the resulted microstructural composition whether it will be bainitic, martensitic or a mixture of both. At low cooling ratios and/or lower levels of alloying, the resulted microstructure will be typically bainitic. At increased alloying levels (when carbon is considered the main element in alloying industry) and adequately high cooling rates, the resulted microstructure will be mostly martensitic. It is likely that the weld nugget includes some reserved austenite after cooling (particularly in TRIP steels, which after all

have been allowed to include reserved austenite) [138]. Despite the microstructural composition of the weld nugget after the welding, a significant impact of welding which is the orientation of grains and size, determined mainly by the trajectory of solidification and the temperature inclines through the cooling as shown in Figure 3.24. It must be noted that voids in the center line are caused by the shrinkage because of the solidification and cooling.

Figure 3.24. Micrograph of Ristenace Spot Welding joint of 3 sheets. The grains direction in the weld nugget extends along with cooling lines vertically. The cooling is directed to the cooled electrode by water horizontally along with the medium line wher the cooling is directed to the su rounding material [158].

Figure 3.25 clarifies that there is no evidence to the microstructures of BM in the FZ and HAZ areas. The microstructures of the FZ is less heterogeneous than the microstructure of the HAZs. The BM microstructures of the steels experienced important microstructural changes in the HAZs joints through RSW process. In order to analyze the microstructures of the HAZ, it is separated into the outer heat-affected zone (OHAZ), the center heat affected zone (CHAZ) and the inner heat-affected zone (IHAZ). As shown in Figure 3.26 that OHAZ microstructures include of tempered bainite and martensite in a ferrite matrix. The bainite formation in the OHAZs may be attributed to the existence of partial re-austenitization through the resistance spot welding process. It is supposed that the temperature in the OHAZs surpassed A1. The microstructures of IHAZ and CHAZ comprise of martensite– austenite (M–A), bainite and martensite constituents (small dark phases) or reserved austenite. These microstructures refer that complete re-austenization over A3 that is the temperature at which ferrite changes to austenite on heating, arose inside the IHAZs and CHAZs.

The formation of M–A through spot welding process (Fig. 3.25 b & c) constituents may be attributed to the dividing of carbon through the transformation to bainite and the post-transformation of carbon-enriched austenite [139]. In addition, bainite and martensite phases are coarser and the fraction of volume for these phases in CHAZs are higher in than in the OHAZs. This is because the highest temperatures in the CHAZ were higher than in the OHAZ. The CHAZ on the DP600 side includes a reasonably coarser prior austenite grains (PAGs) as shown in Figure 3.25. b. This may be caused by the higher temperature on the DP600 side. Moreover, the PAGs in the IHAZs were considerably coarser than in the CHAZs as the highest temperature in the CHAZ was less than in IHAZ. When increase the size of PAG, the structures of bainitic and martensitic in the IHAZ become coarser. As in the CHAZ, the IHAZ on the DP600 contains coarser PAGs to the highest temperature accomplished in the IHAZ of the DP600. This is due to the higher thermal factor of DP600 steel. The FZ microstructure shows a cast structure that is melted through the resistance spot welding process and then is solidified involves of about full columnar coarse lath martensite owing to the columnar and directional solidification from the fusion boundary to the center as clarified in Figure 3.25 d. Formation of Martensite in the FZ is attributed to the inherently high cooling ratio of the resistance spot-welding process owing to the emergence of water cooled copper electrodes and their quenching impact in addition to a short welding cycle. Furthermore, DP steels involves of relatively higher quantities of carbon alloy factors that make the coarse martensite microstructures formation in the FZ in similar steels easier [140].

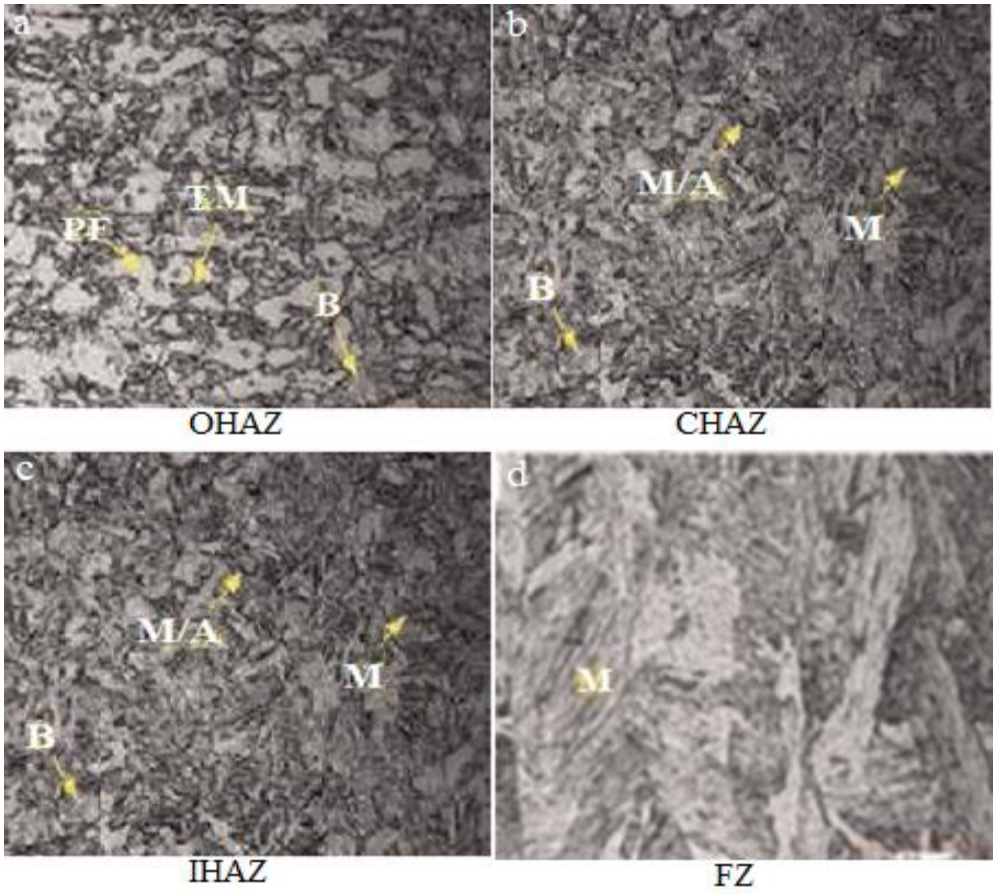

Figure 3.25. The distinctive microstructure of a resistance spot-welded DP600 steel joint where the micrographs locations a to d are indicated: a) DP600 OHAZ; b) DP600 CHAZ; c) DP600 IHAZ; d) FZ. PF: polygonal ferrite; M: martensite; TM: tempered mart ensite; B: bainite; M/A: martensite–austenite [141].

The size of HAZs is narrowed and welding current is decreased. When increase the welding current, HAZs widths on the DP1000 side and on the DP600 side have been decreased by about 43%. The microstructures of FZ for the invented joints with lower welding current are generally composed of coarse martensite with a columnar structure. In terms of the welding current of up to 10 kA, the columnar martensite particles in the FZ became experienced increase in welding current. When the welding current is 10 kA, the columnar martensite grains transform to nearly equated grains.

3.7. MECHANICAL PROPERTIES OF RSW JUNCTION

The most used joining process for DP steel sheets in car structure industry is the Resistance Spot Welding. The microstructural changes occur in the resistance spot-welded joints are highly depend on the welding elements, the base metal (BM) chemistry and the primary microstructure of the BM. the properties of strength and failure for resistance spot welds are functions of the sheet thickness and the harnesses of the weld, the nugget size (NS) and heat-affected zone (HAZ). [142,143]. The quality of resistance spot welding and mechanical behavior depend on the adjacent HAZ that directly affect the crashworthiness and durability of vehicle and the microstructural changes that happen in the weld nugget [144,145]. Pouranvari et al. [146], mentioned that there are three measures are used in order to measure the quality assessment of the resistance spot welds comprising the failure mode, the mechanical properties and the physical weld characteristics (e.g. the electrode indentation, the weld NS and the microstructure of weld area). As perceived that the DP steel has a high ultimate tensile strength (UTS) in the range of (500 to 1200) MPa and the total elongation in the range of (12 ~ 34%) that depend on fractions of bainite, martensite and ferrite [32,147,148]. Prominently, the mechanical properties of (DP and TRIP) steels have higher fatigue strength than equivalent traditional HSLA steels. These benefits reduce these steels ultimate materials for the automotive associated sheet that form functions and operations [149].

3.7.1. Tensile Load Bearing Capacity

Tensile shear strength of welds increases proportionally when the BM tensile strength increases. Instead, cross tension increases when the base is increased. It is noticed that through the service, spot welds in car body structures can expose to both shear loading because of the relative movement or rotation of the tensile loading and neighboring sheets because of the extrication forces applied between the neighboring sheets in the direction normal to the sheets [150,151]. The most frequently used test to assess the mechanical behavior of spot weld are coach peel (CP), cross tension (CT) and the tensile shear (TS) [152]. The diagram representation of the stress state and sample geometry for these loading conditions are shown in Figure 3.26. The

tensile shear (TS), cross tension (CT) and coach peel represent the mainly shear loading (i.e. shear force to the weld interface),56 tensile loading (i.e. normal force to the sheet/sheet interface) [153] and tensile loading persuaded by bending momentum conditions [151] correspondingly.

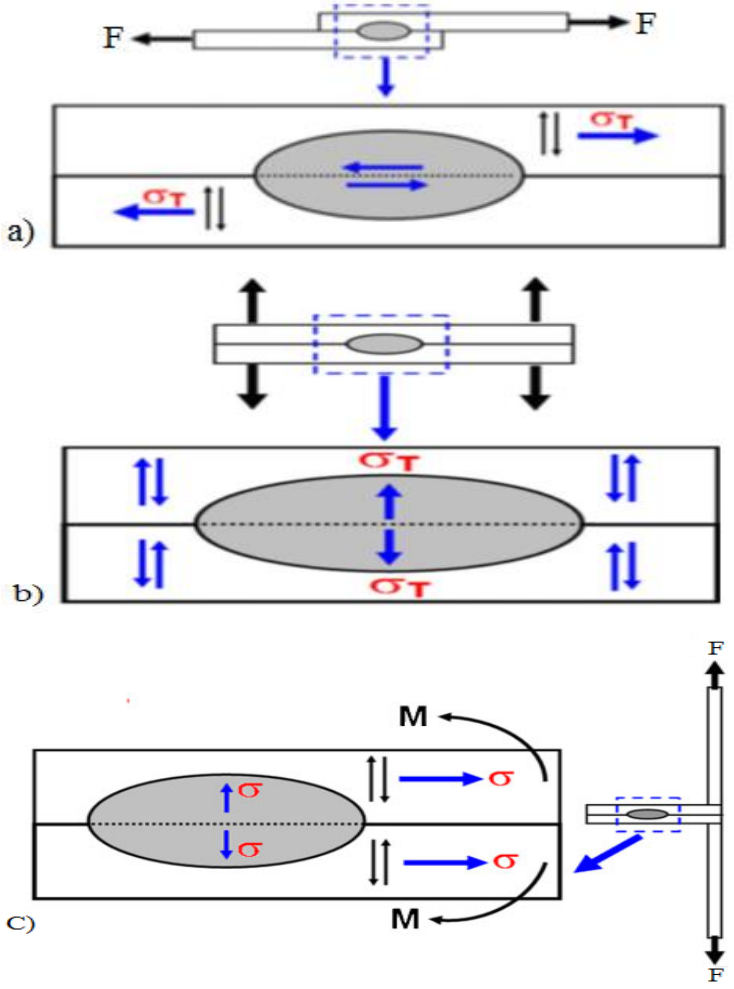

Figure 3.26. Simple models describe the stress distribution at the interface and circumference of a weld nugget through a) TS,[96] b) CT and c) CP tests [200]

3.7.2. Tensile Shear Failure Behavior

In DP600 steels, the interfacial fracture (IF) mode for the weld button has been perceived, particularly with thicker gauges [154-156]. Peterson et al. [156], studied the mechanical properties of weld joints vs. the modes of fracture in the form of lack of fusion, interfacial fracture, thickness fracture and button pull-out. Joaquin et al.

mentioned that the shrinkage voids are one of the main reasons of the interfacial fracture from fatigue tests and tensile shear static. Milititsky et al. [156] performed the tensile shear tests of DP600 samples and perceived solidification cracks and shrinkage. The Figure 3.28 presents the schematic explanation of the failure mode types such as Pullout failure (PF), interfacial failure (IF) and Partial interfacial failure (P-IF). IF spreads beside the centerline of welding and pledgees from the notch between two sheets. Whereas for PF failure which is usually raised at the HAZ or BM that depends on the minimum hardness location with complete withdrawal of weld nugget from one sheet. The preliminary failure location of P-IF is the same as IF. It conveys toward the sheet thickness direction as test load increases. P-IF is frequently convoyed with exclusion existence as clarified in Figure 3.27.

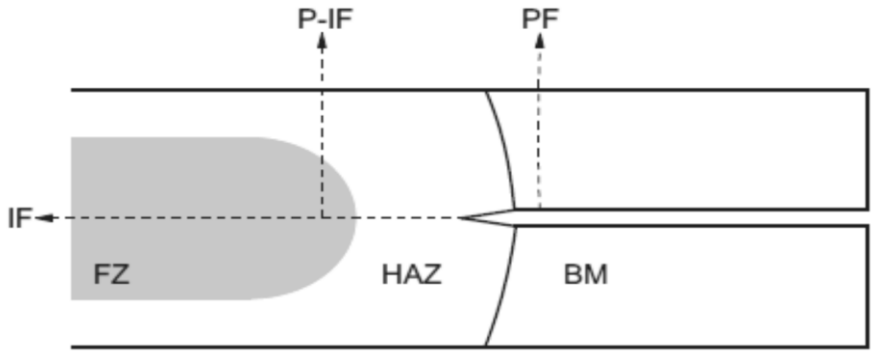

Figure 3.27. Diagram explanation of three distinctive failure modes [177].

The ineffective approaches of resistance spot welding steel are the pull-out of the button, the partial pull-out, and the relational fracture, where the pull-out button is the best, and more energy is engaged through the mode [157]. Zhang et al. [158] proposes that the ineffective approach is basically relied on the size of the fusion area and that this success is predictable to arise under a pull approach as the size of the fusion area increases and increases the least number of spot-spotting to guarantee that the fracture moves out and is directed according to the following relationship:

$$D = K\sqrt{t} \tag{3.2}$$

Where D represents the diameter of the weld nugget in mm, K represents the constant-dependent process ranging from (3 to 6), and t represents the minimum sheet thickness in the mm [152,159].

3.7.3. Stroke Displacement

Figure 2.28 shows a distinctive load displacement spot welding though the tensile shear loading condition. The following parameters can be extracted from the curve of load displacement in order to describe the mechanical behavior of spot welding:

- Peak load Pmax
- Failure energy Wmax at peak load
- Elongation at the peak load Lmax

Wmax is a measure of weld energy absorption competence, and its higher value determines the increase in weld performance consistency against effect loads for example accidents. Lmax is a measure of the joint ductility.

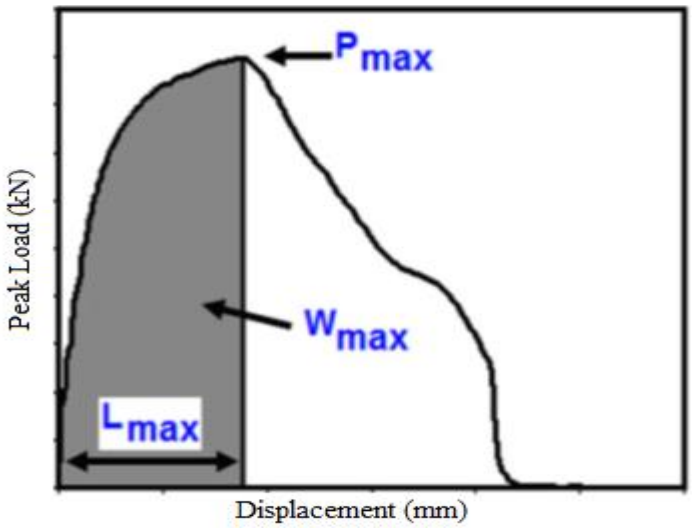

Figure 3.28. Distinctive load–displacement curve thorugh the tensile strength test with the extracted parameters: Wmax: energy absorption; Lmax: elongation at peak load Pmax: peak load; [3].

3.7.4. Hardness Profile

The hardness features of the spot welds is playing a significant role in their mechanical properties and failure mode. Figure 3.29. explains graphic illustration of hardness profiles of resistance spot welds created on normal automotive steels representing three distinct areas conforming to the FZ, which experiences solidification and melting, the HAZ, alongside the FZ that frequently practices solid state stage changes but no melting and natural BM. [160], Fast heating and cooling tempted by resistance spot welding thermal cycles can considerably change the microstructure resulting in an important differences in hardness profile.

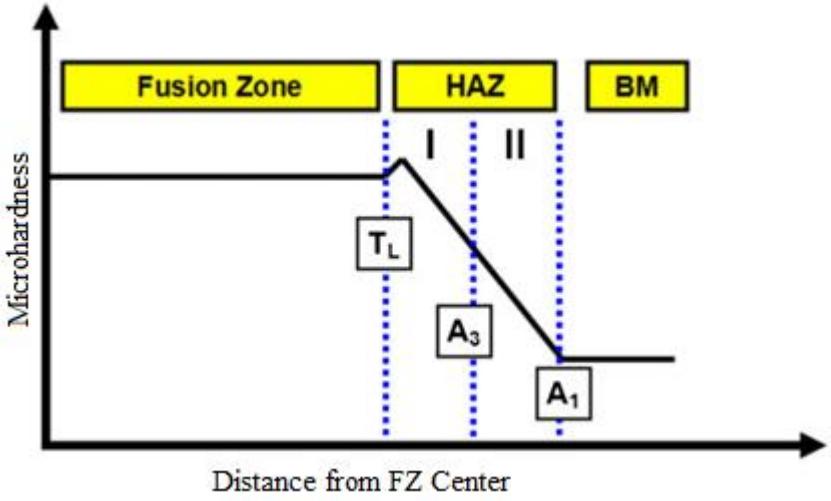

Figure 3.29. Diagram of desntinctive hardness profile of resistance spot welds made [3].

PART 4

EXPERIMENTAL AND THEORETICAL STUDIES (METHODS AND ANALYSIS)

4.1. MATERIALS

Commercial DP600 steel parts is available in sheet metal layers sized in 250mmx250mmx1mm. have been obtained from TOFAŞ AŞ (Bursa/TURKEY) for spot welding experiments and applications. 230VAC heat input, 50Hz frequency and 2500VA power capacity from the SPECTROLAB model LAVFA18A were utilized to determine the chemical composition. The chemical composition of DP 600 sheet steel used in this studied have been given at Table 4.1 and its microstructure have been shown in Figure 4.1. In order to summarize the bulk chemistry of the materials and make further comparison; the carbon equivalent (CE) has been calculated by the yse of Yurioka's formula, the equipment used for microstructure evaluations (Optical microscopy).

Table 4.1. Chemical composition of DP600 Steel (wt.%).

Material	C	Si	Mn	S	Cr	Ni	Al	Ti	V	Sn	Fe
DP 600	0.077	0.253	1.86	0.006	0.177	0.012	0.127	0.002	0.004	0.006	97.472

The welded samples were cut in a plane that was considered vertical to the axis of penetration and then equipped for the metallographic examination on the cross sections of the penetrations. Transverse-transition region views of RSW samples were prepared by following the standard metallographic procedure (grinding and polishing). A sample was mounted, on the ground, Polished samples were exposed to short time etching with 2% nital solution (2% nitric acid + 98% methanol) in order to evaluate the phases. Microstructure analysis has been conducted by the use of Nikon optical microscope.

Microhardness measurements were performed parallel to the axis along the weld metal and ITAB using a Qness Vickers hardness tester with a load of 0.2 kg for 10 seconds.

Figure 4.1. Microstructure view of DP600 steel.

4.2. WELDABILITY OF MATERIALS USED IN EXPERIMENTAL STUDY

The weldability of the steels that are utilized in this research study is determined by the Graville diagram, through which the approach makes use of the carbon equivalent formula (4.1).

The carbon equivalent numbers for the DP600 steels were calculated. It was determined as (**0.46548**) for the DP steels.

$$CE = \%\,C + \frac{Mn+Si}{6} + \frac{Cr+Mo+V}{5} + \frac{Cu+Ni}{15} \quad (4.1)$$

The % carbon content in the Y axis and the determined carbon equivalent number in the X axis for the DP600 steels were assessed in the diagram found in Figure 4.2. The junction point (signed red star) represented the weldability of the steels which were utilized in this research study. Conclusively, it is figured-out that they were the difficult weldable materials.

In order to summarize the bulk chemistry of the materials and make further comparison; the carbon equivalent (*CE*) has been calculated by Equation 4.1. using Yurioka's formula [161]. Some studies examined the mechanical properties of the RSW junction of DP steel. One of these was making by Ml et al. [30], they estimated and reported that carbon equivalents increase the hardness of the weld area, resulting in a very strong correlation between chemical composition and mechanical properties.

The volume fraction of martensite (*fm*) was obtained as 23 %*fm* and remain (*ff*)by standard metallographic image analysis. By assuming that the DP microstructure is a mixture of two phases i.e., ferrite and martensite of nonequal density, calculation of the carbon content within the martensite was performed [162].

$$|\%C|m = \frac{|\%C|a - |\%C|f(1-fm)}{fm} \tag{4.2}$$

where *|%C|m*, *|%C|f* and *|%C|a* are carbon contents of martensite, ferrite and bulk alloy, respectively, and *fm* is the volume fraction of martensite.

By assuming a carbon content of 0.005% in ferrite at room temperature [163], by using the bulk carbon content; the martensite carbon content for all DP steels has been evaluated using equation 4.2. It must be mentioned that the carbon content within martensite increases while decreasing the volume fraction of martensite. For instance, this indicates that higher strength steel is characterized by containing low carbon martensite islands.

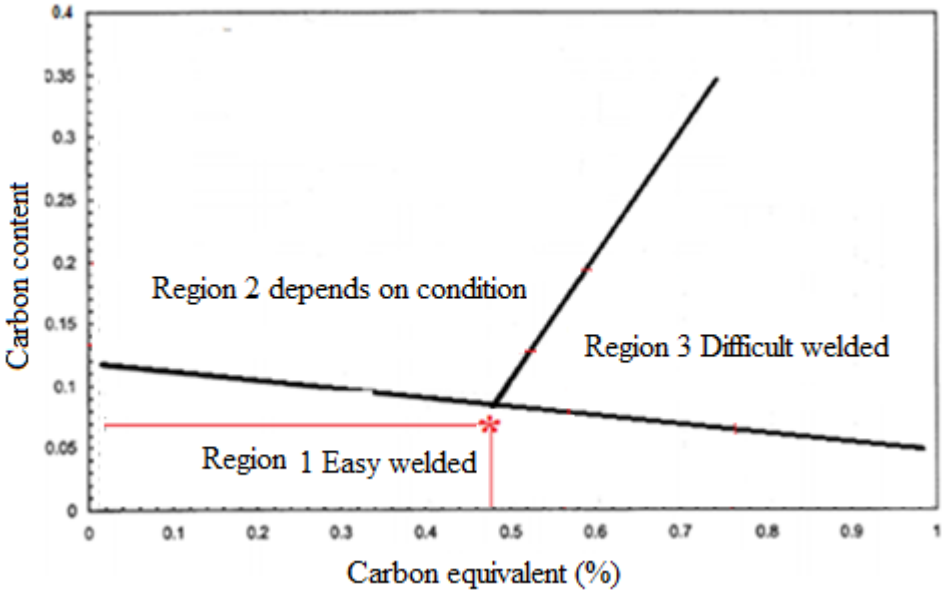

Figure 4.2. The weldability of the steels assessed by Graville diagram.

The region (1) in the diagram was placed in a very good weldable region, where the steels were having low carbon content and with the low hardenability hence, the steel was insensitive for the hydrogen cracking. An opposite postion and observation to the region of (1), was in the region of (3) were the steel presents crack sensetive structure during the welding process due to high carbon content in the composition and the high hardenability hence, the steels in this region were known to be bad weldability.

Hence, the steels that were postioned in region (2) were known to have, had some level of conditional weldable. Even through the high carbon content they showed and revealed the low hardenability this indicated therefore that; they could have been avoided through the hydrogen cracking risk and through the utilization of someof the controlled heat input or the controlled cooling rate [164].

4.3. SAMPLES PART OF RESISTANCE SPOT WELDING

Resistance welding operation of this study in the experimental study, commercial DP 600 sheet steel having 1 mm Dual phase two-dimensional steel was used as base metal. The dimensions of the base metal were 100 mm x 30 mm x 1.0 mm thickness. The samples were designed according to EN ISO 14273 standard for the RSW

operation. The RSW samples were cut to dimensions of 100mmx30mmx1mm as in Figure 4.3 and a sample photograph in Figure 4.4 through the shearing process from the 250mmx250mm sheets. The samples were overlapped for 30 mm. With the consequent size of RSW, overlapped samples were 170 mm. RSW was carried out through the utilization of three different welding currents, 4KA, 6KA and 8kA, two different time 15 and 25 cycles and three different electrode pressures of 3.5, 4.5 and 5.5 bar.

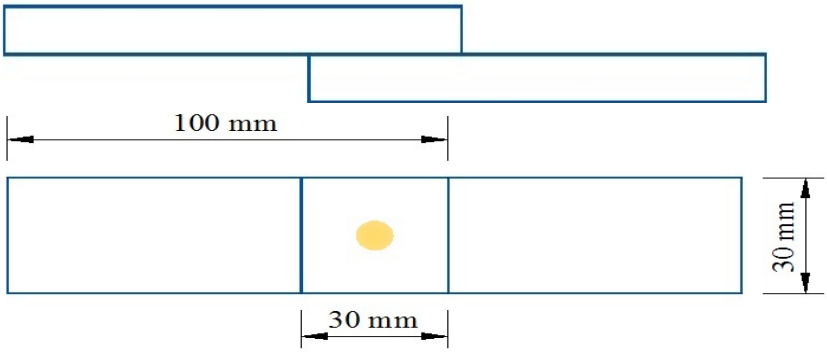

Figure 4.3. Geometry of the sample.

Figure 4.4. RSW sample image.

4.4. RESISTANCE SPOT WELDING PROCESS

The Resistance Spot Welding in this study is made-up of the welding machine, the air compressor for the hydro-pneumatic force and the water cooled spherical with the shape of Cu-Cr electrodes. The detailed information will be mentioned about the equipment will be given below.

4.4.1. Resistance Spot Welding Machine

This study, Spot welding can be operated technically manually, to robotic or with a dedicated spot-welded machine [90,91]. The electrode force and the control of the welding time automatically and immediately. The desired low voltage (5-20 V) and current high intensity (2000–15,000A) is achieved for the welding process from transformations and the pressure is derived from air devices, mechanic and hydraulic [100-102].

The experiments involved the use of an on electric resistance spot welding machine with 120 KVA capacities and a single lever application mechanism. The electrode force was always measured and managed during the experiments. Furthermore, the current welding values have been measured and managed computed by the application of current transformers arranged at upper welding machine and ampere meters. The welding time, holding time and clamping time were changed automatically through the machine's electronic devices [102,165]. The electrodes and electrically placed materials were evenly balanced and predicted to be stable, the contact surface of the electrode was 8.0 mm and a copper alloy was used in the experiment. The resistance welding was obtained in Baykal SPP60 installation. This installation is an AC machine for spot welding as seen in Figure 4.5 fitted with a device for the pneumatic control of the AC phase transfer. The Resistance spot welding machine was equipped with a device for the pneumatic control of the phase shift of the AC current their properties was mentioned in table 4.2. Before their joining, the surface of the work pieces was cleaned and thereafter the welded utilized conical water-cooled Cu–Cr alloy electrodes. The contact surface diameter of the electrode is 8mm [166].

Figure 4.5. Spot welding machine used in this study.

Table 4.2. Spot welding machine properties.

Machine name	**Baykal SPP60 type spot welding machine**
Machine power	60 kW
Supply voltage	380 V (3 phase)
Air pressure feeding the spot arms	6 Bar
Cooling water flow of welding machine	20-25 liter/minute
Cooling Water Flow of Electrodes	4 liter/minute
Electrode diameter	8 mm
Electrode material	Commercial purity Cu-Cr electrodes with truncated conical tip

In Resistance Spot Welding machine to join the Samples in order to fix tensile shear sample properly, The wooden samples holders the molding for joining designed and then manufactured was utilized to readjust the samples during the welding, to avoid axis misalignment and to protect and readjust the sparks from spattering as seam the molding in Figure 4.6. Three-resistance spot welded samples were created singularly for each experiment parameter. The water-cooling system of the electrodes was kept under specific constant water control because of the excess of the heat input.

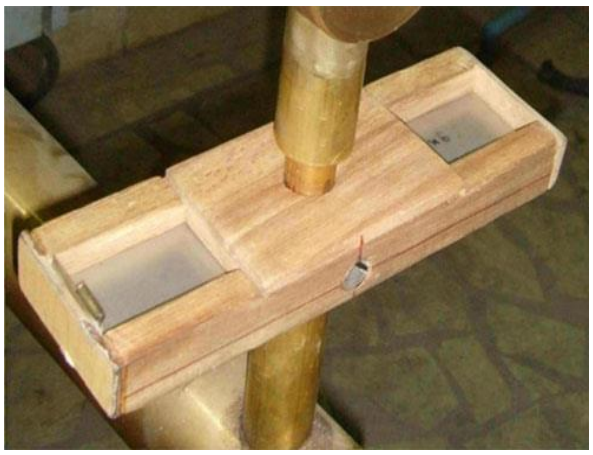

Figure 4.6. Fixture welding sample.

4.4.2. Resistance Spot Welding Parameters

Some of the descriptions about resistance spot welding parameters have been described above. As shown in Figure 4.7 that the weld process is described by force, current and time. At the following parts of this chapter, the whole machine parameters and their effect on spot weld will be discussed. The process of accomplishing and obtaining an excellent weld quality fundamentally begins with a great process design and created that reduces the variables experienced during welding. It must be mentioned that the most relevant welding parameters in the electrical resistance spot welding are time, current intensity and electrode force. An electronically controlled unit is utilized in welding machines in order to acquire the variables of welding. It is not possible to achieve the preferred nucleus diameter without the repositioning of welding current intensity versus welding time excellently. Once the time is held short, the nucleus diameter automatically reduces. Conversely, once it is held longer the amount of molten metal increases and the fused metal spurts out and therefore the strength of welding joint reduces [102]. The parameter values have been chosen in a manner which allows, the minimum nugget diameter of $4\times\sqrt{t}$, where t is the sheet thickness, which was achieved and accomplish after resistance spot welding. Table 4.3 shows the parameters used in this thesis. The weld periods are welded control of 15 cycles, Squeezing time 30, welded on time 15 & 25 Cycles, weld off 20 cycles, holding time 15 cycles and off time 20 cycles with electrode diameter 8 mm Tip, electrode force (F) used with different parameters such

as 3.5, 4.5 and 5.5 bar and the electric current (I) as well as different parameters 4, 6 and 8 KA. select and change these parameters according to xiaodong et. al., Dawel Zhao et. al. and R. Raoelison et. al. RSW parameters utilized in this study are presented in Table 4.3. [38,156]. The time unit is cycle-based (1cycle=0.02s). The RSW adjusting parameters and process steps are shown in Figure 4.7 and 4.8 respectively.

Figure 4.7. Adjusting the parameters.

Table 4.3. Welding parameters using in this study.

Electrode pressure (bar)	Welding current (kA)	Welding time Cycle	Electrode diameter (mm)	Down Electrode Cycle	Squeezing time Cycle	Hold time Cycle
3.5	4, 6 & 8	15 - 25 15 - 25 15 - 25	8	15	30	15
4.5	4, 6 & 8	15 - 25 15 – 25 15 – 25	8	15	30	15
5.5	4, 6 & 8	15 - 25 15 - 25 15 - 25	8	15	30	15

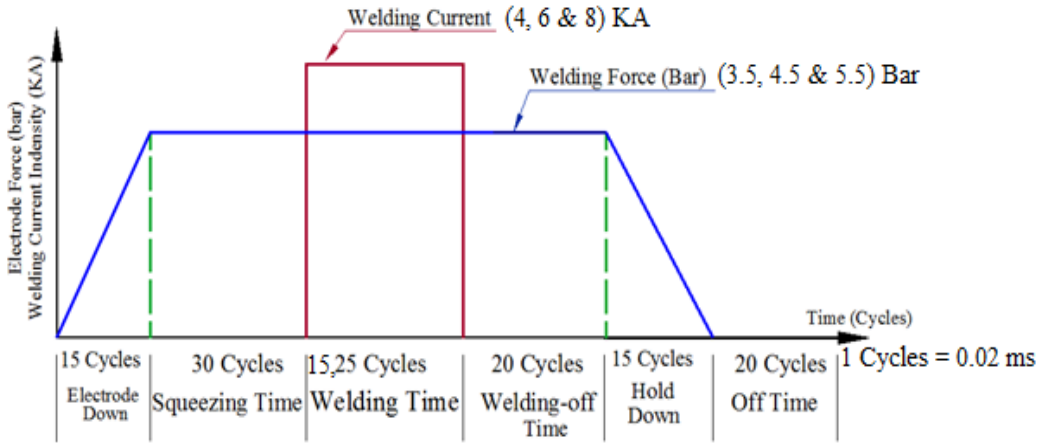

Figure 4.8. RSW process steps.

4.5. MECHANICAL TESTING

The behavior of all the welded samples were under the static load which was determined and predicted by the tensile shear tests. In addition, the couples welded in the different welding parameters were carried out on the hardness measurement for an assessment of the hardness distribution in the Base metal, HAZ and the Weld Nugget. The mechanical test applied for the welded sample was explained in the details that are presented in the following sections.

4.5.1. Tensile Shear Test

In Resistance Spot Welding and conditions that determine the mechanical properties of the weldment, of the tensile shear test samples for each welding parameters were prepared according to DIN EN ISO 14272 standards. The tensile shear test samples were tested by the Schimadzu trademark tensile test machine in Karabük University, The Technology Faculty mechanic test laboratory Figure 4.9. The tensile shear test was carried out at the (2 mm/min) strain rate.

Tensile shear test parameters are the 4kA, 6kA and 8kA welding currents, and 3.5bar to 5.5bar electrode pressures. The samples were tested for each of the experimental parameters and the arithmetic means of these values were calculated. In addition, tensile test was applied to the base material for comparison. In addition to the tensile

shear data which has been generally utilized in the literature, there is now a reference to the parts of the joining made on the nugget welding profile shown in Figure 4.9. In this way, shear data are also considered as stress data. RSW samples had 1mm thickness, 30mm width and 110mm gauge length. The crosshead speed value utilized for the tensile shear test was 2mm/min [166]. During tensile shear tests, maximum tensile shear force value which allows the fracture to occur was evaluated and examined to assess the tensile shear load bearing capacity characteristics of the joint [88]. Base material was also subjected to tensile test. The effects of electrode pressure and welding current on tensile shear force were studied. Authors in [87] reported that micro voids of large size were formed in the low electrode forces of the RSW process. It was observed that nugget solidifies before electrodes were moved away from the weld region. Since the weld nugget was not sufficiently suppressed at relatively lower electrode forces, shrinkage voids were formed because of the low stress during this time [87]. In addition to other approaches, and because of increased electrode progression and clamping as the electrode force increases, the significant parts of the voids are closed, and fewer shrinkage voids occur in the welded area. Any increment of the welding current provides a capable level of current efficiency. Hence, the effectiveness of the welding processes increases [87,167]. Through this discovery, variations of the nugget diameter were investigated in the RSW joints which depended on the welding parameters. The strong relationship between the increment of maximum tensile shear force and the increment of the area been subjected to upcoming stress level was caused by the nugget diameter [5]. Figure 4.10. show Tensile test machine.

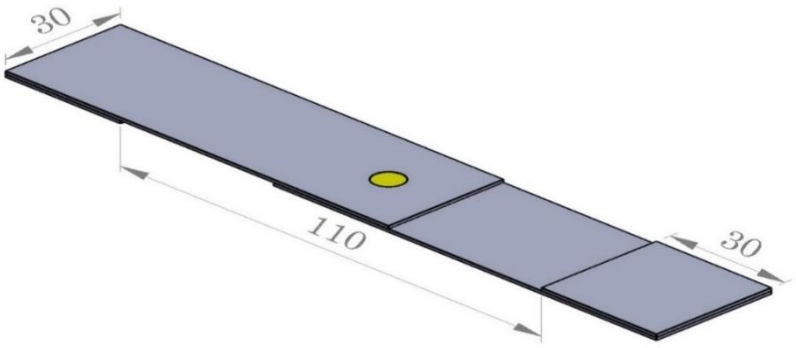

Figure 4.9. Tensile test dimensions.

The performance and quality of spot-welded resistance is very significant for safety design and durability of the vehicle [15]. M. Pradeep et al. [168] observed the process of welding RSW parameters, tensile strength values showing a weaker correlation with higher currents. Also X. Q. Zhang et al. subsequently acknowledged in [169] and noted that the effect of welding enabled welding strength beyond welding time. M. Pouranvari et al. [125] performed a systematic study of the effects of retention time, hardness and mechanical properties of the joints with different thickness levels. The welding force is indeed an important parameter because of the RSW because the force function ensures that there is an electrical contact and keeps the nugget visible from the discharge V. K. Prashanth Kumar et al. [170].

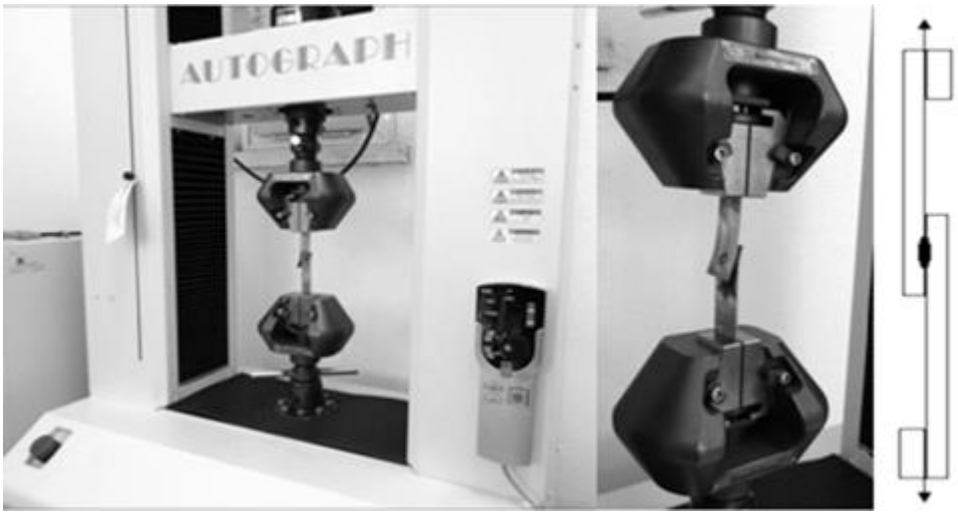

Figure 4.10. Tensile test machine used for testing.

4.5.2. Hardness Measurement

Typical micro-accuracy profile of DP600 steel, which showed important hardness. Because of to the high cooling rate and the high content of alloy elements in the steel in, the hardness may be able to vary by different fields of BM, HAZ and FZ of the samples. The type of Vickers microhardness carried out the examination. 5.903 N operating load samples and tested for all areas of BM, HAZ and FZ with all parameters previously used.

As seen and illustrated in Figure 4.11, The Vickers micro-hardness test using a QNEES type machine with indenter HV0.2 (1.961N) load and dwelling time of 10s calculated time, on the diagonal of the specimen cross section through which the involvement of the weld nugget, and the heat affected zone (HAZ) and that of the base metal used to achieve a diagonal hardness profile. The micro-hardness map using a 0.2 mm grid spacing release, the hardness delivery and individual hardness values in selected areas of the welding component [30,166].

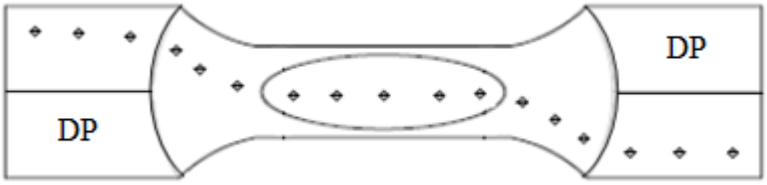

Figure 4.11. The hardness measurement on the diagonal of the weld cross section.

The hardness measurement was then conducted by the Vickers microhardness test machine. The macrograph of the microhardness test machine is also been presented in Figure 4.12.

Figure 4.12. The macrograph of Vickers microhardness test machine.

4.6. METALLOGRAPHIC AND MICROSTRUCTURAL EXAMINATIONS

The welded sample is cut into a plane perpendicular to the weld axis, and then a metallographic examination is prepared on the cross section of the weld. The samples were mounted on the ground, polished areas, and then etched (7-10s).

The commercial availability of DP600 steels was analyzed, As shown in Figure 4.13, the microstructure inspection of the samples was performed using a Nikon Optical DIC microscope and a Zeiss Ultra Plus scanning electron microscope (SEM). In addition, for the fracture surface of the tensile shear and transverse tensile test specimens examined by using SEM and EDS, they jointly analyze the system.

Figure 4.13. The equipment of SEM used for microstructure evaluations.

4.7. RESIDUAL STRESS

Residual stress measurement was conducted by cutting method. In this technique, strain gauge which is an electrical apparatus was used. Firstly, weld region of specimens was cleaned using degreaser, conditioner (acid) and neutralizer (base) respectively. Then strain gauge was glued on the middle of the weld part of specimens. Cutting process was applied to obtain strain values during the cutting via software (System 7000). At the end, Hooke law was applied utilizing elastic modulus

(190 GPa) of samples. So, residual stress was calculated for each sample. Figure 4.14. shows the strain gauge and preparation materials for residual stress measurement.

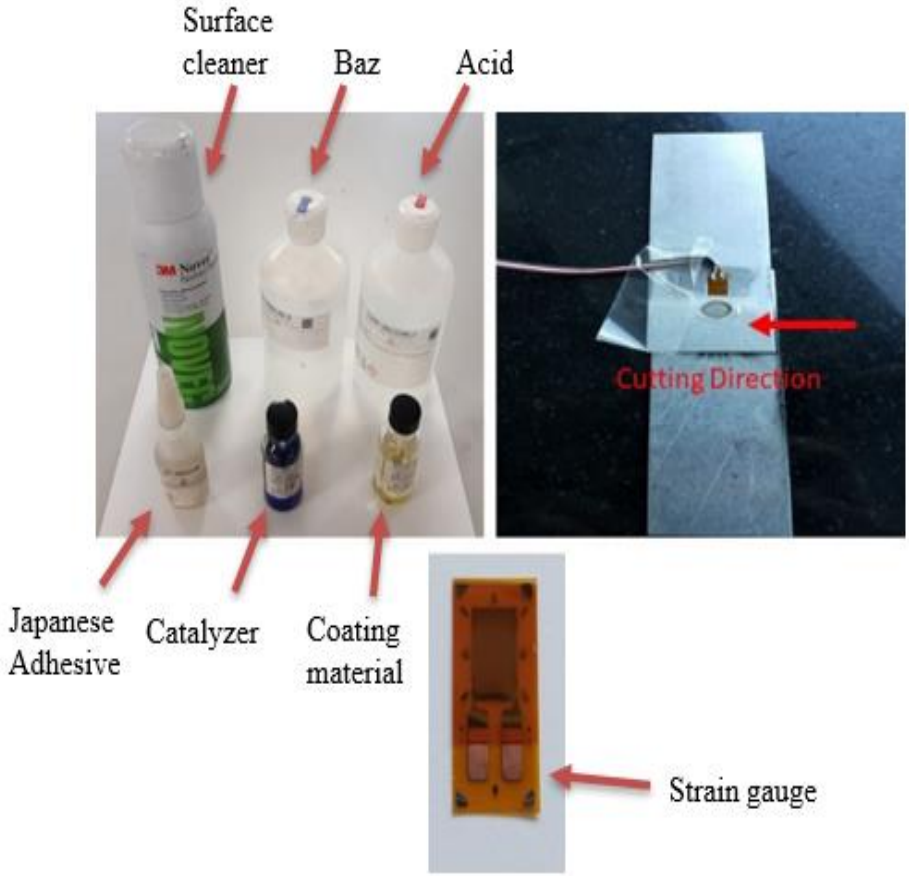

Figure 4.14. Residual stress measurement equipment of specimens**.**

PART 5

MODELING AND SIMULATION, OPTIMIZATION AND ITS TECHNIQUE OF RESISTANCE SPOT WELDING

Resistance spot welding is a technique which have been widely used in many industrial applications for sheet joining purposes. It requires modeling of complex interaction between electrical, mechanical, metallurgical, thermal and phenomena to the process and to get the optimum weld quality.

5.1. MODELING OF RSW

The goal behind the use of simulation software in our study is mainly to explain principles. The use of exact software package is not considered an important issue where it is possible to obtain same results by using similar software packages especially Simufact software, Comsol multi-physics or dedicated purpose-built solutions programmed in third generation programming languages including C++ or FORTRAN. At this study, we will focus on the interaction between the spot welding process and material which will be joined [171]. The simulation results will not highly differ if the mathematical rules and physical equations have been applied correctly conditioning that the model is designed correctly way, and the boundary conditions are applied in the correct way.

The studies on simulation of RSW in this thesis, MiniTab 17 (Taquchi and Anova), Simufact Software are used as the primary software packages. Simufact is the main solver that used in industry in order to simulate the engineering problems including welding range, weld growth curves, weld nugget diameter, and the impact of varying process parameter settings.

5.1.1. Governing Equation

The entire equations used in this study are based on the two-dimensional cylindrical coordinate system. The control equation to calculate the heat generation per unit volume is shown as [172]:

$$q = \frac{1}{R}[\nabla Q]^2 \quad (5.1)$$

Where q is the heat generation per unit, R is the electrical resistivity and V is the electrical potential.

5.2. CLASSIFICATION OF MODELING

5.2.1. Comsol Multiphysics Software

COMSOL Multiphysics software [173-175] was used in order to model the resistance spot welding process. A transient thermoelectrically- mechanical model was developed to model the resistance spot welding process. The structural process module enforces a fixed boundary constrains and force on the modeled geometry.

5.2.2. Simufact Software

A great number of metal working and metal processing production processes is covered by the Simufact software solution. The processes were grouped to application groups 'Forming', 'Joining", and 'Additive'. These three groups of application consist areas of application of our software products Simufact Forming, Simufact Welding, and Simufact Additive. Simufact software help automobile industrialists and their providers by the provision of operations simulation program to check the validity and optimization of joining processes for the construction of car bodies.

5.3. OPTIMIZATION OF RESISTANCE SPOT WELDING

The key step in Taguchi approach is the enhancement of process parameters in order to accomplish high quality without increase the cost. This due to that the process parameters may enhance the quality and the optimal operation which can be obtained from Taguchi approach is insensitive to the change of environmental circumstances and other noise factors. Taguchi approach provides benefits is that it enhances a mean performance property instead of the value within specific characteristics and therefore, it enhances the quality of product. In addition, the experimental design of Taguchi approach is clear, direct and easy apply on many engineering situations which make it strong and simple tool.

The existing experimental study is based on studying the effect and enhancement of welding parameters on the tensile shear strength in the Resistance Spot Welding process. The experimental studies have been performed under changing welding times, welding currents and electrode forces. The welding parameters settings have been determined by the use of Taguchi experimental design of L27 Orthogonal array approach. The optimal welding parameters combination has been determined by the use of analysis of Signal-to-Noise (S/N) ratio. The test of confirmation which has been performed clearly clarifies that it is possible to increase the tensile shear strength of the joint by the combination of the appropriate welding parameters. Therefore, the experimental results confirmed the validity of Taguchi approach that used to promote the welding performance and enhance the welding parameters in the process of welding parameters in resistance spot welding processes.

Statistical analysis software such as Minitab automates calculations and generates graphs, allowing the user to focus more on data analysis and interpretation of results. It is compatible with other Minitab, LLC programs.

5.3.1. Minitab Software

The Minitab is a statistical package developed at the University of Pennsylvania by researchers Barbara F. Ryan, Thomas. Minitab is a software used to teach statistics

and it is a statistical software package for public use and designed for easy interactive use. It is appropriate for teaching applications, but it is strong as a basic tool in order to analyze the research data.

5.4. CLASSIFICATION OF OPTIMIZATION (MINITAB)

Generally, optimization is a process to approximate the least probable value to the process performance at the optimal point for operation parameters. Many investigations have been performed to address the modeling of machining parameters and enhancement to determine the optimal value of the operation.

5.4.1. (Experimental of Desgine) Taquchi

In recent years, the use of Design of Experiment (DOE) has been grown in many applications. It is a scientific approach to identify the parameters associate with specific process and thus, determination of optimal settings for the operation parameters to enhance the performance and capability. Taguchi Method (TM) aims to decrease the number of necessary experiments and through which it is possible to identify the statistical importance safely.

5.4.2. ANOVA

ANOVA can be described as the most commonly used statistical treatment which can be applied on the results of experiments to identify the percentage for the contribution for each parameter against specific level of trust. Depending upon the number of process parameters and their levels, various orthogonal arrays are available. The correct selection of orthogonal array is selected done for current process. If the process parameters have mix levels, then mixed level orthogonal array is selected for experimentation.

PART 6

RESULTS AND DISCUSSION

In this research the theoretical session of this study chapter, the resistance spot weldability of the DP600 steels is clearly examined. To this effect; the functionality of the welding parameters now embodies the welding current, the weld time and the electrode force on the mechanical properties and microstructure of weldment that is now been examined and evaluated in the following section.

6.1. MICROSTRUCTURE

The functional effect of welding parameters involves the electrode force, welding time, and welding current on the microstructure of the DP600 steel weldment which have been evaluated. Moreover, the obtained results have been described and discussed in the following sections of this chapter. The microstructure after the welding process differs from the microstructure before the welding process and this is the main feature that determine the strength of the material and formation capability. As shown in Figure 6.1 that the original microstructure has been destroyed and after the welding process, three regions can be identified [135]:

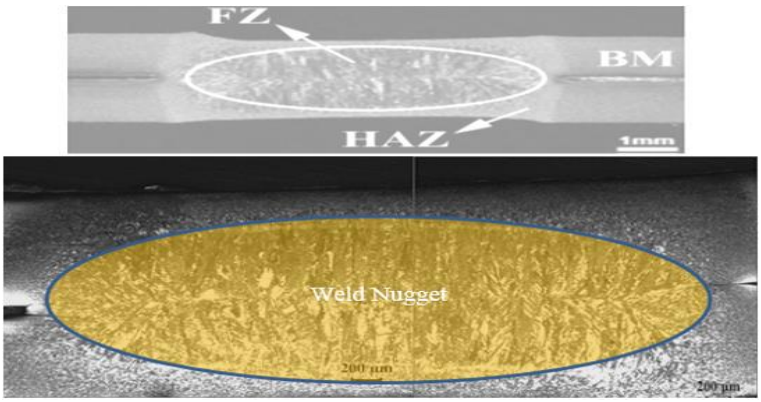

Figure 6.1. Microstructure of DP600.

6.2. THE EFFECT OF WELDING CURRENT ON THE MICROSTRUCTURE

6.2.1. The Effect of Welding Current on Microstructure

The welding current is one of the most valuable welding parameters that have affected the heat input so that the microstructure of the weldment is related and connected with the chemical composition and the welding cooling regime. The current densities of 4, 6, and 8kA which were used for the assessment of the welding currents that affect the microstructure of weldment.

The microstructures of all the weldment were examined and assessed. Furthermore, the microstructure of the samples, which was joined with constant electrode force 3.5 Bar at 4, 6 and 8 kA is presented clearly and is revealed in Figure 6.2- 6.4 respectively. The microstructures of all the weldment were examined and assessed. Furthermore, the microstructure of the samples, which was joined with 3.5, 4.5 and 5.5 Bar electrode force at 4, 6 and 8 kA, is presented clearly and is revealed in Figure 6.2-.6.10 respectively.

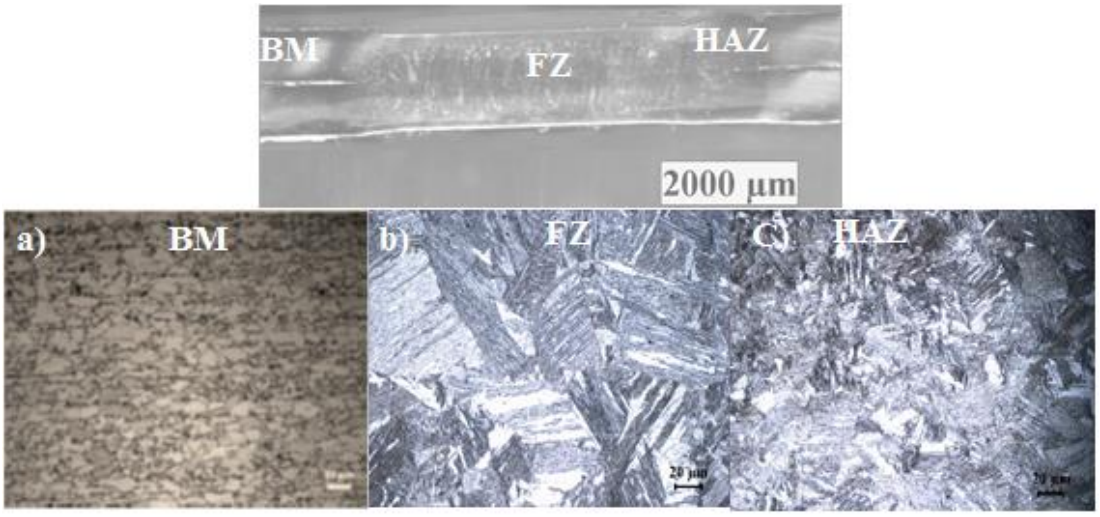

Figure 6. 2. The weld zone profile and its microstructures of DP600 weldment joined with 3.5 Bar electrode force with 4kA welding current. a) base metal (BM), b) Heat Affect Zone (HAZ), c) weld nugget (FZ).

Figure 6.2 a show the microstructure level of the DP600 steels is exclusively involved with a certain amount of martensite phases in ferrite matrix.

The results here show that the DP steel base metal contains the (70 ± 3) % of ferrite and (30±3) % of martensite phases. Figure 6.2 b, Figure 6.3.e, & Figure 6.4 h. illustrates and clearly shows that the microstructure of the HAZ region and c, f, & j) that of the FZ region respectively, in DP600 steel during the process. At parameters of (3.5 Bar with different welding current at 4, 6 and 8 kA). The HAZ region in the DP600 steel of the weldment exhibits the martensitic and the ferritic microstructure. As similarly compare to the DP600 base metal (Figure 6.2 a, Figure 6.3 d & Figure 6.4 g.), the % martensite volume fraction increased to the (50 ± 3)because of the temperature that has been reached between the Ac1 and that of the Ac3 range in the HAZ region while the welding is also been processed, it is partially austenitised and then it has been transformed into the martensite associate with higher cooling regime based on the result of the low heat input [30,152,176]. As a result of the subsequent rapid cooling, the carbon rich austenite transforms to the martensite phase while the ferrite remains as so in the structure [30,177]. The microstructure of the weld nugget decorated predominantly the martensite (Figure 6.2 c, Figure 6.3 f & Figure 6.4 j.). The martensite volume fraction was increased as the location moved towards that of the weld nugget which was as a result of the increment of the heating temperature, which is technically followed by the rapid cooling, which leads to the increments in their hardness [178]. Nayak et al. [179] and Pouranvari et al. [176]. They both collectively indicated that an increasing Si content increases the volume fraction of the martensite phase and then further decreases the amount of the retained austenite in the structure.

The microstructure also occurred predominantly with the martensitic by the weld nugget. As seen in (Figure 6.2 c, Figure 6.3 f & Figure 6.4 j), the weld nugget was exclusively decorated to suit the fully martensite phase because of the temperature that exceeds the Ac_3 so it is completely austenitised and then rapid cooling rate which encourages the martensite transformation of this region [115,180,181].

In the Figure 6.2- 6.4 which did not exhibit difference in terms of the constituent phases which is compared with the structure of the weldment. It has been clarified enough to see that the size and mass of the weld nugget and that of the electrode indentation depth increases but that of the weld nugget height decreases with the

increasing weld current. In addition, the HAZ region of the enlargement has been observed because of the heat input which is found to be associated with the increment of the weld current.

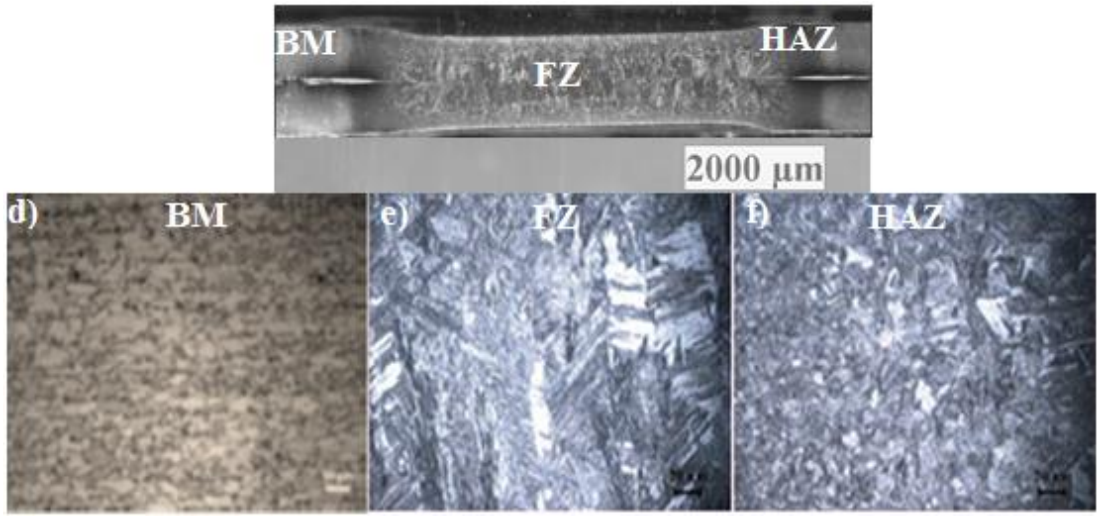

Figure 6.3. The microstructure of weldment joined with 3.5 Bar electrode force with 6kA welding current. a) DP600 base metal (BM), b) DP600 Heat Affect Zone (HAZ), c) DP600 weld nugget (FZ). parameters of (3.5 Bar – 6 kA).

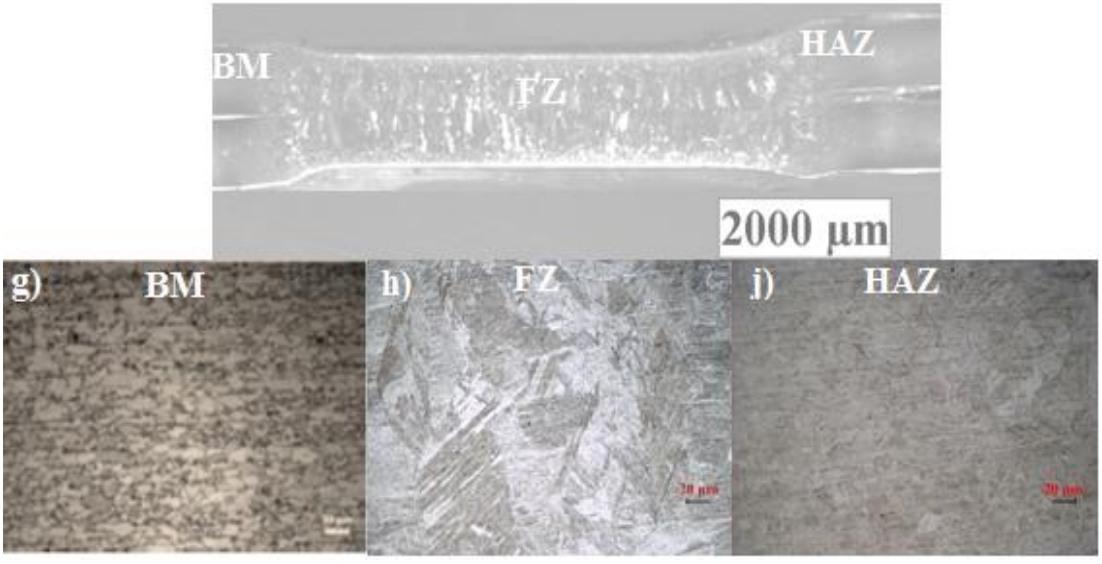

Figure 6.4. The microstructure of weldment joined with 3.5 Bar electrode force with 8kA welding current. a) DP600 base metal (BM), b) DP600 Heat Affect Zone (HAZ), c) DP600 weld nugget (FZ). parameters of (3.5 Bar – 8 kA).

Figure 6.5 b, Figure 6.6e, & Figure 6.7 h illustrate and clearly shows that the microstructure of the HAZ region and c, f, & j) that of the FZ region respectively, in DP600 steel during the process. At parameters of (4.5 Bar with different welding current at 4, 6 and 8 kA). The HAZ region in the DP600 steel of the weldment exhibits the martensitic and the ferritic microstructure. As similarly compare to the DP600 base metal (Figure 6.5 a, Figure 6.6 d & Figure 6.7 g.).

The microstructure also occurred predominantly with the martensitic side by the weld nugget. As seen in (Figure 6.5 c, Figure 6.6 f & Figure 6.7 j), the weld nugget was exclusively decorated to suit the fully martensite phase because of the temperature that exceeds the Ac_3 so it is completely austenitised and then rapid cooling rate which encourages the martensite transformation of this region [115,180,181].

Now, as been, seen and revealed in Figure 6.5, Figure 6.6 and Figure 6.7, the microstructure of the weldment which were joined with the various numbers of the welding current such as, 4, 6, and 8kA at a constant electrode force 4.5Bar, which did not exhibit difference in terms of the constituent phases which is compared with the structure of the weldment. It has been clarified enough to see that the size and mass of the weld nugget and that of the electrode indentation depth increases but that of the weld nugget height decreases with the increasing weld current. Furthermore, the HAZ region of the enlargement has been observed because of the heat input which is found to be associated with the increment of the weld current.

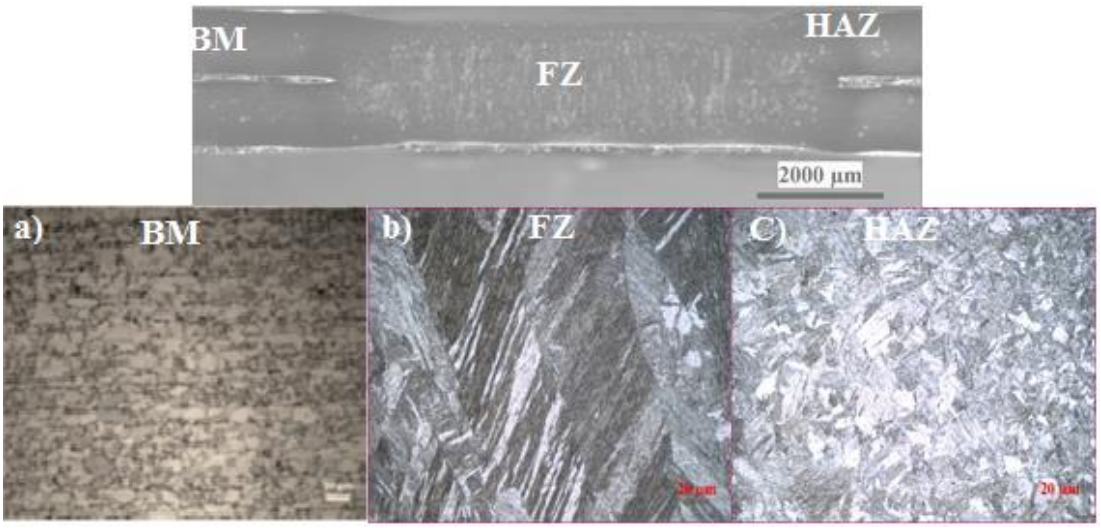

Figure 6.5. The weld zone profile and its microstructures of DP600weldment joined with 4.5 Bar electrode force with 4kA welding current. d) DP600 base metal (BM), e) DP600 Heat Affect Zone (HAZ), f) DP600 weld nugget (FZ).

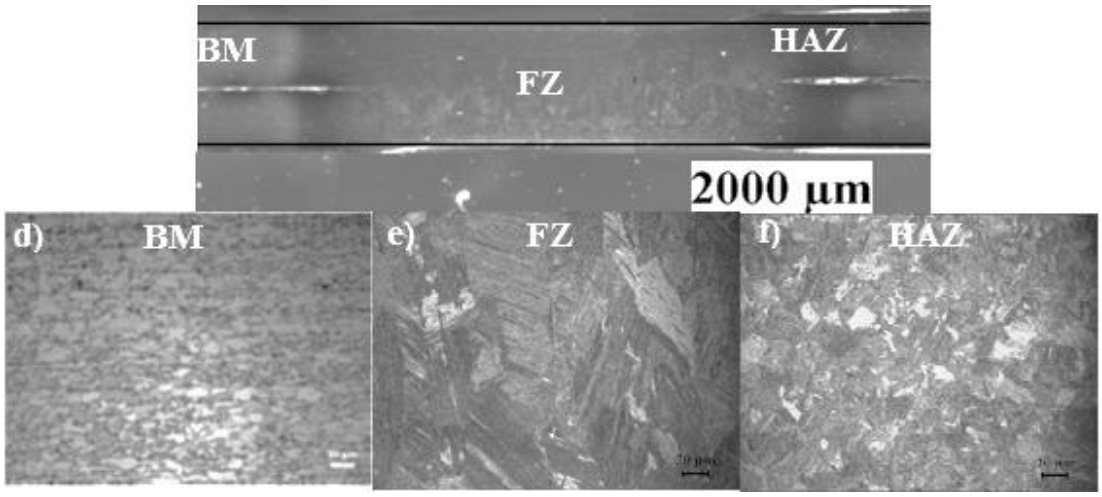

Figure 6.6. The microstructure of weldment joined with 4.5 Bar electrode force with 6kA welding current. d) DP600 base metal (BM), e) DP600 Heat Affect Zone (HAZ), f) DP600 weld nugget (FZ). parameters of (4.5 Bar – 6 kA)

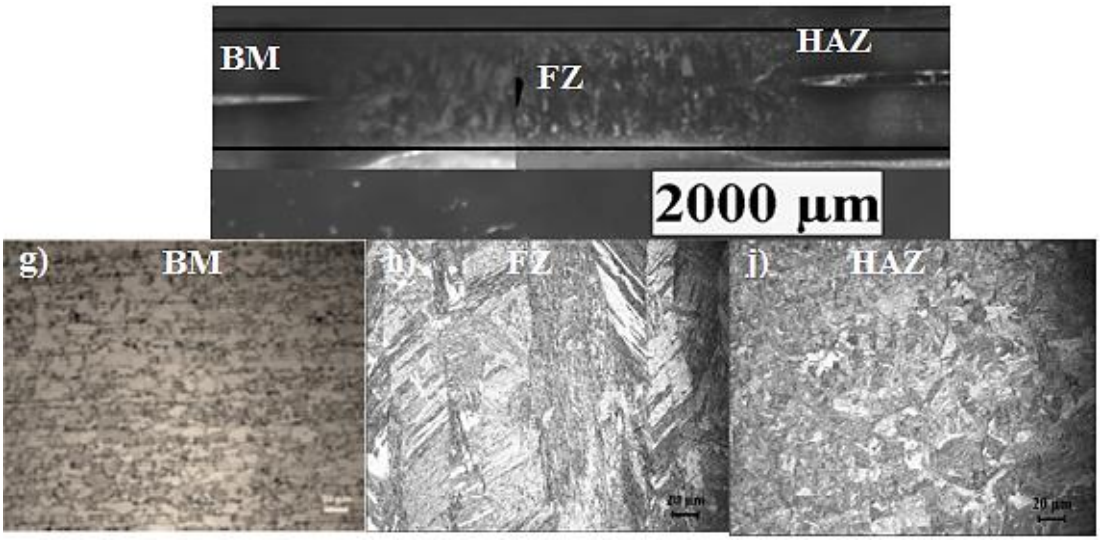

Figure 6.7. The microstructure of weldment joined with 4.5 Bar electrode force with 8kA welding current. g) DP600 base metal (BM), h) DP600 Heat Affect Zone (HAZ), j) DP600 weld nugget (FZ). parameters of (4.5 Bar – 8 kA).

Figure 6.8 b, Figure 6.9e, & Figure 6.10 h. illustrates and clearly shows that the microstructure of the HAZ region and c, f, & j) that of the FZ region respectively, in DP600 steel during the process. At parameters of (5.5 Bar with different welding current at 4, 6 and 8 kA). The HAZ region in the DP600 steel of the weldment exhibits the martensitic and the ferritic microstructure. As similarly compare to the DP600 base metal (Figure 6.8 a, Figure 6.9 d & Figure 6.10 g).

The microstructure also occurred predominantly with the martensitic by the weld nugget. As seen in (Figure 6.8 c, Figure 6.9 f & Figure 6.10 j), the weld nugget was exclusively decorated to suit the fully martensite phase because of the temperature that exceeds the Ac_3 so it is completely austenitised and then rapid cooling rate which encourages the martensite transformation of this region [115,180,181].

Also, has been, seen and revealed in Figure 6.8, Figure 6.9 and Figure 6.10, the microstructure of the weldment which were joined with the various numbers of the welding current such as, 4, 6, and 8kA at a constant electrode force 5.5Bar, which did not exhibit difference in terms of the constituent phases which is compared with the structure of the weldment. It has been clarified enough to see that the size and mass of the weld nugget and that of the electrode indentation depth increases but that of the weld nugget height decreases with the increasing weld current. Moreover,

the HAZ region of the enlargement has been observed because of the heat input which is found to be associated with the increment of the weld current.

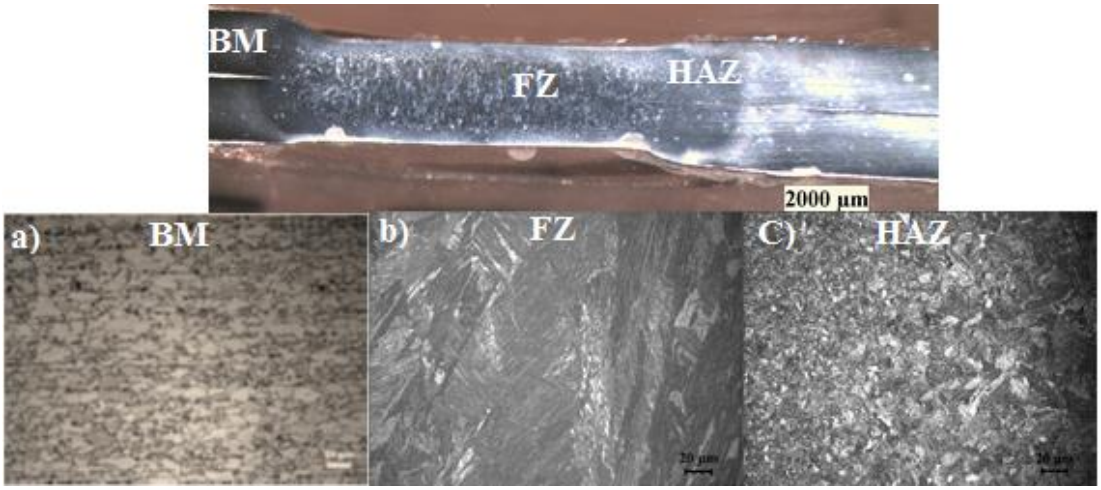

Figure 6.8. The weld zone profile and its microstructures of DP600weldment joined with 5.5 Bar electrode force with 4kA welding current. a) DP600 base metal (BM), b) DP600 Heat Affect Zone (HAZ),c) DP600 weld nugget (FZ).

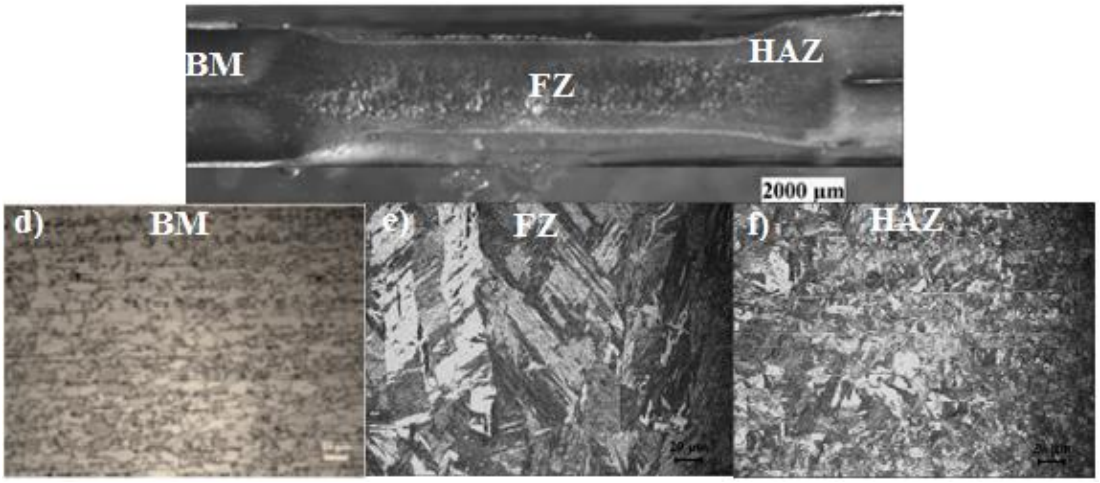

Figure 6.9. The weld zone profile and its microstructures of DP600weldment joined with 5.5 Bar electrode force with 6kA welding current. d) DP600 base metal (BM), e) DP600 Heat Affect Zone (HAZ), f) DP600 weld nugget (FZ).

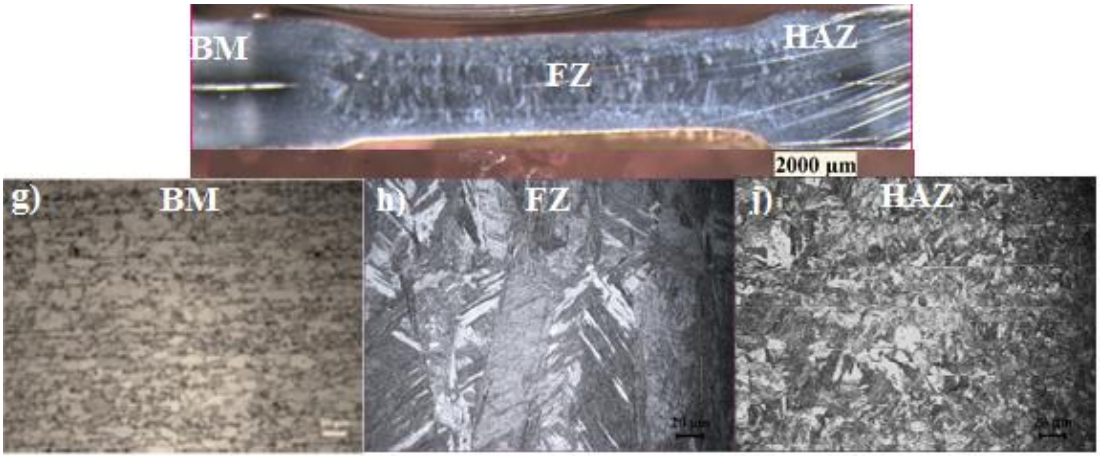

Figure 6.10. The microstructure of weldment joined with 5.5 Bar electrode force with 8kA welding current. g) DP600 base metal (BM), h) DP600 Heat Affect Zone (HAZ), j) DP600 weld nugget (FZ). parameters of (5.5 Bar – 8 kA).

6.2.2. Effect of Electrode Force on the Microstructure of - Dp600 Steel Weldment

In this thesis, the microstructure of the weldment, found to be the most relevant welding parameters was the electrode pressure which, however, affects the microstructure of the weldment which was joined with the 3.5, 4.5 and 5.5Bar had various electrode force were applied through the assessment electrode force. It affects heat input so as microstructure of weldment. In this chapter study, the microstructure of the weldment, which was adjoined with the 3.5, 4.5 and 5.5Bar had various electrode force and of 4, 6 and 8kA welding current, these are clearly, illustrated and shown in Figure 6.11-6.19 respectively.

Figure 6.11 b, Figure 6.12 e, & Figure 6.13 h. illustrates and clearly shows that the microstructure of the HAZ region and c, f, & j) that of the FZ region respectively, in DP600 steel during the process. At parameters of (3.5, 4.5 and 5.5 Bar with constant welding current at 4 kA). The HAZ region in the DP600 steel of the weldment exhibits the martensitic and the ferrite microstructure. As similarly compare to the DP600 base metal (Figure 6.11 a, Figure 6.12 d & Figure 6.13 g.).

The microstructure also occurred predominantly with the martensitic side by the weld nugget. As seen in (Figure 6.11 c, Figure 6.12 f & Figure 613 j), the weld

nugget was exclusively decorated to suit the fully martensite phase because of the temperature that exceeds the Ac_3 so it is completely austenitised and then rapid cooling rate which encourages the martensite transformation of this region [115,180,181]. As illustrated, and revealed in Figure 6.11 to Figure 6.13, the microstructure of the weldment which were joined with the numerous electrode forces such as; 3.5, 4.5 and 5.5Bar at a constant weld current. It, however, did not present the differences in terms of the constituent phases.

The size of the nugget and the electrode indentation has been determined to increase, while the nugget height decreases with the increment of the electrode force. However, the expulsion and inclusion observed clearly because of the high pressure were then associated with increments of the electrode force. It was, thereby, however, reported that the high pressure connected to the electrode pressure and that of the sufficient heat input in the spot welding resulted to the expulsion and the oxide inclusion in the weld nugget [98].

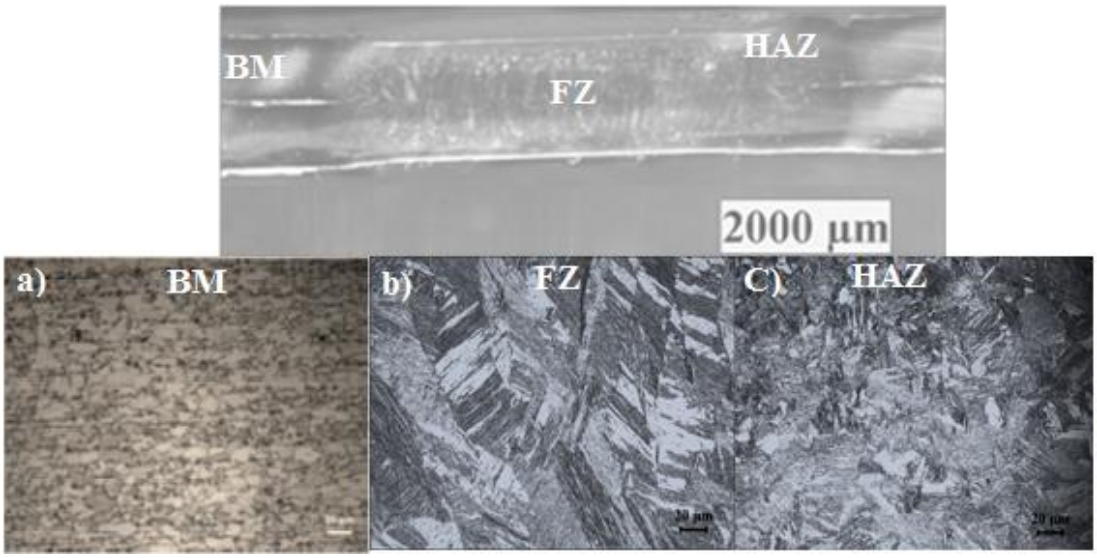

Figure 6.11. The weld zone profile and its microstructures of DP600 weldment joined with 3.5 Bar electrode force with 4kA welding current. a) base metal (BM), b) Heat Affect Zone (HAZ), c) weld nugget (FZ).

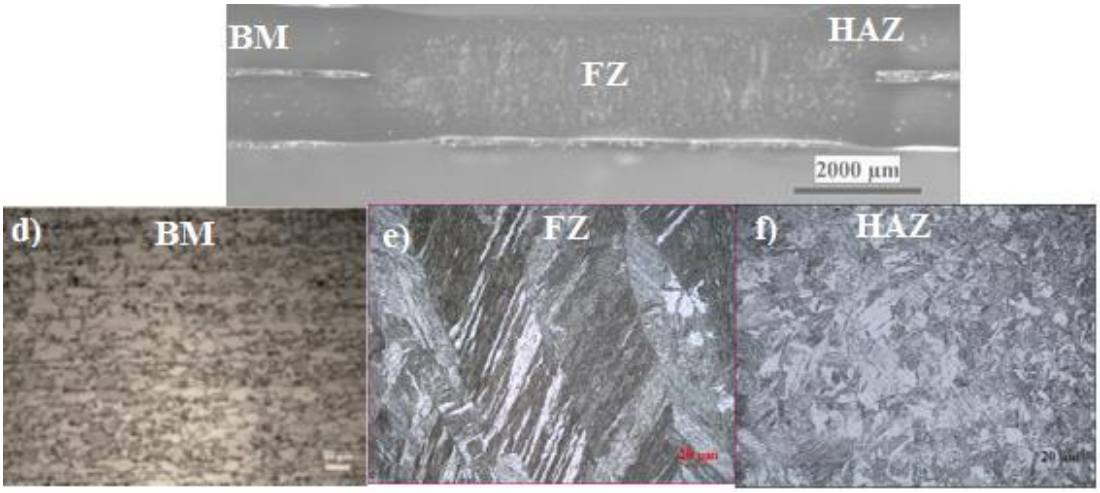

Figure 6.12. The weld zone profile and its microstructures of DP600weldment joined with 4.5 Bar electrode force with 4kA welding current. d) DP600 base metal (BM), e) DP600 Heat Affect Zone (HAZ), f) DP600 weld nugget (FZ).

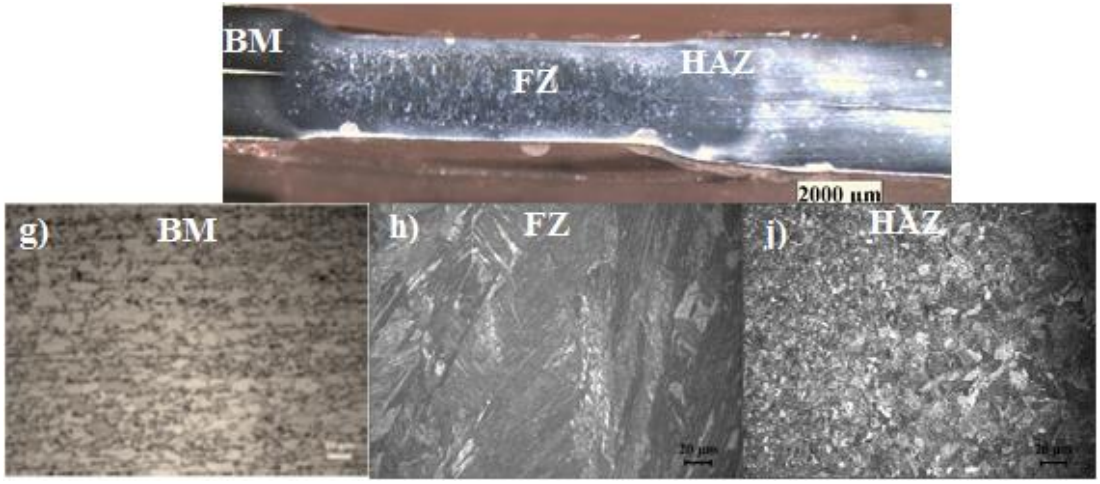

Figure 6.13. The weld zone profile and its microstructures of DP600weldment joined with 5.5 Bar electrode force with 4kA welding current. g) DP600 base metal (BM), h) DP600 Heat Affect Zone (HAZ), j) DP600 weld nugget (FZ).

Figure 6.14 b, Figure 6.15 e, & Figure 6.16 h. illustrates and clearly shows that the microstructure of the HAZ region and c, f, & j) that of the FZ region respectively, in DP600 steel during the process. At parameters of (3.5, 4.5 and 5.5 Bar with constant welding current at 6 kA).

It was found to be the most relevant welding parameters was the electrode pressure which, effects on the microstructure of the weldment. The 3.5, 4.5 and 5.5Bar electrode forces were applied through the assessment electrode force. It affects heat input so as microstructure of weldment. The HAZ region in the DP600 steel of the weldment exhibits the martensitic and the ferritic microstructure. As similarly compare to the DP600 base metal (Figure 6.14 a, Figure 6.15 d & Figure 6.16 g.),
The microstructure also occurred predominantly with the martensitic side by the weld nugget. As seen in (Figure 6.14 c, Figure 6.15 f & Figure 616 j), the weld nugget was exclusively decorated to suit the fully martensite phase because of the temperature that exceeds the Ac_3 so it is completely austenitised and then rapid cooling rate which encourages the martensite transformation of this region [115,180,181]. As illustrated, and revealed in Figure 6.14 to Figure 6.16, the microstructure of the weldment which were joined with the numerous electrode forces such as; 3.5, 4.5 and 5.5Bar at a constant weld current. It, however, did not present the differences in terms of the constituent phases.

The size of the nugget and the electrode indentation has been determined to increase, while the nugget height decreases with the increment of the electrode force. However, the expulsion and inclusion observed clearly because of the high pressure were then associated with increments of the electrode force. It was, thereby, however, reported that the high pressure connected to the electrode pressure and that of the sufficient heat input in the spot welding resulted to the expulsion and the oxide inclusion in the weld nugget [98].

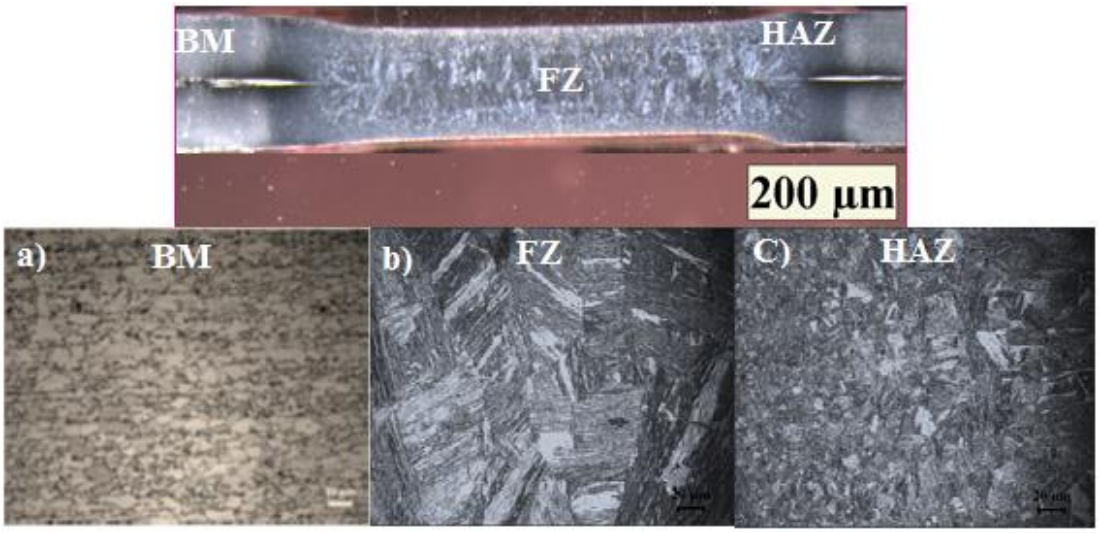

Figure 6.14. The microstructure of weldment joined with 3.5 Bar electrode force with 6kA welding current. a) DP600 base metal (BM), b) DP600 Heat Affect Zone (HAZ), c) DP600 weld nugget (FZ). parameters of (3.5 Bar – 6 kA).

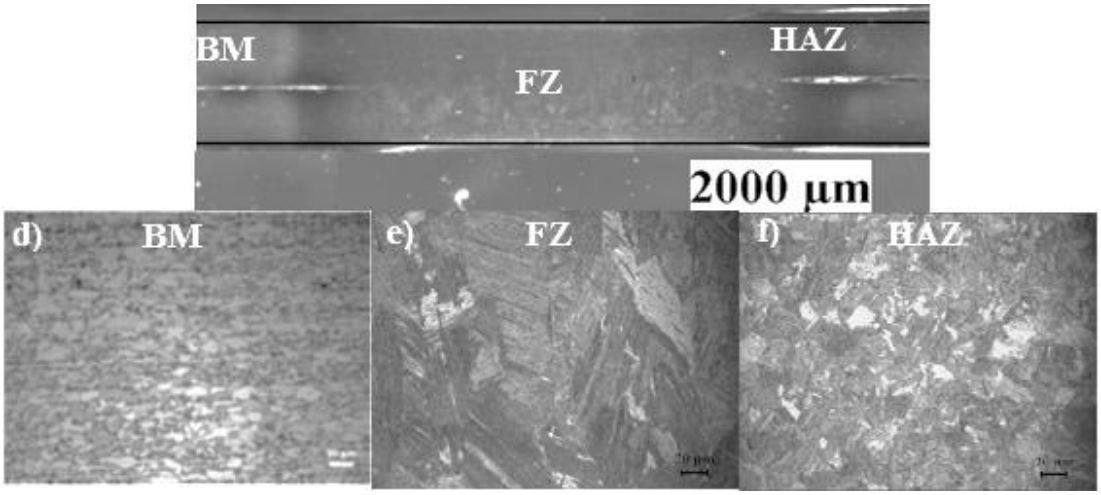

Figure 6.15. The microstructure of weldment joined with 4.5 Bar electrode force with 6kA welding current. d) DP600 base metal (BM), e) DP600 Heat Affect Zone (HAZ), f) DP600 weld nugget (FZ). parameters of (4.5 Bar – 6 kA).

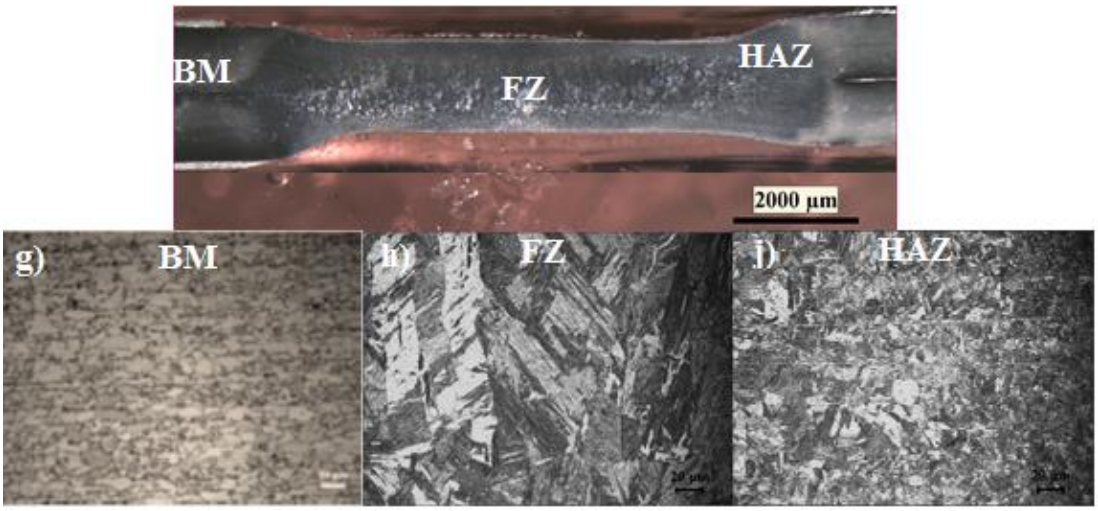

Figure 6.16. The weld zone profile and its microstructures of DP600weldment joined with 5.5 Bar electrode force with 6kA welding current. g) DP600 base metal (BM), h) DP600 Heat Affect Zone (HAZ), j) DP600 weld nugget (FZ).

Figure 6.17 b, Figure 6.18 e, & Figure 6.19 h. illustrates and clearly shows that the microstructure of the HAZ region and c, f, & j) that of the FZ region respectively, in DP600 steel during the process. At parameters of (3.5, 4.5 and 5.5 Bar with constant welding current at 8 kA).

It was found to be the most relevant welding parameters was the electrode pressure which, effects on the microstructure of the weldment. The 3.5, 4.5 and 5.5Bar electrode forces were applied through the assessment electrode force. It affects heat input so as microstructure of weldment. The HAZ region in the DP600 steel of the weldment exhibits the martensitic and the ferritic microstructure. As similarly compare to the DP600 base metal (Figure 6.17 a, Figure 6.18 d & Figure 6.19 g.),
The microstructure also occurred predominantly with the martensitic side by the weld nugget. As seen in (Figure 6.17 c, Figure 6.18 f & Figure 619 j), the weld nugget was exclusively decorated to suit the fully martensite phase because of the temperature that exceeds the Ac_3 so it is completely austenitised and then rapid cooling rate which encourages the martensite transformation of this region [115,180,181]. As illustrated, and revealed in Figure 6.17 to Figure 6.19, the microstructure of the weldment which were joined with the numerous electrode

forces such as; 3.5, 4.5 and 5.5Bar at a constant weld current. It, however, did not present the differences in terms of the constituent phases.

The size of the nugget and the electrode indentation has been determined to increase, while the nugget height decreases with the increment of the electrode force. However, the expulsion and inclusion observed clearly because of the high pressure were then associated with increments of the electrode force. It was, thereby, however, reported that the high pressure connected to the electrode pressure and that of the sufficient heat input in the spot welding resulted to the expulsion and the oxide inclusion in the weld nugget [98].

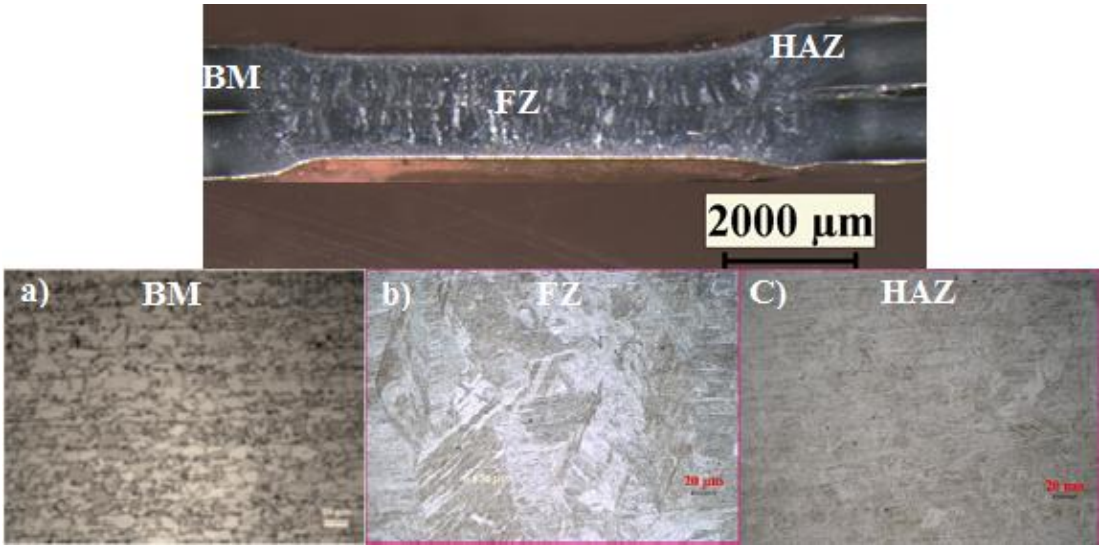

Figure 6.17. The microstructure of weldment joined with 3.5 Bar electrode force with 8kA welding current. a) DP600 base metal (BM), b) DP600 Heat Affect Zone (HAZ), c) DP600 weld nugget (FZ). parameters of (3.5 Bar – 8 kA).

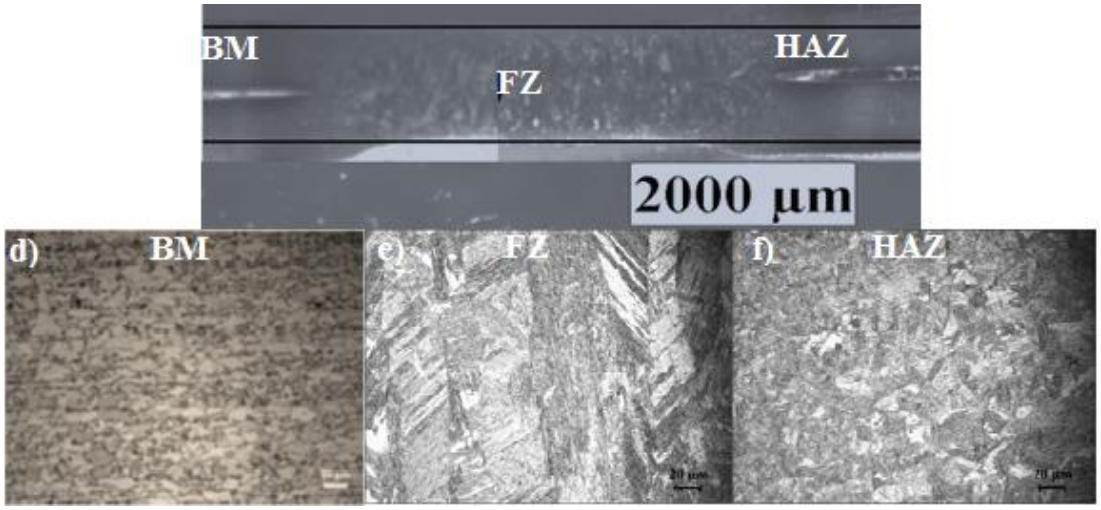

Figure 6.18. The microstructure of weldment joined with 4.5 Bar electrode force with 8kA welding current. d) DP600 base metal (BM), e) DP600 Heat Affect Zone (HAZ), f) DP600 weld nugget (FZ). parameters of (4.5 Bar – 8 kA).

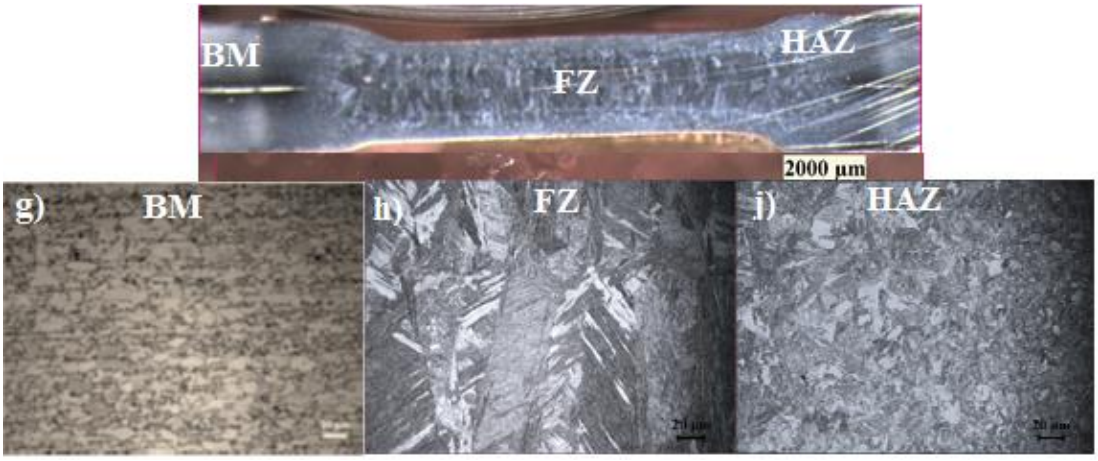

Figure 6.19. The microstructure of weldment joined with 5.5 Bar electrode force with 8kA welding current. g) DP600 base metal (BM), h) DP600 Heat Affect Zone (HAZ), j) DP600 weld nugget (FZ). parameters of (5.5 Bar – 8 kA).

According to our results, we found that the difference in size of nugget and volume fraction is because of the difference in parameters. We noticed that when increase the welding current especially at the parameter 3.5 bar and 8kA, the size of nugget and volume of fraction will be increased accordingly. Also, when the forced is increased more than 3.5 bar, we noticed that the explosion occur at the nugget point.

6.3. NUGGET FORMATION

In this study, nugget formation during RSW have been studied by experimental and results have been given at Figure 6.20. as nugget profile and Table 6.1 and Figure 6.2. As seen on these, the mean diameter of the nugget had been measured as been up to approximately 8,25 mm in 3,5 Bar, 25 cycles and 8 kA in and it can be used for DP600 steel. These results can be explained by 5√t rule (t: material thickness), which was recommended to be appropriate rule according to Japanese and German standards [181].

According to Wang Y et. al. [3], the nugget formation during RSW may be separated by three specific stages: recovery and progress, growing, and reach to equilibrium [11]. During the development stage, which is rapid, typically lesser than even 1 cycle, the nugget starts to be forming owing to the melting of the metal. In the development period, which occurs in the following 2-4 cycles, the nugget grows rapidly then the growing grade failures with time. This is due to the reduction in current quantity and heating amount produced by the increase in the interaction portion between the electrode and workpiece. As a final point, the nugget growth accomplishes maintenance after almost 4 cycles. The periods of the development stage for steel alloys are much bigger than that of Mg alloys and Al alloys.

It could be also shown at Figure 6.20 and Table 6.1 that increasing the current, increase the diameter of nugget, while decrease with increasing the pressure. As presented just when the increase of time increases by both the diameter of nugget and penetration rate of the welding that is at a stable electrode load and raises with a current level of increase. This discloses the features of welding links that include of the nugget size, the heat the impacted region width and the height, peak load, indentation depth and failure modes in the tensile shear test. Thus, it can be noticed from this that the extreme movement, peak load, penetration ratio and failure energy are monotonically raising with the fusion size.

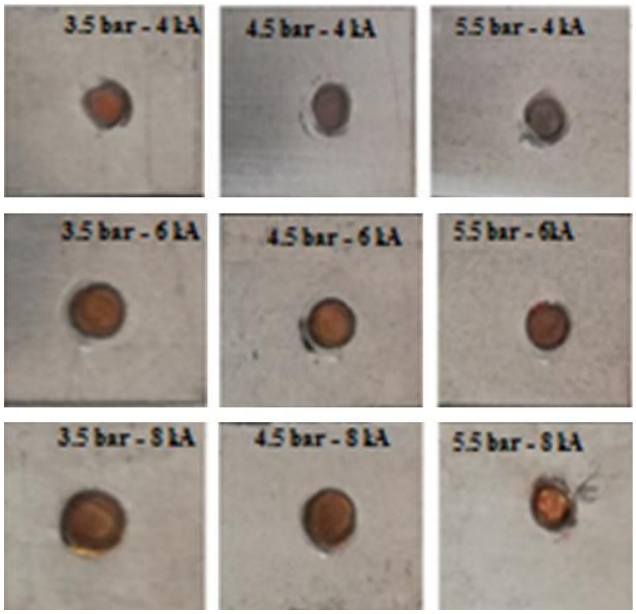

Figure 6.20. Macro photography of weld nuggets of RSW samples.

Table 6.1. Changing of weld nugget with welding current and electrode force clamping load at 25 cycles.

Electrode Force (Bar)	Welding Current (kA)	Nugget Diameter (mm)`
3.5	4	5.52
	6	6.15
	8	8.25
4.5	4	4.85
	6	5.73
	8	7.80
5.5	4	4.45
	6	5.64
	8	7.50

Table 6.2. Changing of weld nugget with welding current and electrode force/ clamping load at 15 cycles.

Electrode Force (Bar)	Welding Current (kA)	Nugget Diameter (mm)`
3.5	4	4.62
	6	5.87
	8	7.67
4.5	4	4.08
	6	5.52
	8	7.55
5.5	4	3.82
	6	5.24
	8	7.31

6.4. SIMU FACT SIMULATION

The Simufact software results can be clarified as follows. At constant value of clamping load and when increase the welding current, the nugget diameter and penetration ratio will be increased. While at constant value of welding current and increasing the clamping load, we found that the nugget diameter and penetration ratio will be decreased. These results show that the optimal value of nugget size is obtained at 8kA and 3.5 bar. As well as, the least value of nugget size is obtained at 5.5 bar and 4kA. It is clear from Figure 6.21 the modeling of samples and that the major phase index, it is almost martensite.

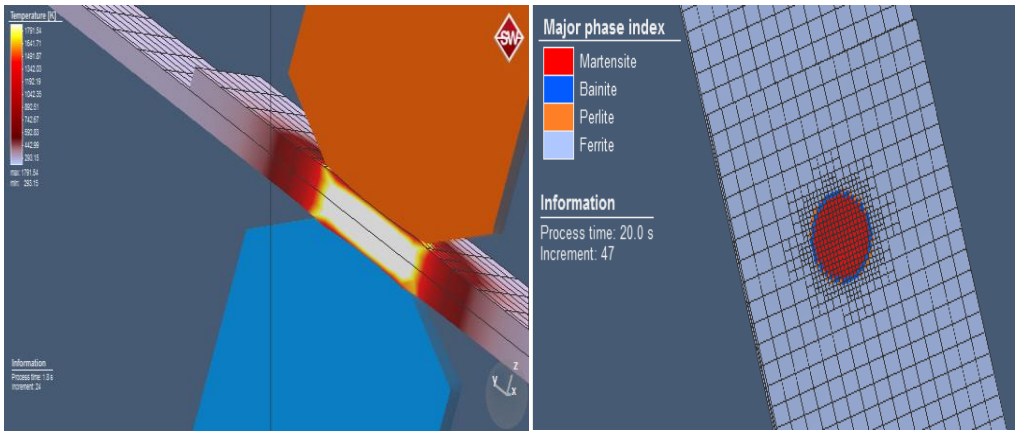

Figure 6.21. Modeling of sample and the majer phase.

Through the following figures 6.22, we can see that the volume fraction of martensite increases when the welding current decreases and it does not effect by change of clamping load. The volume fraction of martensite is about 91.0 to 93 % at FZ and with welding current 4kA whereas volume fraction of martensite at the welding current 6kA is from 80.0 to 88 % and it is 30 to 70 % with welding current value of 8kA.

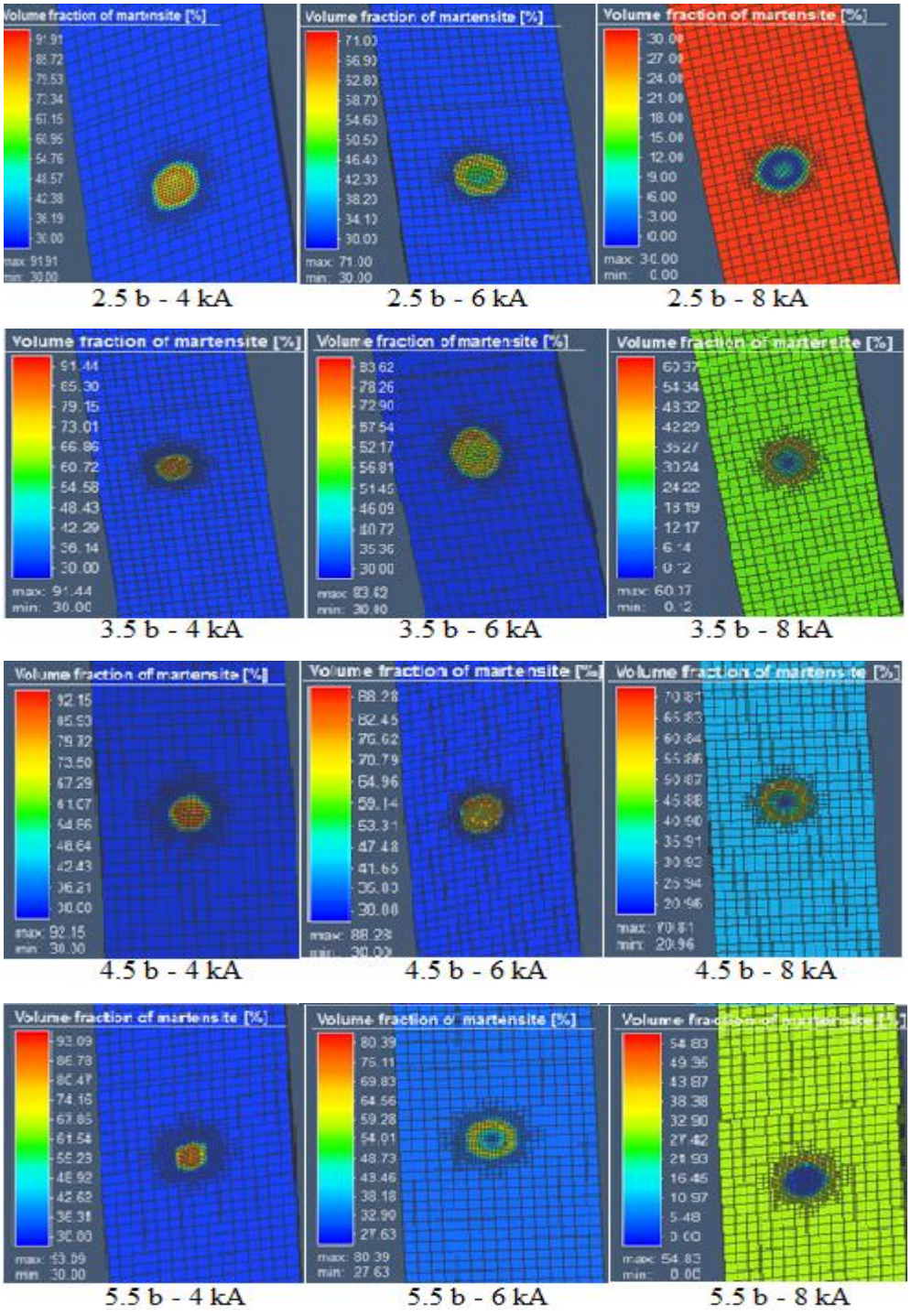

Figure 6.22. The Volume fraction of martensite transformation.

At the following figure 6.23, we see that the volume fraction of ferrite increases when the welding current decreases and it does change by change occur in clamping load. The volume fraction of ferrite at FZ is about 4% with welding current 4kA while the volume fraction of ferrite at welding current 6kA is about 5-10 % and it is

from 7 to 32 % with welding current value of 8kA. When we compare these results with results in the literature review, we can find that the results are too close from each other.

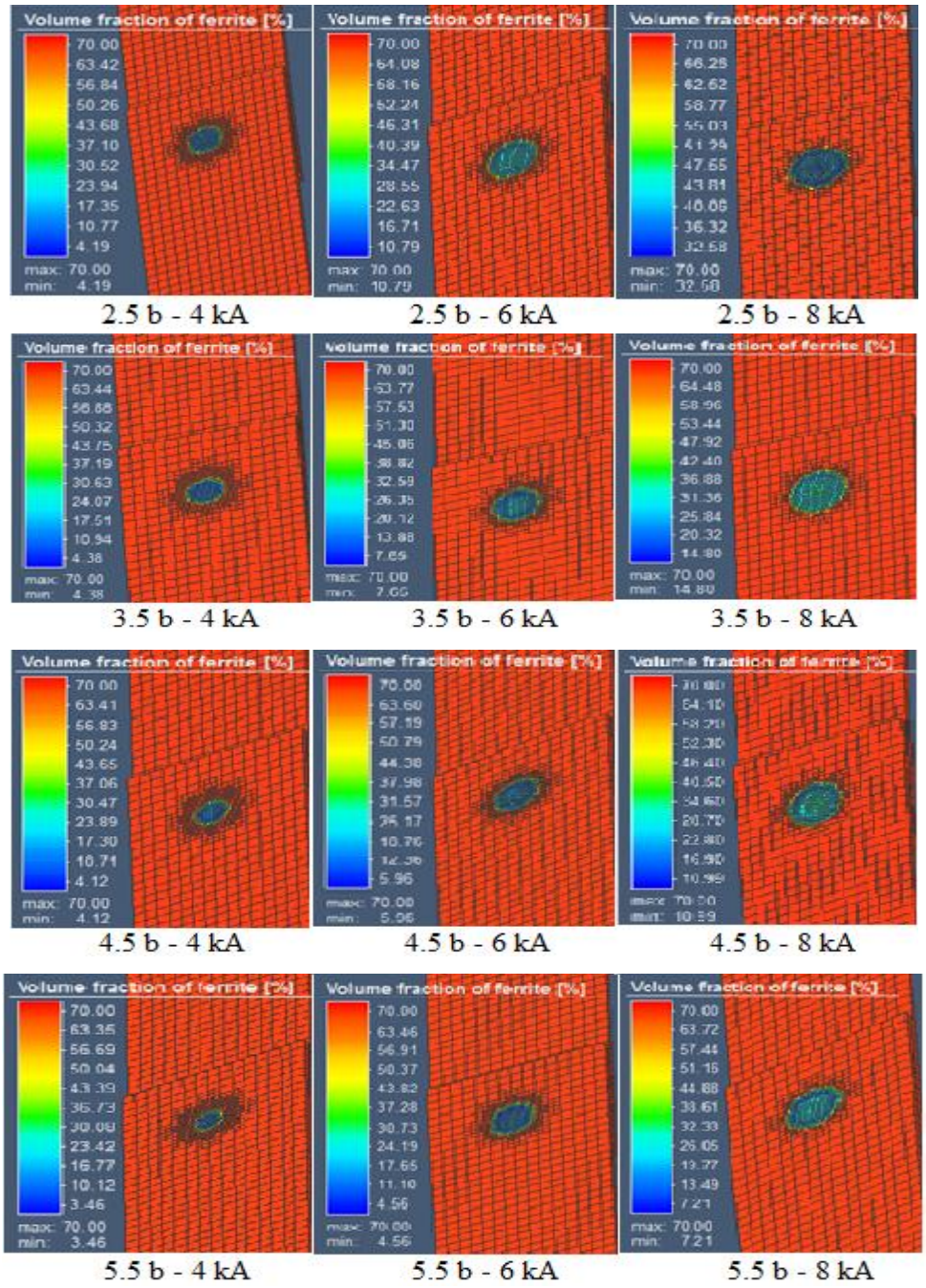

Figure 6.23. Volume fraction of ferrite at FZ.

As clear in Figure 6.24. that the main elements in DP 600 steels are C, Fe, Mn and Cr and their percentages are 0.08%, 97.48%, 1.86% and 0.18% respectively.

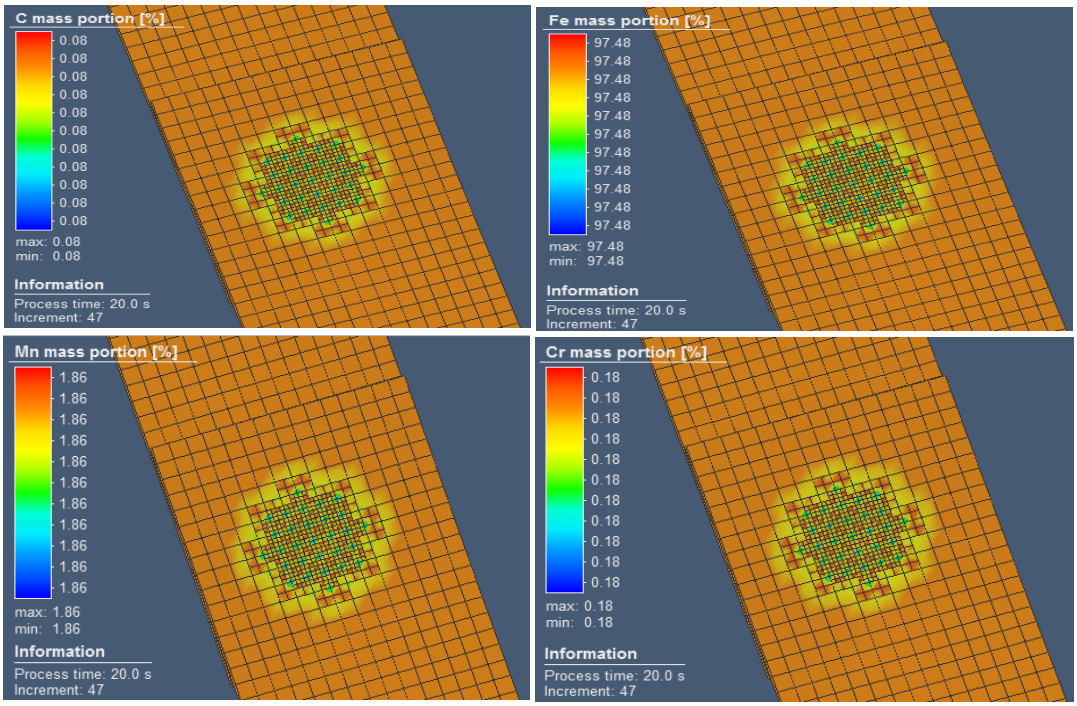

Figure 6. 24. The contents of carbon, iron, manganese and chrome.

As clear in Figure 6.25. a, Figure 6.25. b, Figure 6.25. c that when increase current, the nugget formation is increasing accordingly. Also, in cases of Figure 6.25.d, Figure 6.25.e and Figure 6.25.f and Figure 6.25.g, Figure 6.25.h and Figure 6.25.j, the nugget formation is increasing when the welding current increases.

Whereas in Figure 6.25.a, Figure 6.25.d and Figure 6.25.g, at fixed welding current with 4 kA, the nugget formation reduces when increase the clamping load. Moreover, in cases of Figure 6.25.b, Figure 6.25.e and Figure 6.25.h, we can see that the nugget size decreases when we fix. the current at 6 kA and increase the clamping load from 3.5 bar up to 5.5 bar by incremental value of 1 bar. Finally, it is clear from the results in Figure 6.25.c, Figure 6.25.f and Figure 6.25.j that the nugget size decreases by increasing clamping force with fixed current.

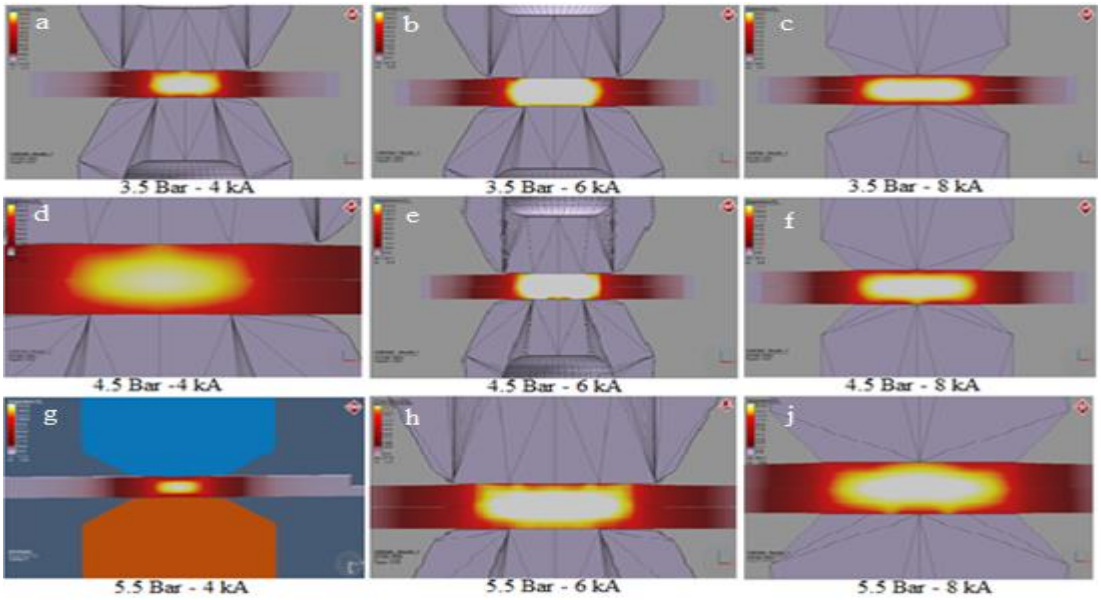

Figure 6.25. Nugget size formation in simufact software.

The optimal value of nugget formation is obtained with clamping of 3.5 bar and current 8 kA while least size of nugget is obtained with clamping load of 5.5 bar and current of 4 kA.

When we make comparison between software results and our experimental results, we found that they are close from each other. These results can be shown in Figure 6.26 where the left sides represent the nugget shape of our experimental results and the right sides represents the software results. Figure 6.26.a, Figure 6.26.b and Figure 6.26.c at constant load of 3.5 bar and welding current 4, 6 and 8kA, we notice that when increase the welding current, the nugget diameter will be increased. The same results happen with Figure 6.26.d, Figure 6.26.e and Figure 6.26.f at constant force 4.5 bar. In addition, in Figure 6.26.g, Figure 6.26.h and Figure 6.26.j the same case happens with constant force 5.5 bar.

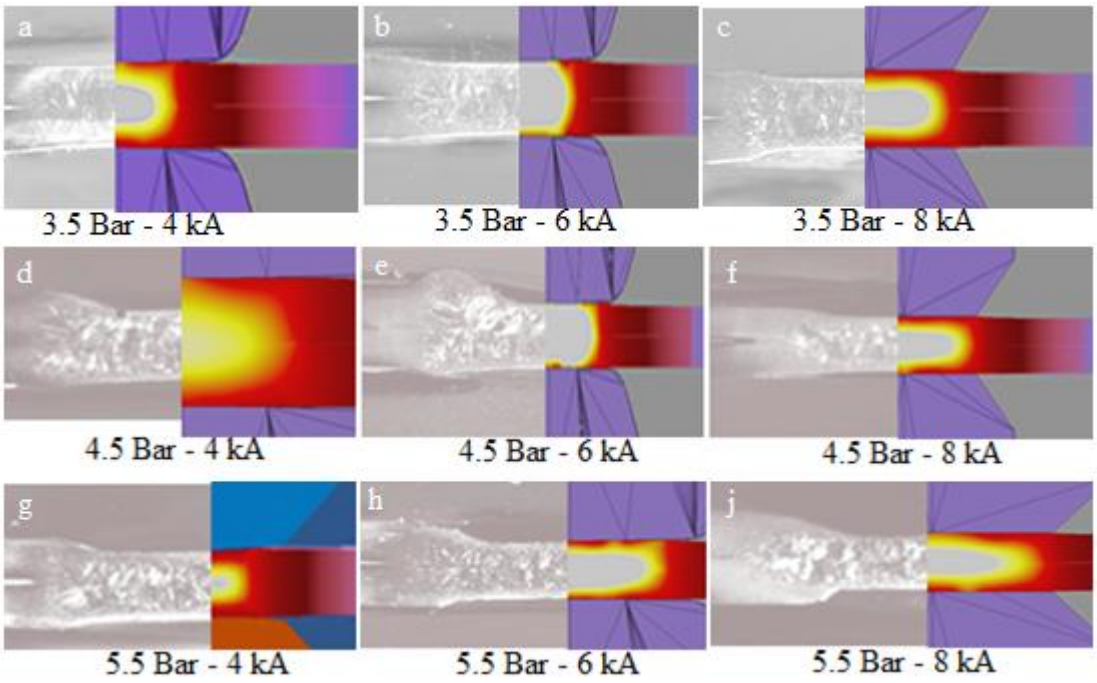

Figure 6.26. Nugget formation in simufact software and experimental results.

6.5. TENSILE SHEAR TEST

6.5.1. Maximum Tensile Shear Strength Values

The values presented below state, and the curves reveal the results achieved in the tensile test. The actual results are whether current (I) 4, 6 and 8 kA parameters are applied with a variable force (F) of 3.5, 4.5 and 5.5 Bar. Max. load completed and achieved when built at 3.5 Bar with 8 kA it found 14.573 kN. This implies; the load was proportional to the increment of the current at a fixed force of 3.5 Bar. Although and when this force increased more than the rate and the height of 3.5 Bar it reduced the tensile load, which was found in all cases with an increase in the current, increase the load as shown in Figure 6.27. Also found the second point at the same weld current 8 kA is 13.998 kA, then decreased to 13.326kA at 6 kA and 4.5 Bar, next strength was 13.064 kA at the same parameters 6 kA and 4.5Bar. In the parameters of 3.5 Bar and 4kA the strength was 12.989 kN and 12.778 kN at 8 kA, then decrease to 12.762 kN at electrode force 4.5 Bar and welding current 4 kA, and 12.497 kN at 6 kA and 5.5Bar, finally decrease to 12.350 kN at 4 kA and 5.5 Bar.

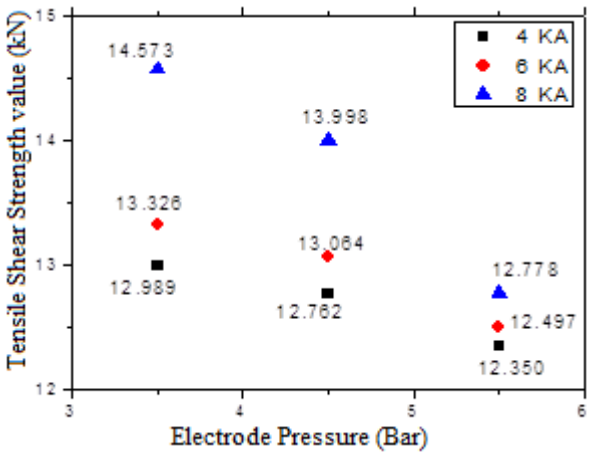

Figure 6.27. Maximum tensile shear force values obtained at 25 cycles.

6.5.2. Tensile Shear Load Bearing Capacity vs Current With Clamping Load

Tensile shear test results as current vs tensile load bearing capacity with clamping load have been given at Figure 6.28. shows that when increase clamping load from 3.5 bar to 4.5 bar, tensile shear decreases, and the decreasing value is 0.0178. While increasing the clamping load from 3.5 bar to 5.5 bar, the value of tensile shear will be decreased, and the decreased value is 0.052. Also, increase the clamping load from 4.5 bar to 5.5 bar, the value of tensile shear decreases, and its decreasing value will be 0.033. The above results are under the welding current value of 4kA and welding current 25 cycles. As shown in Figure 6.22 when the tensile shear decreases and its decreasing value is 0.045 when increase the clamping load from 4.5 bar to 5.5 bar while the tensile shear decreases with value of 0.066 when increase the clamping load from 3.5 bar to 5.5 bar and finally, tensile shear decreases with decreasing value of 0.02 when increase the clamping load from 3.5 bar to 4.5 bar. The welding current value of the above results is 6 kA and welding current 25 cycles.

When increase the clamping load from 3.5 bar to 4.5, 3.5 bar to 5.5 bar and 4.5 to 5.5 bar, the tensile shear will be decreased with decreasing values of 0.041, 0.14 and 0.095 respectively. It must be mentioned that the welding current value to the above results is 8 kA and welding time is 25 cycles.

That tensile load bearing capacity increasing with increasing the weld current. However, increasing proportion of tensile load bearing capacity is changing depending on clamping load and increasing current. These are the effect of current 4, 6 and 8, and each as of the clamping load of 3.5, 4.5 and 5.5, respectively. As shown in the three curves that when increasing the current, the tensile shear strength will be increased at the three loads. However, we notice that at the force 5.5 and when the current increases from 4 to 6 and then 8, the tensile strength will be simply increased. when the current increases from 4, 6 and 8, the tensile shear strength highly increases. Also, we notice that this curve at the load 3.5 and especially at the current 8 is with greater registered strength and less value at the load 5.5 with the current 4. This relationship is considered positive relationship between the current and tensile shear strength. The results clarified that increasing the welding current increases the tensile shear force. Also, the optimal value is obtained at welding current of 8kA with clamping load 3.5 bar.

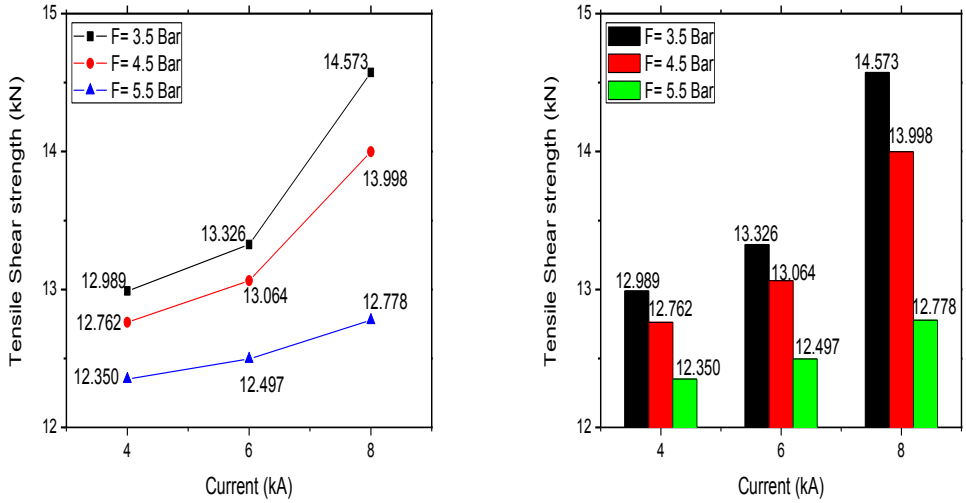

Figure 6.28. Effect of current on tensile shear strength at different parameters at 25 cycles.

In the Figure 6.29. The value of tensile shear is decreased, and its decreasing value is 0.15 when the clamping load increase from 4.5 bar to 5.5 bar whereas its decreasing value is 0. 172 when increase the clamping load from 3.5 bar to 5.5 bar and finally, the value of tensile shear is decreased and decreasing value is 0.15 when increase the clamping load from 4.5 bar to 5.5 bar the value of welding current is 4kA and welding current 15 cycles.

When increase the clamping load from 3.5 bar to 4.5 bar, the value of tensile shear will be decreased, and the decreasing value is 0.067. Also, when increase the load of clamping from 3.5 bar to 5.5 bar, the tensile shear value is decreasing and the decreased value is 0.133 and finally, when the clamping load is increased from 4.5 bar to 5.5 bar, the value of tensile shear is decreased and the decreasing value is 0. 149. The value of current welding to the above results is 6kA and welding current 15 cycles. The tensile shear value is decreased with decreasing value of 0.074, when increase the clamping load from 3.5 bar to 4.5 bar while its value is decreased with decreasing value of 0.242, when increase the clamping load from 3.5 bar to 5.5 bar and finally, the value of tensile shear is decreased and the decreasing value is 0.16 when increase the tensile shear from 4.5 bar to 5.5 bar. The welding current value to the above results is 8 kA and welding current 15 cycles. It is clear from our results that when increase the welding current, the tensile shear force increase. Moreover, the welding current of 8kA with clamping load of 3.5 bar gives the optimal value.

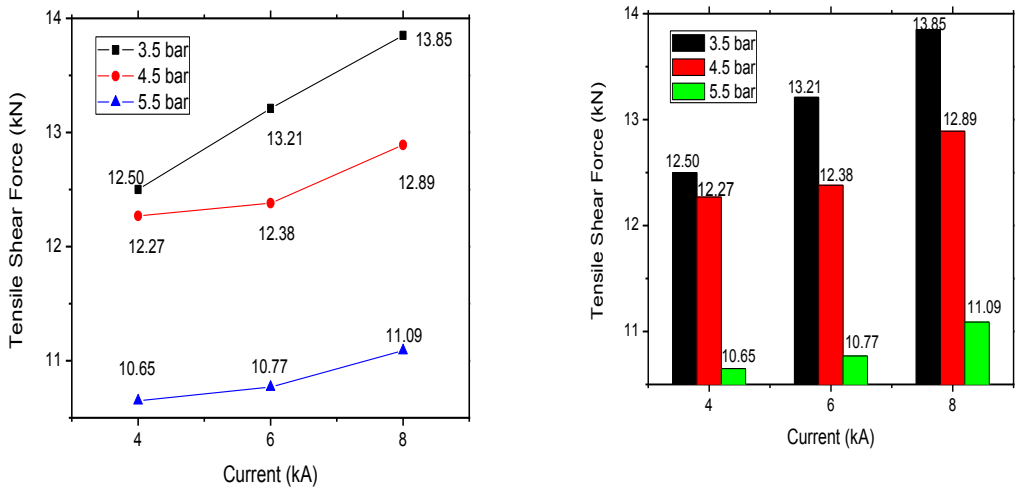

Figure 6.29. Effect of current on tensile shear strength at different parameters at 15 cycles weld time.

6.5.3. Tensile Shear Load Bearing Capacity vs Clamping Load With Current

What we found also in Figure 6.30. When increase the welding current from 4kA to 6kA, the tensile shear will be increased, and the increased value is 0.025. While increasing the welding current from 4kA to 8kA, the tensile shear will be increased,

and its increasing value is 0.122. Finally, when increase the welding current from 6kA to 8kA, the tensile shear force will be increased, and the increased value is 0.093. The above results are under clamping load of 3.5 bar. The tensile shear is increased and it's increased valued is 0.023 when increasing the welding current from 4kA to 6kA and its value is also, increasing when increase the welding current from 4kA to 8ka with increasing value of 0.096 while it is increasing when increase the welding current from 6kA to 8kA with increasing value of 0.071. The above-mentioned results are under clamping load of 4.5 bar. When increase the welding current from 4kA to 6kA, 4kA to 8kA and 6kA to 8kA with clamping load of 5.5 bar, the tensile shear will be increased accordingly and the increasing values are 0.011, 0.034 and 0.022 respectively. It must be mentioned that the welding time value to the above results is 25 cycles.

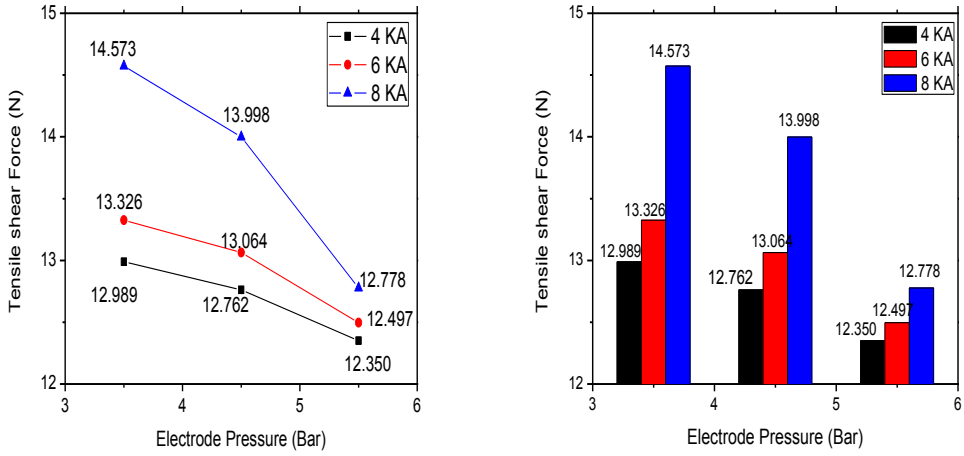

Figure 6.30. Effect of force on tensile shear strength at different parameters at 25 cycles.

Also, in this work we found in Figure 6.31 that when increase the welding current from 4kA to 6kA, the tensile shear will be increased, and the increased value is 0.056. While increasing the welding current from 4kA to 8kA, the tensile shear will be increased, and its increasing value is 0.11. Finally, when increase the welding current from 6kA to 8kA, the tensile shear force will be increased, and the increased value is 0.048. The above results are under clamping load of 3.5 bar. The tensile shear is increased and it's increased valued is 0.0089 when increasing the welding current from 4kA to 6kA and its value is also, increasing when increase the welding

current from 4kA to 8ka with increasing value of 0.051 while it is increasing when increase the welding current from 6kA to 8kA with increasing value of 0.041. The above-mentioned results are under clamping load of 4.5 bar. When increase the welding current from 4kA to 6kA, 4kA to 8kA and 6kA to 8kA with clamping load of 5.5 bar, the tensile shear will be increased accordingly and the increasing values are 0.011, 0.041 and 0.029 respectively. It must be mentioned that the welding time value to the above results is 15 cycles.

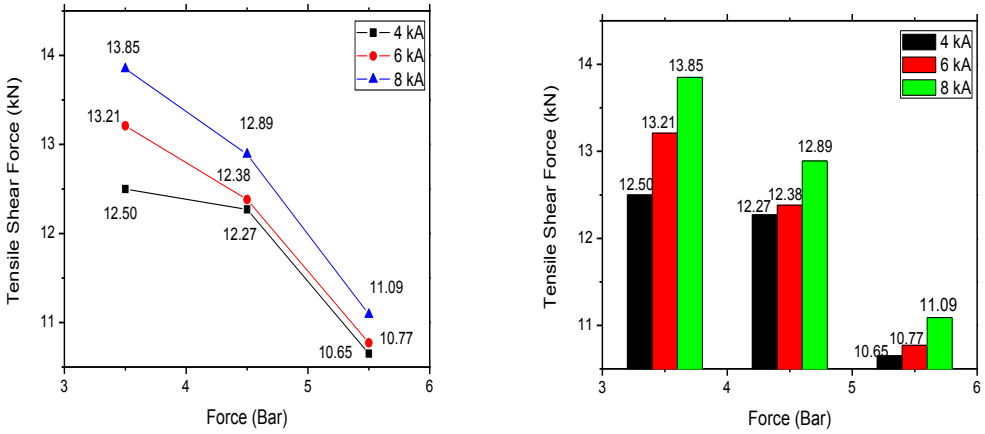

Figure 6.31. Effect of force on tensile shear force values obtained at 15 cycles weld time.

The effect of force of tensile shear strength is negative relationship between the force and tensile shear strength as shown above in the figure 6.30 and 6.31. three curves it is the relationship between the effect of force 3.5, 4.5 and 5.5 Bar with the current for each of 4, 6 and 8 respectively. We notice at these curves that curve where its current value is 8 kA at the force 3.5 Bar. It is considered the highest value for tensile shear strength and this curve decreases by increasing the load from 3.5, 4.5 and 5.5 Bar which means negative relationship with high decrease from the fore 5.5 Bar. While in terms of the curve which is the same current 6 kA, we realize that the curve looks like the curve with current 8 but the value of the curve is less than the previous values. As well as, the value of tensile shear decreases when increase also, we notice that the third curve represents the least values and it has negative relationship with the force and the value of current is 4.that means when increase the clamping load after 3.5 Bar the tensile shear force will decrease.

6.5.4. Effects of the Clamping Load on Nugget Formation

Figure 6.32 shows that when increase the welding current values from 4kA to 6kA, 4kA to 8kA and 6kA to 8kA, the nugget diameter values will be increased and the increasing values are 0.11, 0.49 and 0.34 respectively. The clamping load for the above results is 3.5 bar. What we showed also, the nugget diameter values would be increased, and the increased values are 0.181, 0.61 and 0.36 when the welding current values increase from 4kA to 6kA, 4kA to 8kA and 6kA to 8kA respectively. The clamping load to the above results is 4.5 bar. Lastly, at clamping load value of 5.5 bar, we found that the nugget diameters are increased, and the increased values are 0.27, 0.68 and 0.33 when increase the welding current values from 4kA to 6kA, 4kA to 8kA and 6kA to 8kA respectively. It must be mentioned that the welding time is 25 cycles.

It is clear from our results that when increase the clamping load more than 3.5 Bar, the Nugget formation will decrease. Moreover, the welding current of 8kA with clamping load of 3.5 bar gives the optimal value.

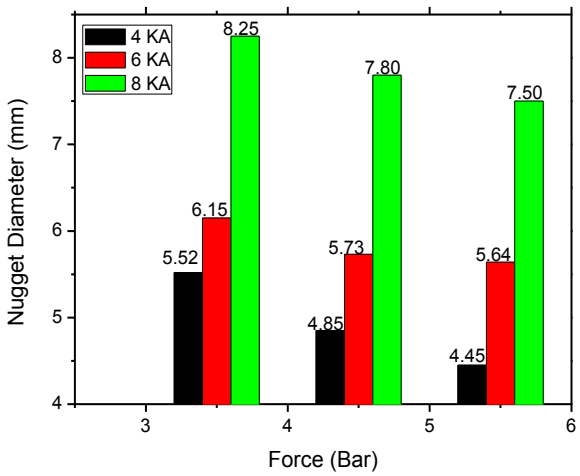

Figure 6.32. Effects of the clamping load on nugget formation at time 25 cycles.

Figure 6.33 shows that when increase the welding current values from 4kA to 6kA, 4kA to 8kA and 6kA to 8kA, the nugget diameter values will be increased and the increasing values are 0.27, 0.66 and 0.31 respectively. The clamping load for the above results is 3.5 bar. What we showed also, the nugget diameter values would be

increased, and the increased values are 0.35, 0.85 and 0.37 when the welding current values increase from 4kA to 6kA, 4kA to 8kA and 6kA to 8kA respectively. The clamping load to the above results is 4.5 bar. Lastly, at clamping load value of 5.5 bar, we found that the nugget diameters are increased, and the increased values are 0.372, 0.91 and 0.39 when increase the welding current values from 4kA to 6kA, 4kA to 8kA and 6kA to 8kA respectively. It must be mentioned that the welding time is 15 cycles.

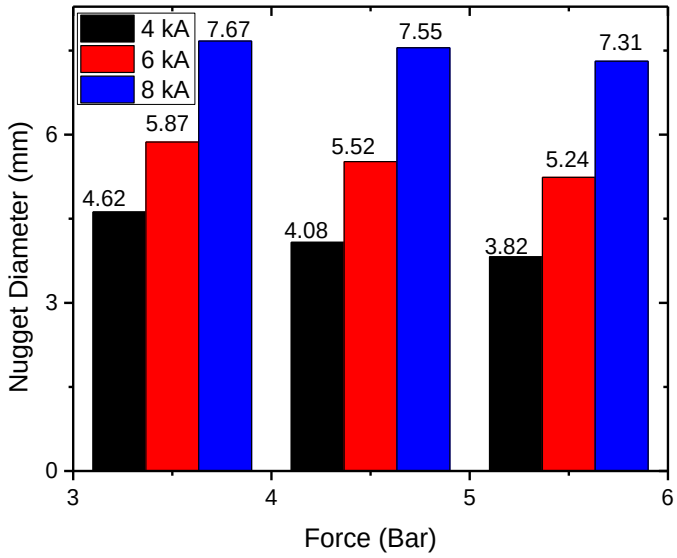

Figure 6.33. Effects of the clamping load on nugget formation at time 15 cycles.

The Figure 6.34 focuses and discloses the relationship between diameter of the nugget and the electrode load (clamping load) in spot welding with comprise the results of this research (Experiment), software results (Simufact simulation) and literatures results. The main factor for in the experiment presented is the nugget diameters as known. This is because of the different diameter of nugget is main reason for increasing/decreasing or changing of strength values. In order to achieve and see/obtain the preferred strength or optimization of mechanical properties in junctions of RSW, experimentally studies and may simulation studies be useful. That's way, in this study have been performed.

As clear in the blue curve, the results of this research refer to that effected of clamping load on the nugget diameter increases gradually to some extent point from

the load which is 3.5 bar and then it decreases by increasing the clamping load. While in terms of software results, the diameter increases by simple increasing or curving to the amount of the clamping 4.5 Bar and then decreases by increasing that clamping. Finally, other researchers or literatures results, It must be mentioned that effect of clamping load on nugget diameter starts from 1.5 Bar and the nugget diameter is simply increasing at the beginning and then increases to the maximum diameter during the load with 3.5 Bar and then decreases steeply.

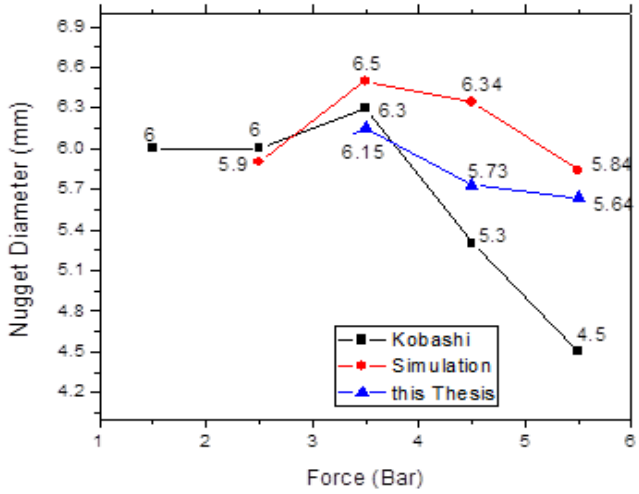

Figure 6.34. Comparison between the of the original results with simulation and researcher results on clamping load on nugget formation.

In this study, nugget formation during RSW have been studied by experimental also software analysis and results of them given by comparatively with close literature results. The effect of the clamping load on nugget growth was studied via experiment with a load range of 3.5 Bar to 5.5 Bar with increment 1 Bar and via simufact software simulation with a load range of 2.5 Bar to 5.5 Bar with increment 1 Bar. The experimental results of the relationship between the diameters of the nugget with the magnitude of the load is shown in Figure 5.1. And Figure 5.2. In literature the effect of clamping load on nugget formation and nugget diameter also studied by several researcher T. Kobashi et. al [128] used a load range of 1.5 Bar to 5.5 Bar with increment 1 Bar in their studied. They reported these effects that increasing the clamping load creates two conflicting effects: expanding the heated contact area and diffusing the current density. Experimental results of different clamping load versus

nugget size diameter of the weld samples of 6 kA and 25 Cycle have been given for comparing with simufact simulation results of these samples and results of T. Kobashi et. al. from literature at Figure 35 The clamping load amounted 3.5 have been shed with each of value of the welding current 4, 6 and 8. It is found that the diameter of nugget at the current 8 is greater than 4 and 6 and when increase the value of the load from 3.5 to 4.5 bar the value of the nugget diameter has decreased and when the value of the load has increased again to 5.5 bar, the value of diameter has decreased more. Then, these values are derived at the time 15 and 25 and it is noticed at these results that the value of diameter with time 25 is greater than the value of diameter in time 15 as shown in the figure. Maximum nugget dimeter is obtained by 3.5 Bar - 8 kA samples at 25 cycles welding time and minimum nugget diameter was obtained by 5.5 Bar - 4 kA samples at 15 cycles welding cycles, It is obvious that the current value of 8 kA and 3.5 Bar are the most effected than 6 and 4 kA and 4.5 and 5.5 Bar respectively. The nugget dimeters decreasing with increasing clamping load more than 3.5 Bar, could be evaluated as have been almost the same for different current samples.

As clear in the Fig. 6.35 above. It is obvious definite there are similarity in the results of this thesis and Simufact results, while there are some different between these results compared with other researchers, thus because there are different in the parameters such as materials, Electrode diameter and materials thickness etc.

6.6. EFFECTS OF WELDING CURRENT ON NUGGET FORMATION

The main factors in the experiment presented in this Figure 6.35 and Figure 6.36 are the nugget diameters. This is because of the different diameter of nugget release change the strength of RSW junctions. Also, to obtain and preferred nugget diameter, to accomplish the true and precise value of welding current or other parameters.

When the subject is about increasing the thickness, a higher welding current may be necessary to present and generate a nugget. This requires the use of a much larger diameter of nugget. The use of a higher welding current joined with the application of a larger diameter electrode generates a greater weld nugget. It is significant to sign

that the large welds of diameters have high strength capabilities. In this Fig., the impact for each of the nugget diameters with welding current are obviously seen with the differences and similarities.

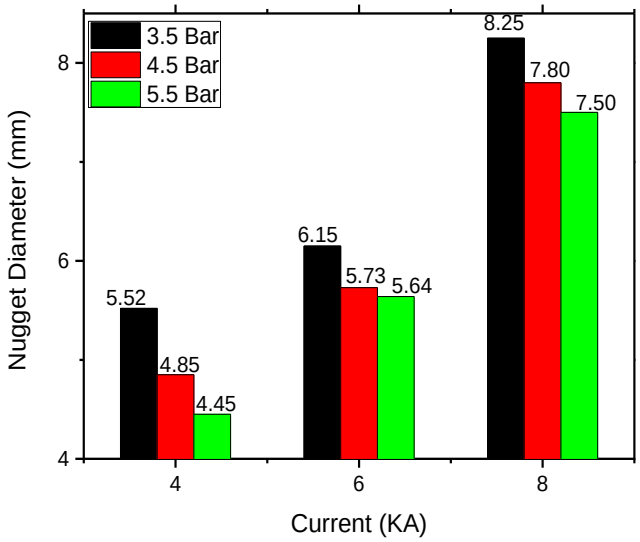

Figure 6.35. Effect of the current on nugget formation at 25 cycles weld time.

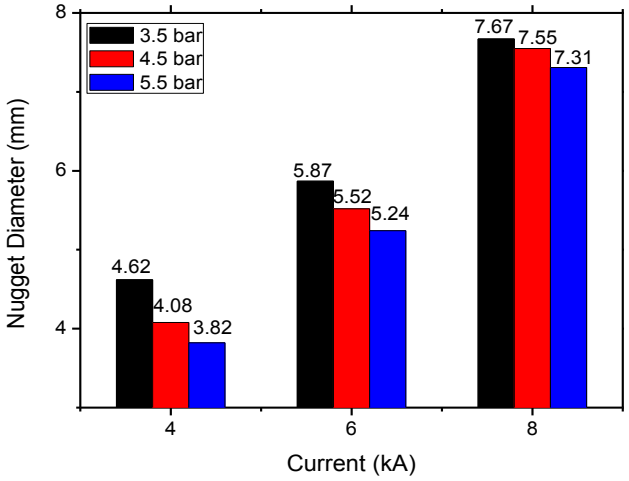

Figure 6.36. Effect of the current on nugget formation at 15 cycles weld time.

The main factors in the experiment presented in this Figure 6.35 and Figure 6.36. are the nugget diameters. This is because of the different diameter of nugget release change the strength of RSW junctions. Also, to obtain and preferred nugget diameter, to accomplish the true and precise value of welding current or other parameters.

When the subject is about increasing the thickness, a higher welding current may be necessary to present and generate a nugget. This requires the use of a much larger diameter of nugget. The use of a higher welding current joined with the application of a larger diameter electrode generates a greater weld nugget. It is significant to sign that the large welds of diameters have high strength capabilities. In this Fig., the impact for each of the nugget diameters with welding current are obviously seen with the differences and similarities. Instead, the effects of welding factors on the nugget size are reliable with the effect and influence of the welding factors on the mechanical possessions of joins. Later, it is rationally to follow that the welding influences the nugget size, whereas the mechanical properties of the sample are straight organized by the size of synthesis. When the electrode pressure and the current is too low, it is not possible to form the nugget because the temperature generation is less than the required temperature in order to melt the joint [184]. When the current increase, the heat production will be increased quickly and then the heat accumulates between the basic mineral. Thus, the upper and lower steel plate will be melted in order to form the nugget formation process. When the current of nugget is more than the critical value, the heating speed will be quick because of the high welding current [185]. Since the effect of electric cooling is basically completed through the cooling water cycle, the generated heat in welding joint cannot be exported quickly through the electrode under the condition of fast quick heating quick. The corona bond around the nugget may not configured yet and the high temperature molten steel extrudes out of the joint and then it forms splashes, that results in the dimensions of decreased nugget, and shrinkage which may occur more easily. At this time, the corona bond around the nugget would not yet have formed, and the high temperature molten steel extrudes out of the joint and then it forms splashes that results in the dimensions of nugget reduced and shrinkage which could happen more easily. Figure 6.35 shows the relationship between average of current and diameter of the nugget at the welding time 25. Each of the load of 3.5, 4.5 and 5.5 have been used with the current 4, 6 and then with 8. As shown in Figure 4, it is found that whenever the value of current is increased from 4 to 6, the value of diameter is increased and also when increase the current from 6 to 8 kA, the value of diameter is increased more than the first increase. As well as, we found that the value of diameter at the load 3.5 Bar is greater than 4.5 and 5.5 bar. Therefore, we

conclude that that the greatest value of welding diameter at the current 8 kA and clamping load 3.5 Bar. Moreover, same values of clamping and current are used and the same relationship between intensity of current and diameter of nugget, but the time of welding has been changed from 25 to 15. So, it is noticed as shown in the Figure 6.36. that diameter of nugget in each of the stages at the current 4, 6 and 8 and at the load 3.5, 4.5 and 5.5 at the welding time 25 greater than the diameter of nugget at the time 15 Cycles. Thus, we concluded that the greater diameter of the nugget is at the load 3.5, current 8 and welding time 25 Cycles.

In this thesis, in addition to experimental study, simulation using simufact software have also been made for comparing with experimental results and estimating more results without doing more experiment. Weld current and weld clamping load with two different cycle have been studied in experiment Figure. 6.37 clearly indicates and reveals the results of the effectiveness of welding current on nugget size through a comparison between the results of this thesis and the results of simulations and other researchers. As seen this graphic, in experimental studies, nugget dimeter is changing from 4.85 to 7.8mm with increasing current from 4 up to 8kA with 4.5 Bar and in literature was changing from 4.3 to 7.2mm and with Simufact Simulation was changing from 3.6 to 7.05mm when kept the clamping load fixed 4.5 Bar.

In condition of kept constant clamping load as 3.5 Bar, Maximum nugget dimeter is obtained by 3.5 Bar - 8 kA samples and minimum nugget diameter was obtained by 5.5 Bar - 4 kA samples, it is obvious that the current value of 8 kA is the most effected than 6 and 4 kA.

The nugget dimeters decreasing with increasing clamping load more than 3.5 Bar, could be evaluated as have been almost the same for different current samples. It was obvious to assert that from the seen the results the welding time had a very minor effect on the nugget size in comparison with welding current whereas the electrode force was kept slightly constant. The strength and properties of welding are determined and thus, the main body through quality of the weld nuggets. As mentioned literature [186], the most efficient parameters in this process are usually: the current intensity, the welding time, the sheet thickness and that of the material,

the geometry of the electrodes and electrode tip diameter, and the electrode force. In the most carried out researches [187], a mechanical electrical thermal coupled model in a finite element analysis environment is created. Via simulating this process, the phenomenon of nugget formation and the effects of process parameters on this phenomenon could be simulated and understood. As showed comparatively with literature in experimental results of resistance spot welding of DP600 sheet steel like other metal sheet such as Al and Mg, it was observed that the nugget diameter is increasing with increasing currents but decreasing with increasing clamping load.

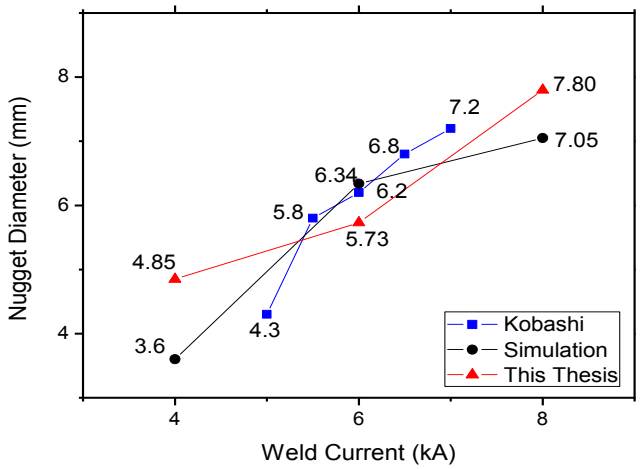

Figure 6.37. Changing of the nugget diameter with weld current. At this Fig, simufact simulation, a literature.

The three curves in the Figure 6.37 are influenced and impacted differently due to the increase in the welding current as this increment creates an increase for nugget size diameter, through this there is a revealed observation that shows the similarities in the results and closed to each other which indicates a level of success.

6.7. THE FAILURE MODE ANALYSIS OF TENSILE TESTED DP600

In the experimental material part, various failure modes of resistance spot welding of DP600 steel are analyzed, of tensile specimen observed by scanning electron microscope (SEM). The fracture mode in most of the samples occurs at BM and HAZ regions. Images for each region (BM, HAZ and FZ) were taken by SEM device as shown in Figure 6.38 a), b) and c).

There are usually two phases in the microstructure DP steel, body centered cubic (bcc) ferrite and body center Tetragonal martensite as in Figure 6.38 (a), while (b) the Micro-component Martensite and ferrite in HAZ are thinner than either of BM and FZ. Due to Incomplete austenitization in HAZ and form the grain of austenite. So, the lath Martensite is thought to form and contains very thin Lath or retained austenite between laths, and There may be some lower bainite as in Figure 6.38 (c).

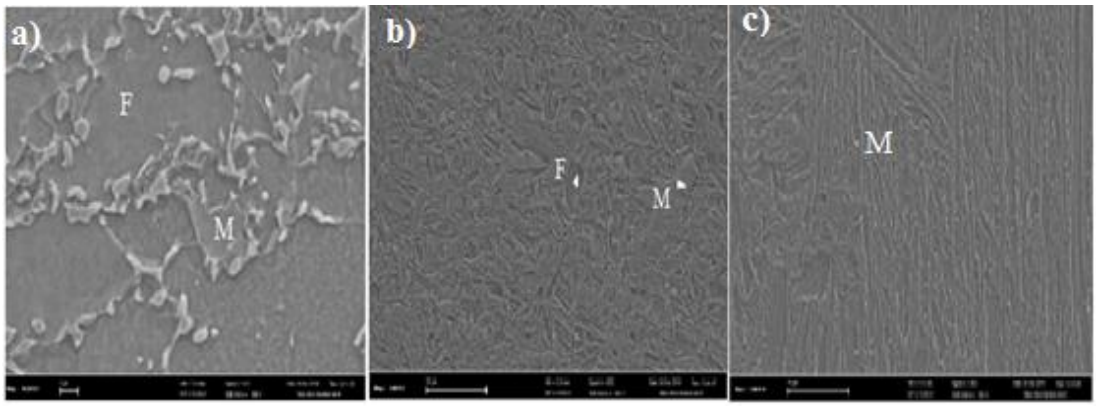

Figure 6.38. The microstructure of DP600 a) BM, b) HAZ and c) FZ.

To identify the type of failure mode, macroscopic inspection was made on the spot-welding samples, which passed the tensile shear strength. The PF is generally always preferred to the failure mode. The failure occurs at base metal in Figure 6.39, The pullout failure mode at HAZ in Figure 6.40 and Figure 6.41 in the same region.

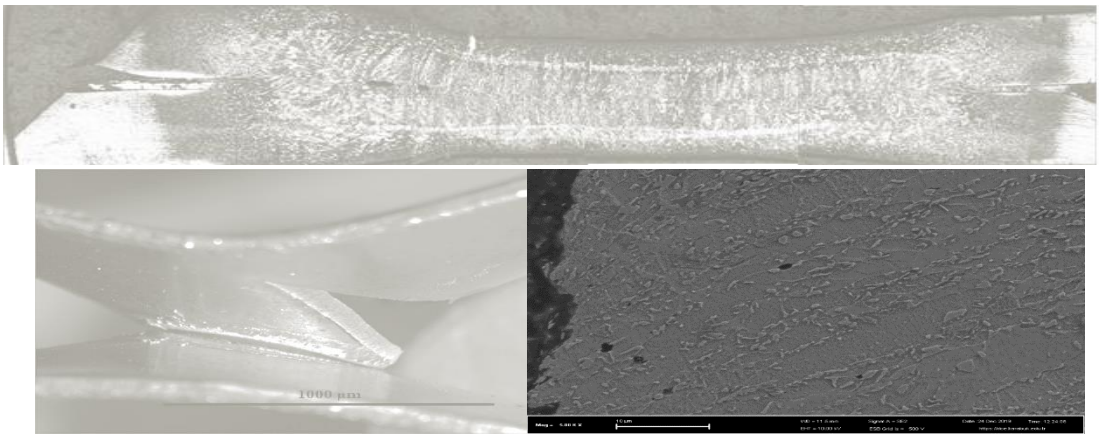

Figure 6.39. Failure mode in resistance spot welding for BM.

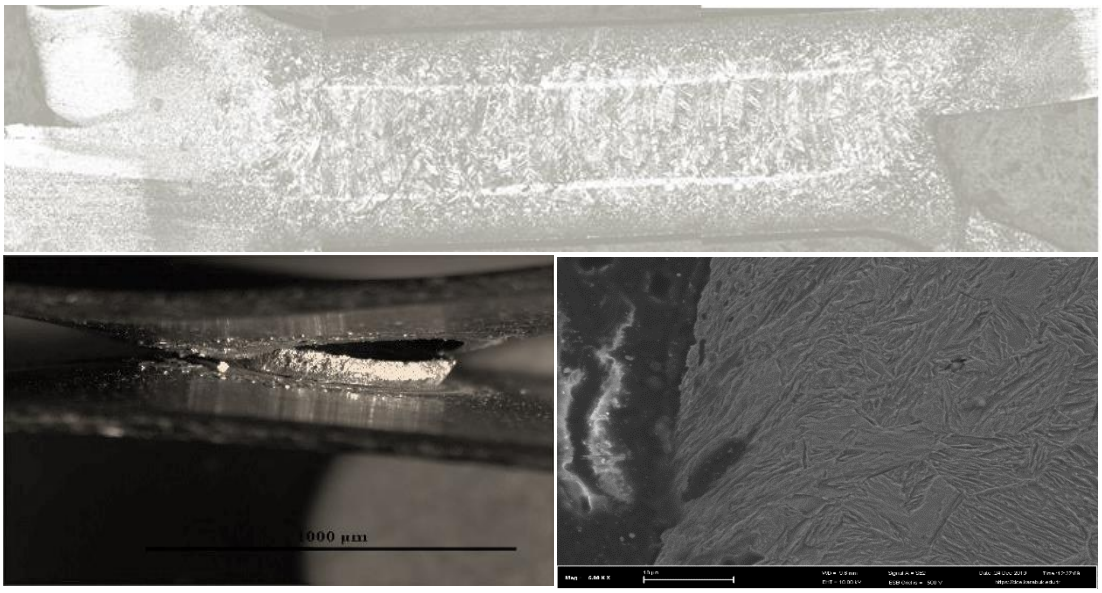

Figure 6.40. Failure mode pull out in resistance spot welding for HAZ.

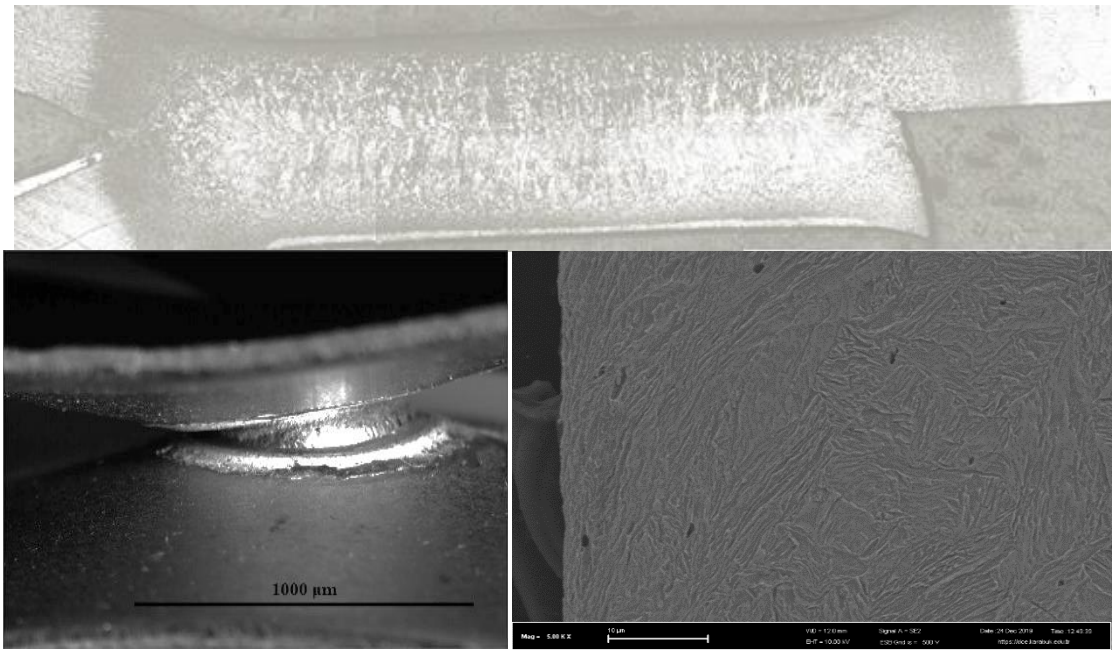

Figure 6.41. Failure mode pull out in resistance spot welding for HAZ.

6.8. HARDNESS MEASUREMENT

Hardness is essentially crossed on the joint surface. While the FZ zone's hardness values are more than 400-450 and for the HAZ which is 300-350 HV it can be connected to the martensite and the bridal ranks, hence, and the hardness of the Bas

bass are estimated to be less than 300 HV per HV and then it can be attributed to the ferrite phase [188].

The chemical composition and initial microstructure of the BM determine the hardness profile of spot welds of carbon steels that may show hardening in FZ and HAZ in addition to softening in the HAZ.

$$\text{Hardening ratio} = \frac{\text{HFZ}}{\text{HBM}} = \frac{410.13}{200.4} = 2.05\ HV \quad (6.1)$$

$$\text{Softening ratio} = \frac{\text{Hmin}}{\text{HBM}} = \frac{200}{200.4} = 1.0\ HV \text{ , For welding time 25 Cycles}$$

Where HBM, HFZ and Hmin are BM hardness, FZ hardness and minimum hardness in HAZ.

$$\text{Hardening ratio} = \frac{\text{HFZ}}{\text{HBM}} = \frac{400}{190} = 2.1\ HV \quad (6.2)$$

$$\text{Softening ratio} = \frac{\text{Hmin}}{\text{HBM}} = \frac{281}{190} = 1.48\ HV \text{ , For welding time 15 Cycles.}$$

Figure 6.42, Figure 6.43 and Figure 44. shows that Nugget hardness is 2.05 times greater than the hardness of the base metal, and about 1.9 times the HAZ is valued at approximately 410.13 HV and valued at approximately 200.4 HV and 213.68 HV for base metal and affected heat zone respectively for weld time 25 Cycles. Nugget weld strength is 2.05 times more than base metal, which is consistent with the results reported by Rathbun et al. [32]. For welding time 15 Cycles, nugget hardness is 2.1 HV times greater than the hardness of the base metal and about 1.2 HV more than HAZ hardness. Nugget expresses more hardness and strength to the martensite formation. Figure 6.42 shows that the hardness at clamping load of 3.5 bar is greater than the hardness with clamping load of 4.5 bar and 5.5 bar.

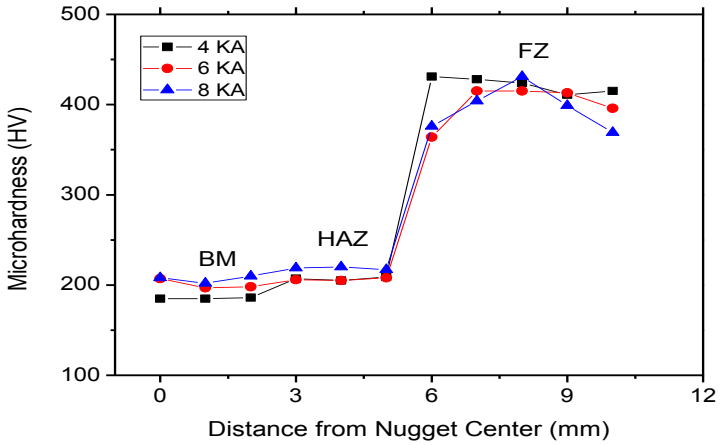

Figure 6.42. Microhardness profile with force 3.5 bar at different current.

It is shown in Figure 6.43 that the hardness at FZ is more than HAZ and BM. We can conclude from this result that hardness at spot welding is always better. Also, when increase the welding current the hardness will be increased.

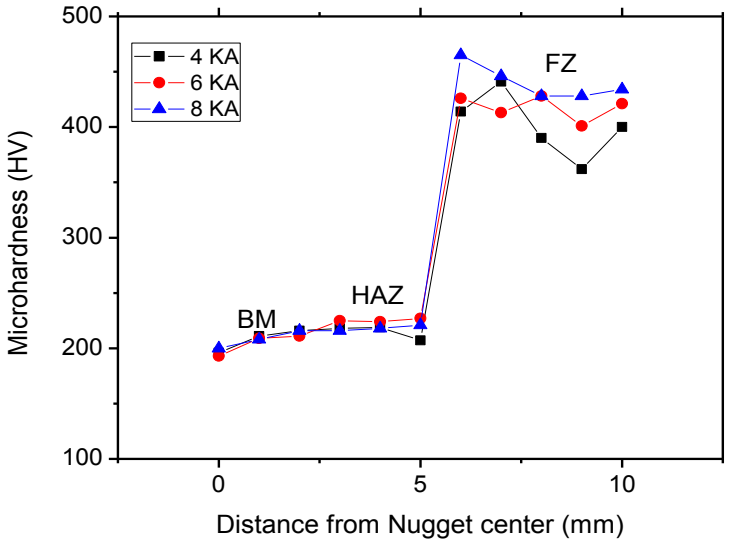

Figure 6.43. Microhardness profile with force 4.5 bar at different current.

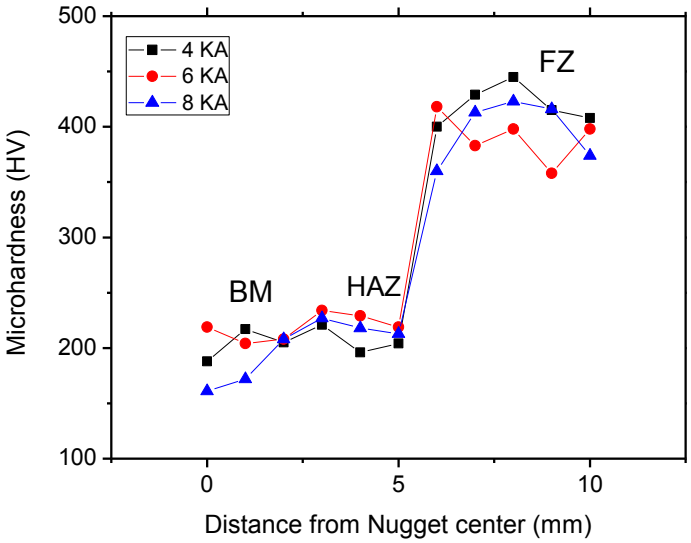

Figure 6.44. Microhardness profile with force 5.5 bar at different current.

It is clear from Figure 6.44 that when increase the clamping load up to 5.5 bar, the hardness at welding current 8 kA is less than the hardness with welding current 4 kA.

6.9. RESIDUAL STRESS

The residual stress values of specimen's vs clamping force have been given at Figure 6.45 and Figure 6.46. Cutting method with strain gauge is generally used to understand stress type and content in specimens as a destructive technique. Stress values were calculated via Hooke's law after strain values obtained via software during cutting. The following formula was used to calculate stress measurement results.

$$\sigma_{longitudinal} = -E.\varepsilon \tag{6.3}$$

Where $\sigma_{longitudinal}$ is the residual stress, E is the elastic modulus of steel sheet and ε is the strain value. Results clearly show that compression stress which play important role to enhance the mechanical performance of materials. The value of 6 kA welded samples, 5.5Bar possess highest stress, which can exhibit better hardness and strength. When welding current changed, compressive residual stress increases.

At clamping load 3.5, 4.5 and 5.5Bar with 6 kA welded sample has 19.1, 24 and 27.2 MPa stress value as shown in Figure 6.45, So, it can be deduced that the clamping load might be more effective than welding current to determine the residual stress performance these results at welding time of 25 Cycles. However, at 15 weld time of 15 cycles, also the value of 6kA welded samples but with4.5 Bar possess highest stress, which can exhibit better hardness and strength, instead of 5.5Bar. When welding current changed, compressive residual stress increases. The value was 34.2 MPa as shown in Figure 6.46.

Residual stress values give information about the mechanical properties of materials. If it is known, fatigue and tensile properties of specimens can be predicted. If the compressive residual stress is higher, material exhibits better fatigue performance. If the specimens have tensile residual stress, fatigue performance is lower. So, researchers can see the mechanical performance of specimens after welding process via residual stress measurement with strain gauge technique which is practicable and economic process compared to other techniques.

We noticed that when increase load, the stress will be increased. At the load 3.5 bar, we found that the stress at 8kA is higher than the stress at 4kA and 6kA. While at the load 4.5, 5.5Bar, it is found that stress at 6kA is higher than 4kA and 8Ka respectively. These results are at the time 25 cycle. Whereas at 15 cycle, we found that the highest stress is at the load 4.5 bar and 6kA.

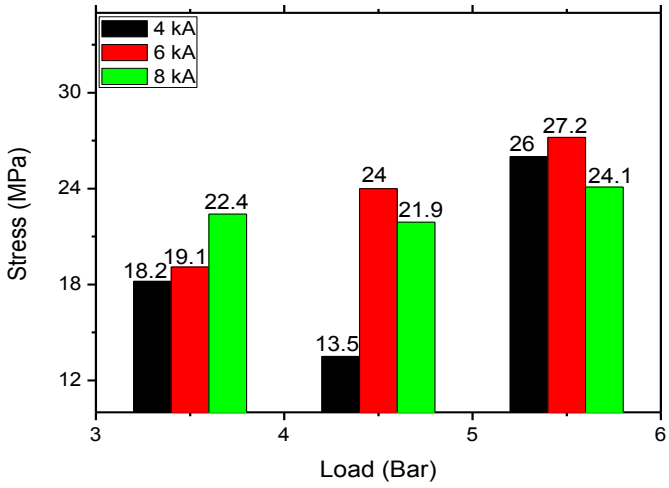

Figure 6.45. Residual stress values of samples at time of 25 cycles.

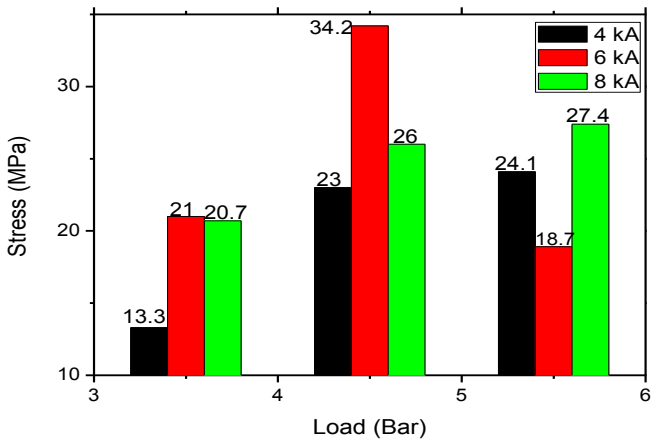

Figure 6.46. Residual stress values of samples at time of 15 cycle.

6.10. MINITAB TAQUCHI

Taguchi parametric design methodology has been adopted. The experiments have been performed by the use of L27 Orthogonal Array (OA) with two parameters (electrode force and weld current) with three levels (level 1, level 2 and level 3). the process parameters, their symbols and their values at different levels.

The values in the tables and curves the tensile test results and Nugget Diameter results that they are clearly with the facts compared to the results of Taguchi and Minitab 17 software, with current (I) parameters of 4,6 and 8 KA parameters other fixed, force (F) 3.5 bar. We get the maximum load when it is built 3.5 bar with 8 KA. In addition, a steady stream of 3.5 was prepared with different forces 3.5, 4.5 and 5.5 bar.

6.10.1. Taguchi Design

Taguchi Orthogonal Array Design

L27(3^2)
Factors: 2
Runs: 27

Optimization of Results with Taguchi Method obtained as a result of the experiments made according to the experimental setup of the tensile-shear strength values of Taguchi. The results obtained from the experiments with the help of the method Converted to Signal / Noise ratio and decibels Strength and Signal / Noise ratios.

$$S/N = -10\log\left(\frac{1}{n}\sum_{t=1}^{n}\frac{1}{yi^2}\right) \quad (6.4)$$

yi: Performance response, i: the observation value, n: indicates the number of tests in one trial. S / N of pull shear according to" largest best". The graph showing the rate change.

6.10.2. Tensile Shear Strength

For maximum tensile shear the optimum combination of experiments determined. This result increases the parameter values for optimum tensile shear values has been reached. The use of Taguchi experiments to find out which parameter values should be used to achieve optimum test results of tensile shear strengths of welded parts combined with spot resistance welds. As a result of the experiments, welding current value 8kA, welding time 25 cycles, and electrode force 3.5 Bar values have reached optimum results. In these combinations, maximum tensile shear values were obtained. The results showed that the optimum tensile shear result was achieved with increasing welding parameters.

6.10.2.1. The Effect of Parameters on Signal to Noise Ratio

In this thesis Table 6.3 and graph 6.47 for S/N ratio explain the analysis of Taguchi where it is found that the optimal value of S/N is 22.68 for level (1) of force. this value is found with clamping force of 3.5 bar and 22.77 for level (3) of welding current 8kA. The obtained results by minitab (Taguchi) are compatible with experimental results where the optimal value of the experimental results is found with same value of welding current and clamping load. Taguchi Analysis, the Tensile strength versus force; Current Response for Signal to Noise Ratios Larger is better.

Table 6.3. The response analysis for signal to noise ratios.

Level	F	I
1	22.68	22.07
2	22.45	22.25
3	21.97	22.77

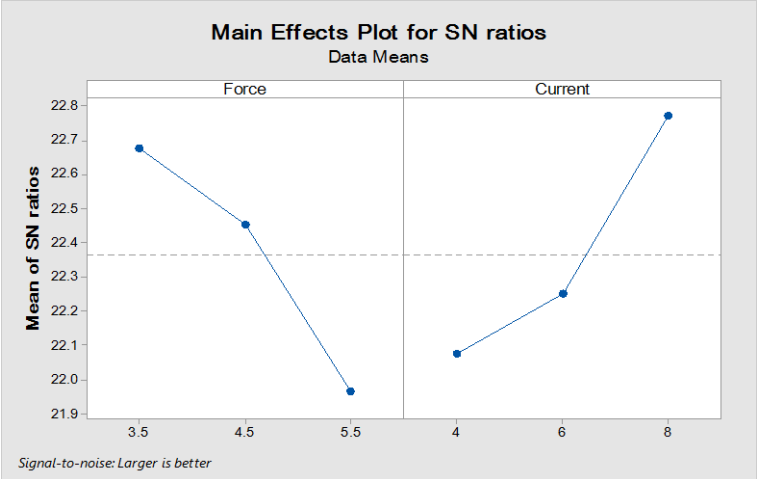

Figure 6.47. The main response effects plot of parameters for signal to noise.

At the left side of Figure 6.48 represents the force effect on single to noise. The relationship between clamping force and single noise is inverse relationship. We notice that at force of 3.5 bar and welding current 8kA, the highest value is 23.271 as it is reported in table 6.4 and increasing the force more than 3.5 bar at fixed current, the plots will be decreased. While the right side of Figure 6.48 represents the effect of welding current on single to noise. The relationship between welding current and single noise is proportional. We notice that when the welding current increases, the single to noise increases accordingly at constant force.

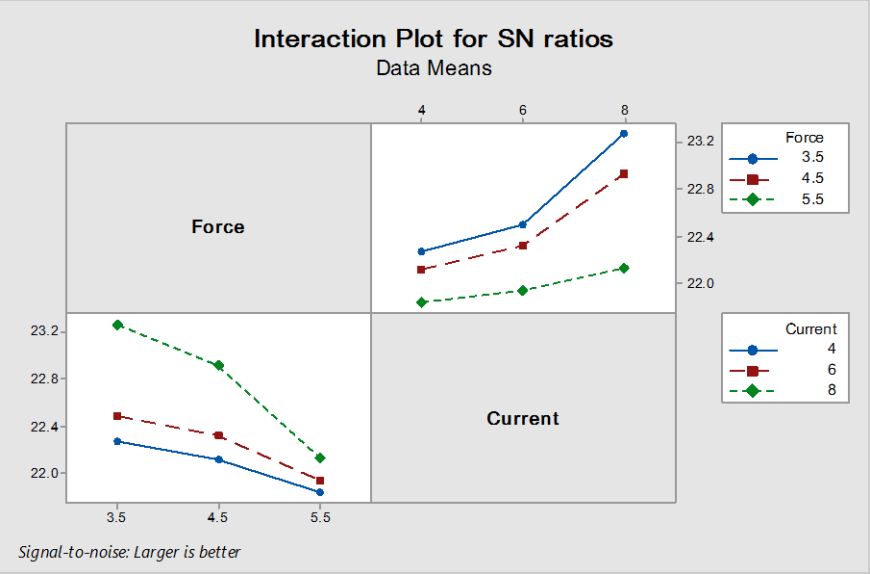

Figure 6.48. Interaction the effect of force and current on signal to noise.

As clear in table 6.4. at maximum tensile strength the signal to noise is maximum, while the signal noise is minimum value is 21.833 at clamping force 5.5 bar and welding current of 4 Ka. when the tensile shear is minimum that mean the signal, noise is depending on the parameters and proportional with the welding current and reverse with clamping load after 3.5 Bar.

Table 6.4. The results of interaction the effect of the parameters for signal to noise.

Force	Current	Tensile shear strength	S/N Ratio
3.5	4	12.989	22.272
3.5	6	13.326	22.494
3.5	8	14.573	23.271
4.5	4	12.762	22.118
4.5	6	13.064	22.322
4.5	8	13.998	22.921
5.5	4	12.350	21.833
5.5	6	12.497	21.936
5.5	8	12.778	22.129

6.10.2.2. The Analysis of Parameters for Means

In Table 6.5 and graph 6.49 for means, explain the analysis of Taguchi where it is found that the maximum value of the means in table 6.5. is 13.63 for level (1) of

force. this value is found with clamping force of 3.5 bar and 13.78 for level (3) of welding current 8kA. Also, it clear in graph 6.49.for the left side for the clamping load the first and second point in permitted region while at right side for the welding current only the first point found it in the permitted region.

Table 6.5. The response analysis for means.

Level	F	I
1	13.63	12.70
2	13.27	12,96
3	12.54	13.78

Figure 6.49. The main response effects plot of parameters for means.

We found that the maximum value at level (1) for clamping load 3.5 bar and at level (3) for welding current 8 KA. This means that the Tensile shear is proportional to the current at a constant force of 3.5 bar. While the force increases more than 3.5 the load when it increases the force.

6.10.3. Nugget Diameter

6.10.3.1. The Analysis of Parameters on Signal to Noise Ratio

Taguchi Analysis, nugget diameter versus Force; Current for S/N Response for Signal to Noise Ratios, Larger is better.

In this research Table 6.6 and graph 6.50 for S/N ratio explain the analysis of Taguchi where it is found that the maximum value of S/N in table 6.6. is 16.32 for level (1) for clamping load of 3.5 bar and 17.89 for level (3) of welding current 8kA. The graph 6.50 it clearly that the first point from both sides of clamping load and welding current in the permitted region. The obtained results also are compatible with experimental results where the optimal value of the experimental results is found with same value of welding current and clamping load, these values investigate the optimum value occur at 3.5 Bar with 8 kA.

Table 6.6. The response analysis for signal to noise ratios.

Level	Force	Current
1	16.32	13.84
2	15.57	15.32
3	15.16	17.89

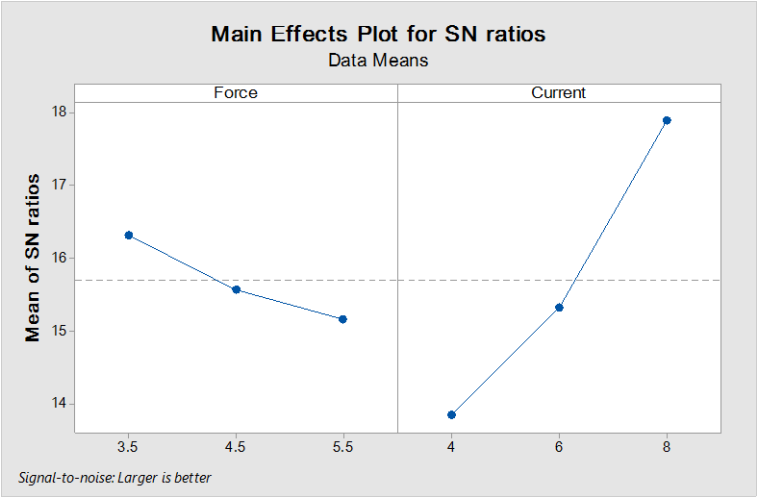

Figure 6.50. Response effect of parameters for signal to noise.

It is clear at the graph of the interaction plot for S/N At the left side of Figure 6.51 represents the Nugget Diameter effect on single to noise. The relationship between the diameter of the Nugget and single noise is inverse relationship with clamping load, while it is proportional with welding current. It is clear that in Figure 6.51 that when the welding current increases, the single to noise increases accordingly at constant force.

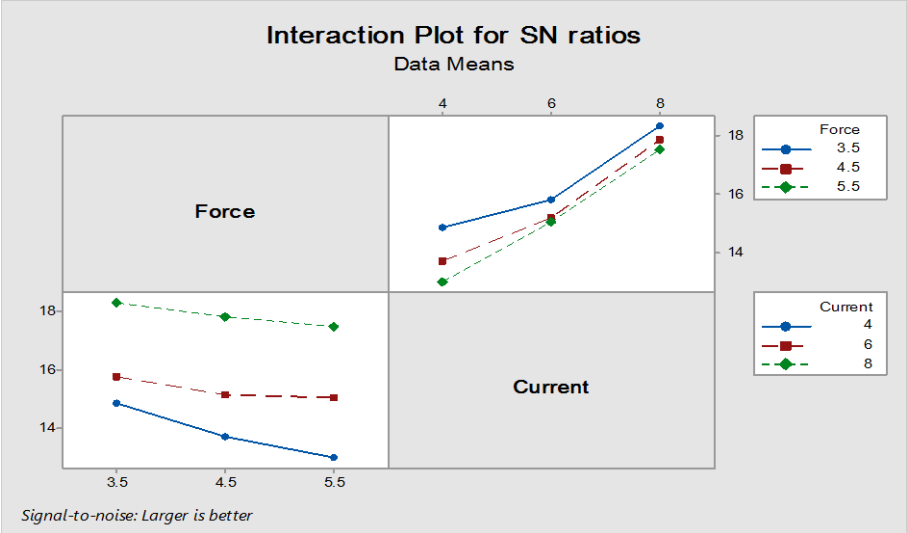

Figure 6.51. Interaction the effect of force and current on signal to noise.

As the results in table 6.7. We notice that at force of 3.5 bar and welding current 8kA, the highest value is 18.329 as it is reported in table 6.7 and increasing the force more than 3.5 bar at fixed current, the plots will be decreased and the minimum value is reported 12.967. While the right side of Figure 6.51 represents the effect of welding current on single to noise.

Table 6.7. The results of interaction the effect of the parameters for signal to noise.

Force	Current	Nugget Diameter	S/N Ratio
3.5	4	5.52	14.839
3.5	6	6.15	15.778
3.5	8	8.25	18.329
4.5	4	4.85	13.715
4.5	6	5.73	15.163
4.5	8	7.80	17.842
5.5	4	4.45	12.967
5.5	6	5.64	15.026
5.5	8	7.50	17.501

6.10.3.2. The Analysis of Parameters for Means

In Table 6.8 and graph 6.52 for means, explain the analysis of Taguchi where it is found that as a results in table 6.8. The maximum value of means is 6.640 for level (1) of force. this value is found with clamping force of 3.5 bar and 7.850 for level (3)

of welding current 8kA. Also it clear in graph 6.52.for the left side for the clamping load and righ side for the welding current only the first point found it in the permitted region.

Table 6.8. The response Analysis for means.

Level	Force	Current
1	6.640	4.940
2	6.127	5.840
3	5.863	7.850

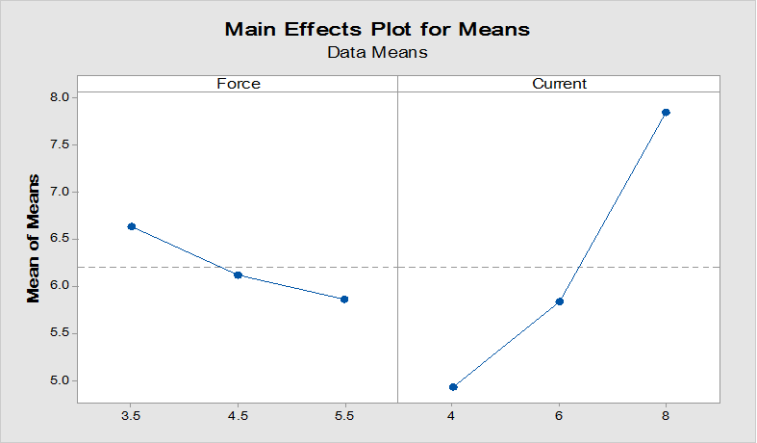

Figure 6.52. The main Response effects plot of parameters for means.

6.10.4. Analysis Variance (ANOVA)

ANOVA gives additional results and which the parameters more effect as shown in Figure 6.42. we have force 3.5, 4.5 and 5.5 bar, and welding current 4, 6 and 8kA. The obtained results of tensile shear test at 3.5, 4.5 and 5.5 bar with results of 4 kA to 8 kA with increment 2 kA, while by using Variance (Anova) we can get the results between that parameters.

6.10.4.1. The Analysis of (ANOVA) For Tensile Shear Strength

The analysis of variance (Anova) is applied to the experimental results to determine that the percentage contribution of each parameter is related to a specific trust level.

It is clear from table 6.9. show the results of tensile shear strength for the parameters of welding current are more effect than that of clamping load.

Table 6.9. Analysis variance (ANOVA) for tensile shear.

Source	DF	Seq ss	Adj ss
Force	2	1.84610	1.84610
Current	2	1.91430	1.91430
Total	8	4.16364	4.16364

Also, by using the analysis of Anove we can get on the results of any parameters for the welding current or clamping load as showing in graph 6.53. we get on the results of tensile shear strength at the parameters of clamping load 3.5, 4.5 and 5.5 Bar and of welding current 4 – 8 kA with increment 2 kA.

The maximum value of the results was at clamping load of 3.5 bar with welding current of 8 kA, while the minimum results at clamping load of 5.5 bar with 4 kA.

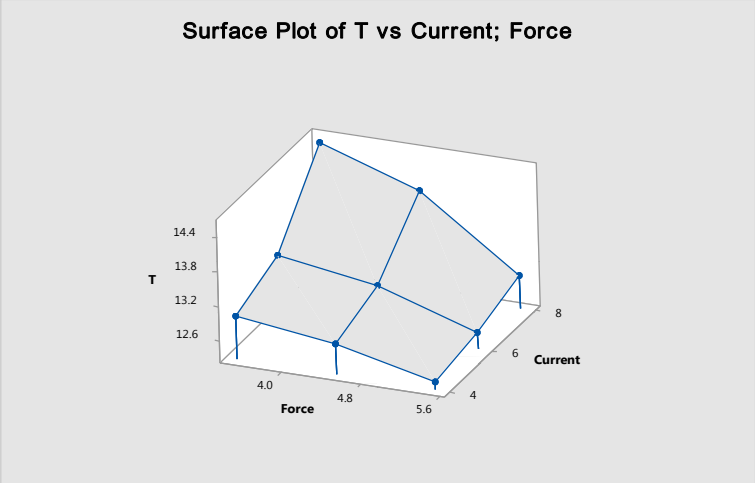

Figure 6.53. The analysis of ANOVA for tensile shear.

6.10.4.2. The Analysis of (ANOVA) for Nugget Diameter

The analysis of variance (Anova) is applied to the experimental results to determine that the percentage contribution of each parameter is related to a specific trust level.

It is clear from table 6.10. show the results of Nugget Diameter for the parameters of welding current are more effect than that of clamping load.

Table 6.10. Analysis of variance (ANOVA) for nugget diameter.

Source	DF	Adj ss	Adj ms
Force	2	2.8082	1.4041
Current	2	39.9546	19.9773
Total		43.0080	43.0080

Moreover, by using the Anove we can get on the results of the nugget diameter for any parameters for the welding current or clamping load as showing in graph 6.53. The max. results were at clamping load 3.5 and 8 kA welding current, while the minimum was at 5.5 bar with 4 kA.

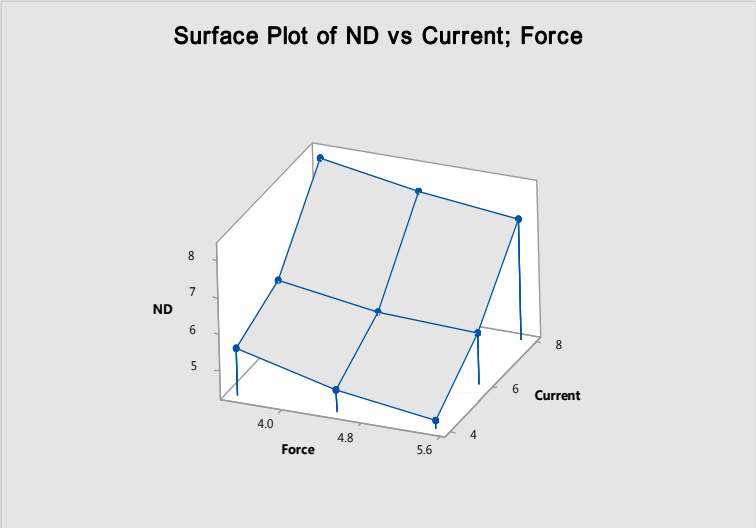

Figure 6.54. The analysis of ANOVA for Nugget Diameter.

PART 7

CONCLUSION

In this study, an experimental study and simulation investigations of resistance spot welding (RSW) were conducted on DP600 sheet steel, which is used in automotive industry, to get the optimum strength values for the strength of welding nugget such as tensile shear force, mechanical properties, microstructure, microhardness, welding nugget size diameter (penetration and indentation) and residual stress. In the experimental work, samples of 15 mm overlap joint were prepared for spot welding from two similar sheets of DP600 steel with dimensions of 100 X 30 X 1 mm. The samples were welded under different parameters. A range of electrode forces from 3.5 bar to 5.5 bar with 1.0 bar increment were applied with 8 mm electrode tip diameter to make the spot welding and for each clamping force three values of welding currents of 4 kA, 6 kA and 8 kA were used. The welding time for all the samples was 25 cycles and 15 cycles. To get the average tensile shear force for each welding procedure, three samples welded with the same parameters were tested. In this research, Simufact software was used to simulate the welding process for a sample with the same dimensions of experimental sample and under the same experimental welding parameters to validate the experimental results of nugget dimension, phase diagram and mass volume fraction. In order to get the optimum values of tensile shear force and nugget size, Minitab software (Taquchi and Anova) results were compared with the experimental results.

From the results of present study, the following conclusions can be made:

- As the welding current increases the tensile shear strength increases at constant clamping load and welding time whereas increasing the clamping load leads to decrease the tensile shear strength at fixed welding current and welding time. Increasing welding time increases the tensile shear strength.

- For the welding time of 25 cycles, at clamping load of 3.5 bar, the tensile strength was 12.989 kN when the welding current was 4 kA, by increasing the current up to 6 kA the tensile shear strength increased to 13.326 kN, the tensile shear strength reached a value of 14.573 kN, which is the optimum value, when the welding current raised up to 8 kA. Increasing the clamping load to 4.5 bar, and applying a welding current of 4, 6 and 8 kA the values of tensile shear strength was 12.762, 13.064 and 13.998 kN respectively. For 5.5 bar clamping force, the tensile strength was 12.350 kN when the welding current was 4 kA, while increasing the welding current to 6 and 8 kA the tensile shear strength was 12.497 and 12.778 kN respectively.
- For the welding time of 15 cycles, at clamping load of 3.5 bar the tensile shear strength was 12.50 kN at 4 kA welding current, increasing the clamping load to 4.5 and 5.5 bar decreased the tensile shear strength to 12.27 and 10.65 kN respectively. Raising up the welding current to 6 kA with applied clamping loads of 3.5, 4.5 and 5.5 bar resulted in tensile shear strength of 13.21, 12.38 and 10.77 kN. Finally, applying 8 kA welding current, the recorded tensile shear strength was 13.85, 12.89 and 11.09 kN at clamping load of 3.5, 4.5 and 5.5 bar respectively.
- According to optical microscopic images and the Scanning Electron microscope (SEM), the phase of base metal contains of a certain amount of hard martensite phase in a soft ferrite matrix, which is changed to a certain amount of ferrite in martensite phase in HAZ while in FZ the phase is almost of lath martensite lath Martensite is thought to form and contains very thin Lath or retained austenite between laths. To identify the type of failure mode, macroscopic inspection was made on the spot-welding samples, which passed the tensile shear strength. the PF is generally always preferred to the failure mode. The failure occurs at base metal in this research almost occur pullout failure mode at HAZ and BM.
- The Simufact software results presented the percentage of volume mass fraction in each zone. Moreover, the Simufact results showed the percentage of main elements in DP600. By using Simufact software we get on that the volume mass fraction of Martensite for different parameters. As welding current increase the volume fraction of martensite is decrease, while the

increase at FZ than that of HAZ and BM, the clamping load does not effect on it. The volume fraction of martensite is about 91.0 to 93 % at FZ and with welding current 4kA whereas the volume fraction of martensite at the welding current 6kA is from 80.0 to 88 % and it is 30 to 70 % with welding current value of 8kA. The volume fraction of ferrite at FZ is about 4% with welding current 4kA while the volume fraction of ferrite at welding current 6kA is about 5-10 % and it is from 7 to 32 % with welding current value of 8kA. When we compare these results with results in the literature review, we can find that the results are too close from each other. The percentage of main elements in DP600 are 0,08% C, 97.48% Fe, 1.86% Mn and 0.18% Cr. The phase diagram of Simufact results agreed with the experimental results reported in the literature.

- It has been clarified enough that the size and mass of the welding nugget and the electrode indentation depth increase with the increase of the welding parameters, while the welding nugget height decreases.
- As the welding current increases the Nugget formation increases at constant clamping load and welding time whereas increasing the clamping load leads to decrease the nugget size at fixed welding current and welding time. Increasing welding time increases the Nugget formation**.**
- For the welding time of 25 cycles, at clamping load of 3.5 bar, the Nugget formation was 5.52 mm when the welding current was 4 kA, by increasing the welding current up to 6 kA the Nugget formation increased to 6.15 mm, the Nugget formation reached a value of 8.25 mm, which is the optimum value, when the welding current raised up to 8 kA. Increasing the clamping load to 4.5 bar, and applying a welding current of 4, 6 and 8 kA the values of Nugget formation was 4.85, 5.73 and 7.80 mm respectively. For 5.5 bar clamping load, the Nugget formation was 4.45 mm when the welding current was 4 kA, while increasing the welding current to 6 and 8 kA the Nugget formation was 5.64 and 7.50 mm respectively.
- For the welding time of 15 cycles, at clamping load of 3.5 bar the Nugget formation was 4.62 mm at 4 kA welding current, increasing the clamping load to 4.5 and 5.5 bar decreased the Nugget formation to 4.08 and 3.82 mm respectively. Raising up the welding current to 6 kA with applied clamping

loads of 3.5, 4.5 and 5.5 bar resulted in Nugget formation of 5.87, 5.52 and 5.24 mm. Finally, applying 8 kA welding current, the recorded Nugget formation was 7.67, 7.55 and 7.31 mm at clamping load of 3.5, 4.5 and 5.5 bar respectively.

- Also, by using the Simufact software as the welding current increases the Nugget formation increases at constant clamping load and welding time whereas increasing the clamping load leads to decrease the nugget size at fixed welding current and welding time. Increasing welding time increases the Nugget formation**.**
- At clamping load of 2.5 bar, the Nugget formation was 5.9 mm, increase the clamping load up to 3.5 the nugget diameter increase to 6.5 mm at 6 kA whereas the nugget formation were 3.7, 6.5 and 7.9 mm at 4, 6 and 8 kA respectively at 3.5 bar and welded time of 25 cycles, while at 15 cycles were 4.3, 6.2 and 6.8 mm. when increase the load to 4.5 the nugget size was reduced to 6.34 mm finally the clamping load increased up to 5.5 the nugget formation decreased and reached to 5.64. At the case of welding current 4 kA the nugget diameter was 3.6 mm while when increase the welding current from 4 to 6 kA the nugget formation also increases to 6.34 and then reached to 7.05 mm at welding current 8 kA.
- The optimum values of the nugget formation for different welding parameters were estimated and compared with experimental results and there was a good agreement between both results. which was that values at welding current 8 kA and 3.5 bar clamping load.
- The experimental results of this study were compared with the Simufact software and the simulation results reported by Kobashi, who used Abaqus software to predict the size and the shape of the nugget for steel sheet metal. The comparison showed that the behavior of the clamping load and welding current effects on the nugget size is the same in all studies mentioned above, in which the optimum nugget diameter occurs at 3.5 bar.

  In the case of clamping load, the nugget diameter for the Simufact results are higher than the experimental results. The maximum difference was about 0.61 mm at 4.5 bar clamping load whereas the minimum difference was 0.2 mm at 5.5 bar. The nugget diameter results of Kobashi are higher than that of

experimental results before the optimum clamping load, after that the kobashi results start to drop to reach the maximum difference of 1.14 mm less than the experimental results at 5.5 bar clamping load. For the case of welding current, the maximum difference in results of nugget diameter between the Simufact software results are less than the experimental results by 1.25 mm at 4 kA. While the maximum difference between Kobashi and experimental results are 0.7 mm at 5 kA.

- The microhardness at FZ is higher than that of HAZ and BM as a result of the microstructure of the FZ is almost martensite phase. Increasing the welding time causes an increase in hardness. The results showed that the FZ hardness ratio is 2.05 times greater than the hardness of the BM metal, and about 1.9 times the HAZ. The value of hardness at FZ approximately 410.13 HV whereas It is 200.4 HV and 213.68 HV at BM and HAZ respectively. Softening ratio is 1.0 HV, these results at welding time of 25 cycles. For 15 cycles welding time, the FZ hardness was 400 HV, 336.1 HV and 190 HV for BM and HAZ respectively. The hardness ratio is 2.1 times greater than the hardness of base metal, and about 1.2 times more than HAZ, the softening ratio is about 1.48 HV.
- At the load 3.5 bar, the residual stress at 8kA is higher than the stress at 4 kA and 6 kA. While at the load 4.5, 5.5 bar, it is found that the stress at 6 kA is higher than 4 kA and 8 kA.
- At welding time of 25 cycles with clamping load 3.5, 4.5 and 5.5 bar with 6 kA welded sample has 19.1, 24 and 27.2 MPa stress. So, it can be deduced that the impact of clamping load might be more effective than welding current to determine the residual stress performance. However, at 15 cycles welding time, the value of stress at 6 kA welded samples with 4.5 bar possess the highest stress of 34.2 MPa, which can exhibit better hardness and strength, instead of 5.5bar in the case of 25 cycles welding time. Therefore, the effect of clamping load is more effective than the effect of welding current on residual stress at welding current 25 cycles.
- The results showed in Minitab software Taquchi (DOE) and analysis of Anova the effect of welding current is more effect of clamping load. At the welding current increase the tensile shear and Nugget formation increase at

constant the time whereas increase the clamping load lead to decrease the tensile shear and nugget formation.

- For tensile shear strength, the max. value of S/N and the value of means for Tensile shear were 22.68 and 13.63 for level (1) for the force when the clamping load is 3.5 bar. While it found 22.77 and 13.78 for level (3) of welding current at welding current 8kA respectively. While the max. and min. interaction effect values were 23.271 and 21.833 at parameters of clamping load and welding current of 3.5 and 5.5 bar and 8 and 4 kA respectively. The results get by using the analysis of ANOVA the effect of welding current is more than the effect of clamping load with percentage of 46% and 44% respectively.
- For Nugget formation the max. value of S/N and the means value were 16.32 and 6.640 for level (1) for the force when the clamping load is 3.5 bar. While 17.89 and 7.850 for level (3) for welding current at 8 kA respectively. Whereas the max. and min. interaction effect were 18.329 and 12.967 at parameters of clamping load and welding current of 3.5 and 5.5 bar and 8 and 4 kA respectively. The Anova results for the effect of the parameters of welding current and clamping load for Nugget formation were 92% and 6.5% respectively.

In the light of this study, some recommendations can be advised :

- To use the Software to measure the cracks and corrosion also to simulate the tensile shear test to compare the results with experimental work.
- To measure the volume fraction of martensite and ferrite by using experimental work to compare it with the results of software.
- to use the thermocouple at the HAZ and FZ during spot welding.

REFERENCES

1. Pouranvari, M. and Marashi, S. P. H., ‘Critical review of automotive steels spot welding: process, structure and properties’, ***Science And Technology Of Welding And Joining***, 18 (5): 361–403 (2013).

2. Cooman, B. and Speer, J., "Materials Design–the Key to Modern Steel Products, ed. by K," ***Garbracht, Bad Harzburg,*** 271 (1): 381-404 (2007).

3. Pouranvari, M. and Marashi, S., "Critical review of automotive steels spot welding: process, structure and properties," ***Science and Technology of Welding and Joining***, 18 (1): 361-403 (2013).

4. Maggi S. and Murgia, M., "Introduction to the metallurgic characteristics of advanced high-strength steels for automobile applications," ***Welding International***, 22 (1): 610-618 (2008).

5. Tumuluru, M. D., "Resistance spot welding of coated high-strength dual-phase steels," ***Welding Journal,*** 8 (1): 31-37 (2006).

6. Wei, S. Lv, D. R., Liu, Lin, L. Xu, R. J., "Similar and dissimilar resistance spot welding of advanced high strength steels: welding and heat treatment procedures, structure and mechanical properties," ***Science and Technology of Welding and Joining,*** 19 (1): 427-435 (2014).

7. Roncery, L. M. Weber, S. and Theisen, W., "Welding of twinning-induced plasticity steels," ***Scripta Materialia,*** 66 (1): 997-1001 (2012).

8. Kearns, W. H., "AWS welding handbook,welding processes resistance and solid state welding and other joining processes", ***Amer Welding Society, Aman***, 1220-1230 (1980).

9. Unruh, G. C., "Understanding carbon lock-in," ***Energy policy,*** 28 (1): 817-830 (2000).

10. Emadi, A., "Handbook of automotive power electronics and motor drives," ***CRC press,*** Florida, USA, 23-25 (2017).

11. Krauss, G., "Steels: heat treatment and processing principles," ***ASM International 1990,*** 497 (1990).

12. Pouranvari, M., and Marashi, S. P. H., "Critical review of automotive steels spot welding: process, structure and properties," ***Science and Technology of Welding and Joining,*** 18 (1): 361-403 (2013).

13. Mayyas, A. A., Qattawi, M. Omar, and Shan, D., "Design for sustainability in automotive industry: A comprehensive review," ***Renewable and Sustainable Energy Reviews,*** 16 (1): 1845-1862 (2012).

14. Aslanlar, S. A., Ogur, Ozsarac, U. and Ilhan, E. "Welding time effect on mechanical properties of automotive sheets in electrical resistance spot welding," ***Materials & Design***, 29 (1): 1427-1431 (2008).

15. Williams, N. and Parker, J. "Review of resistance spot welding of steel sheets Part 1 Modelling and control of weld nugget formation," ***International Materials Reviews,*** 49 (1): 45-75 (2004).

16. Messler, R. W., "Principles of welding: processes, physics, chemistry, and metallurgy," ***John Wiley & Sons,*** Texas, USA, 45-51 (2008).

17. Erden, M., "The effect of the sintering temperature and addition of niobium and vanadium on the microstructure and mechanical properties of microalloyed PM steels," ***Metals,*** 7: 329 (2017).

18. Tamarelli, C. M., "The evolving use of advanced high-strength steels for automotive applications," ***Steel Market Development Institute,*** Michigan, USA, 41-44 (2011).

19. Barabash, Z., Barabash, R., Liu, O. W. and Feng, Z.. "Microscopic deformation in individual grains in an advanced high-strength steel," ***Jom,*** 65 (1): 21-28 (2013).

20. Govik, A., Nilsson, L. and Moshfegh, R., "Finite element simulation of the manufacturing process chain of a sheet metal assembly," ***Journal of Materials Processing Technology,*** 212 (1): 1453-1462 (2012).

21. Mesplont, C., "Phase transformations and microstructure-mechanical properties relations in complex phase high strength steels," ***Ghent University,*** Belguim, 66-71 (2002).

22. De, A., "Spot welding", ***Science and Technology of Welding and Joining,*** 13(3): 213-214 (2008).

23. Khan, M. Kuntz, M. and Zhou, Y. "Effects of weld microstructure on static and impact performance of resistance spot welded joints in advanced high strength steels," ***Science and Technology of Welding and Joining,*** 13 (1): 294-304 (2008).

24. Tumuluru, M. "The effect of coatings on the resistance spot welding behavior of 780 MPa dual-phase steel," ***Welding Journal-New York,*** 86 (1): 161 (2007).

25. Zhang, P. Xie, J., Wang,Y. and Chen, J. "Effects of welding parameters on mechanical properties and microstructure of resistance spot welded DP600 joints," ***Science and Technology of Welding and Joining***,16 (1): 567-574 (2011).

26. Nayak, S., Zhou, Y. V. Hernandez, B. and Biro, E., "Resistance spot welding of dual-phase steels: heat affected zone softening and tensile properties," **in *Proceedings of the 9th International Conference on Trends in Welding Research, Chicago, Illinois, United States,*** 641-649 (2012).

27. MI, K., Biro, E., and Zhou, Y. "Microstructure and mechanical properties of resistance spot welded advanced high strength steels," ***Materials Transactions,*** Washington, D. C., 435 (2008).

28. Chemin. F.,R. A.. Valente. T., Barreto, L. M. and Marcondes, V. P., "An experimental approach for blankholder force determination for DP600 with different material flow strain rates in the flange during stamping,"***Proceedings of the Institution of Mechanical Engineers, Part B: Journal of Engineering Manufacture,*** 227 (1): 417-422 (2013).

29. Kuziak, R., Kawalla, R. and Waengler, S., "Advanced high strength steels for automotive industry," ***Archives of Civil and Mechanical Engineering,*** 8 (1): 103-117 (2008).

30. Irie, T. S., Satoh, K., Hashiguchi, I. and Hashimoto O., "Metallurgical factors affecting the formability of cold-rolled high strength steel sheets," ***Transactions of the Iron and Steel Institute of Japan,*** 21 (1): 793-801 (1981).

31. Furukawa, T., Morikawa, H., Endo, M. Takechi, Koyama, H. K. O., "Process Factors for Cold-rolled Dual-phase Sheet Steels," ***Transactions of the Iron and Steel Institute Of Japan,*** 21 (1): 812-819 (1981).

32. Takechi, H. and Abe, M., "Manufacturing techniques for high strength steel sheets for automotive applications," ***Nippon steel technical report. Overseas,*** London, UK, 9-18 (1984).

33. Llewellyn, D. and Hillis, D., "Dual phase steels," ***Ironmaking & Steelmaking,*** 23 (1): 471-478 (1996).

34. Rocha, R. Melo, T., Pereloma, E. and Santos, D., "Microstructural evolution at the initial stages of continuous annealing of cold rolled dual-phase steel," ***Materials Science and Engineering: A,*** 391 (1): 296-304 (2005).

35. Ma, C. D., Chen, L. S. Bhole, D., Boudreau, Lee, G. A. and Biro, E. "Microstructure and fracture characteristics of spot-welded DP600 steel," ***Materials Science and Engineering: A,*** 485 (1): 334-346 (2008).

36. Long, X. and Khanna, S. K., "Fatigue properties and failure characterization of spot welded high strength steel sheet," ***International Journal of Fatigue,*** 29 (1): 879-886 (2007).

37. Kankanamge, N. D. and Mahendran, M. "Mechanical properties of cold-formed steels at elevated temperatures," ***Thin-Walled Structures,*** 49: 26-44 (2011).

38. De Cooman, B. C., K. G. Chin, and Jinkyung Kim. "High Mn TWIP steels for automotive applications." ***New Trends and Developments in Automotive System Engineering***, New Yurk, USA, 101-128 (2011).

39. Rana, R. and Singh, S. B. *"Automotive steels: design, metallurgy, processing and applications,*" **Woodhead Publishing,** London, UK, 10-11 (2016).

40. Kumar, A. Singh, S. and Ray, K. "Influence of bainite/martensite-content on the tensile properties of low carbon dual-phase steels," ***Materials Science and Engineering: A,*** 474 (1): 270-282 2008.

41. Saeidi, N. and Ekrami, A., "Comparison of mechanical properties of martensite/ferrite and bainite/ferrite dual phase 4340 steels," ***Materials Science and Engineering: A,*** 523 (1): 125-129 2009.

42. Ramazani, A., Pinard, P. Richter, S. Schwedt, A. and Prahl, U., "Characterisation of microstructure and modelling of flow behaviour of bainite-aided dual-phase steel," ***Computational Materials Science,*** 80 (1): 134-141 (2013).

43. Park K., Nishiyama, M. Nakada, N. Tsuchiyama, T. and Takaki, S., "Effect of the martensite distribution on the strain hardening and ductile fracture behaviors in dual-phase steel," ***Materials Science and Engineering: A,*** 604 (1): 135-141 (2014).

44. Avramovic-Cingara, G., Ososkov, Y., Jain, M. and Wilkinson, D., "Effect of martensite distribution on damage behaviour in DP600 dual phase steels," ***Materials Science and Engineering: A,*** 516 (1): 7-16 (2009).

45. Mazinani, M. and Poole, W., "Effect of martensite plasticity on the deformation behavior of a low-carbon dual-phase steel," ***Metallurgical and Materials Transactions A,*** 38 (1): 328-339 (2007).

46. Peng-Heng, C. and Preban, A., "The effect of ferrite grain size and martensite volume fraction on the tensile properties of dual phase steel," ***Acta Metallurgica,*** 33 (1): 897-903 (1985).

47. Jiang, Z. Guan, Z. and Lian, J., "Effects of microstructural variables on the deformation behaviour of dual-phase steel," ***Materials Science and Engineering: A,*** 190 (1): 55-64 (1995).

48. Calcagnotto, M. Ponge, D. and Raabe, D., "Effect of grain refinement to 1μm on strength and toughness of dual-phase steels," ***Materials Science and Engineering: A,*** 527 (1): 7832-7840 (2010).

49. Calcagnotto, M., Adachi, Y. Ponge, D., and Raabe, D., "Deformation and fracture mechanisms in fine-and ultrafine-grained ferrite/martensite dual-phase steels and the effect of aging," ***Acta Materialia,*** 59 (1): 658-670 (2011).

50. Speich, G. "Physical metallurgy of dual-phase steels," ***Fundamentals of Dual-Phase Steels***, ***Los Alamos National Lab.,*** New Mexico, USA, 3-45 (1981).

51. Morais, W. A. d. and Borges, H. C., "Condições Técnico-Econômicas Para Viabilizar o Emprego de Aços Planos de Elevada Resistência Mecânica em Aplicações Práticas," ***Tecnologia em Metalurgia, Materiais e Mineração,*** 6(1): 1 (2009).

52. Pouranvari, M. Marashi, S. and Safanama, D., "Failure mode transition in AHSS resistance spot welds. Part II: Experimental investigation and model validation," ***Materials Science and Engineering: A***, 528 (1): 8344-8352 (2011).

53. Tong, W. Tao, H. Zhang, N. Jiang, X., Marya, M. P. L., "Deformation and fracture of miniature tensile bars with resistance-spot-weld microstructures," ***Metallurgical and Materials Transactions A,*** 36 (1): 2651-2669 (2005).

54. Amirthalingam, K., "Women's rights, international norms, and domestic violence: Asian perspectives," ***Human Rights Quarterly,*** South Korea, 683-708 (2005).

55. Waterschoot, T., Kestens, L. and De Cooman, B., "Hot rolling texture development in CMnCrSi dual-phase steels," ***Metallurgical and Materials Transactions A,*** 33 (1): 1091 (2002).

56. Amirthalingam, M., "Microstructural development during welding of TRIP steels," ***PhD thesis, Material Science and Engineering, Delft University,*** 115(1): 20-32 2010.

57. Garrido, F. Illera, V. and Garcia-Gonzalez, M., "Effect of the addition of gypsum-and lime-rich industrial by-products on Cd, Cu and Pb availability and leachability in metal-spiked acid soils," ***Applied Geochemistry,*** 20 (1): 397-408 (2005).

58. Meng, Q., Li, J. Wang, J., Zhang, Z. and Zhang, L. "Effect of water quenching process on microstructure and tensile properties of low alloy cold rolled dual-phase steel," ***Materials & Design,*** 30 (1): 2379-2385 (2009).

59. Thomas, G., Speer, J. and Matlock, D., "Quenched and partitioned microstructures produced via Gleeble simulations of hot-strip mill cooling practices," ***Metallurgical and Materials Transactions A,***42 (1): 3652-3659 (2011).

60. Kim, T., Park, H. and Rhee, S. "Optimization of welding parameters for resistance spot welding of TRIP steel with response surface methodology," ***International Journal of Production Research***, 43 (1): 4643-4657 (2005).

61. Granbom, Y., "Structure and mechanical properties of dual phase steels," ***An Experimental and Theoretical Analysis,*** UK, London, 12-16 (2010).

62. Das, D. and Chattopadhyay, P. P., "Influence of martensite morphology on the work-hardening behavior of high strength ferrite–martensite dual-phase steel," ***Journal of Materials Science,*** 44 (1): 2957-2965 (2009).

63. Smith, W. F., "Structure and properties of engineering alloys", ***McGraw-Hill,*** New York, USA, 12-16 1993.

64. Oliver, C., Randy, J. and Daniel E. G., "Dual Phase Steel Characterization for Tube Bending and Hydroforming Applications." **In** ***Materials Science Forum,*** 706 (1): 2066-2071 (2012).

65. Speich, G., Demarest, V. and Miller, R., "Formation of austenite during intercritical annealing of dual-phase steels," ***Metallurgical and materials transactions A,*** 12 (1): 1419-1428 (1981).

66. Lanzillotto, C. and Pickering, F., "Structure–property relationships in dual-phase steels," ***Metal Science***, 16 (1): 371-382 (1982).

67. Güral, A., Bostan,B. and Özdemir, A., "Heat treatment in two phase region and its effect on microstructure and mechanical strength after welding of a low carbon steel," ***Materials & Design,*** 28 (1): 897-903 (2007).

68. Kadkhodapour, J., Schmauder, S., Raabe, D., Ziaei-Rad, S., Weber, U. and Calcagnotto, M,. "Experimental and numerical study on geometrically necessary dislocations and non-homogeneous mechanical properties of the ferrite phase in dual phase steels," ***Acta Materialia,*** 59 (1): 4387-4394 (2011).

69. Sodjit, S. and Uthaisangsuk,V., "Microstructure based prediction of strain hardening behavior of dual phase steels," ***Materials & Design,*** 41 (1): 370-379 (2012).

70. Sarwar, M. and Priestner, R., "Influence of ferrite-martensite microstructural morphology on tensile properties of dual-phase steel," ***Journal of Materials Science,*** 31 (1): 2091-2095 (1996).

71. Loisy, C. and Cerepi, A. "Radon-222 as a tracer of water–air dynamics in the unsaturated zone of a geological carbonate formation: Example of an underground quarry (Oligocene Aquitain limestone, France)," ***Chemical Geology***, 296 (1): 39-49 (2012).

72. Matlock, D. K., Speer, J. G. and Moor, E. "Recent AHSS Developments for Automotive Applications: Processing, Microstructures, and Properties," ***In Workshop ASPPRC,*** **Germany**, 10-12 (2012).

73. Paralikas, J. Salonitis, K. and Chryssolouris, G., "Robust optimization of the energy efficiency of the cold roll forming process," ***The International Journal of Advanced Manufacturing Technology***, 69 (1): 461-481 (2013).

74. Vural, M. and Akkus, A. "On the resistance spot weldability of galvanized interstitial free steel sheets with austenitic stainless steel sheets," ***Journal of materials processing technology,*** 153 (1): 1-6 (2004).

75. Kahraman, N., "The influence of welding parameters on the joint strength of resistance spot-welded titanium sheets," ***Materials & Design***, 28 (1): 420-427 (2007).

76. Sun, D., Lang, B. Sun, D. and Li, J., "Microstructures and mechanical properties of resistance spot welded magnesium alloy joints," ***Materials Science and Engineering****: A,* 460 (1): 494-498 (2007).

77. McCallum, B. "Characterization of DP600 Steel Subject to Electrohydraulic Forming," ***Archives Of Civil And Mechanical Engineering,*** Paris, France, 11-13 (2014).

78. Zhang, X., Chen, G. Zhang,Y. and Lai, X., "Improvement of resistance spot weldability for dual-phase (DP600) steels using servo gun," ***Journal of Materials Processing Technology,*** 209 (1): 2671-2675 (2009).

79. Han, L. Thornton, M. and Shergold, M. "A comparison of the mechanical behaviour of self-piercing riveted and resistance spot welded aluminium sheets for the automotive industry," ***Materials & Design,*** 31 (1): 1457-1467 (2010).

80. Qiu, R., Iwamoto, C. and Satonaka, S., "Interfacial microstructure and strength of steel/aluminum alloy joints welded by resistance spot welding with cover plate," ***Journal of Materials Processing Technology***, 209 (1): 4186-4193 (2009).

81. Pouranvari, M. and Marashi, S., "Failure mode transition in AHSS resistance spot welds. Part I. Controlling factors," ***Materials Science and Engineering: A,*** 52 (1): 8337-8343 (2011).

82. Kearns, W., "Welding Processes, AWS Welding Handbook, American Welding Society," ***Macmillan Press Ltd.,*** London, 30-36 (1980).

83. Cui, Y. and Lundin, C. D., "Austenite-preferential corrosion attack in 316 austenitic stainless steel weld metals," ***Materials & Design,*** 28 (1): 324-328 (2007).

84. Özyürek, D., "An effect of weld current and weld atmosphere on the resistance spot weldability of 304L austenitic stainless steel," ***Materials & Design,*** 29 (1):597-603 (2008).

85. Mudali,U. K. B., Rao, A., Shanmugam, R. and Raj, B., "Corrosion and microstructural aspects of dissimilar joints of titanium and type 304L stainless steel," ***Journal of Nuclear Materials,*** 321 (1): 40-48 (2003).

86. Yang, Y. and Lee, S., "A study on the joining strength of laser spot welding for automotive applications," ***Journal of Materials Processing Technology,*** 94 (1): 151-156 (1999).

87. Nong, N., Keju, O., Yu, Z. Q. Zhiyuan, T. and Feipeng, L. "Research on press joining technology for automotive metallic sheets," ***Journal of Materials Processing Technology,*** 137 (1): 159-163 (2003).

88. Al-Jader, M. A., "Investigation of spot welding electrode tip wear and a non-destructive test of plastic joining in the automotive industry," ***Liverpool John Moores University,*** Liverpool, UK, 20-21 (2014).

89. Cecil, D. G., "Resistance projection welding system and method for welding a fastener element to a workpiece," ***Google Patents,*** Kalifornia, USA, 20-26 (1998).

90. Matteson, R. P. "Electric resistance welder having capability of consistent seam welding and heat-treating," ***Google Patents,*** Kalifornia, USA, 12-14 (1997).

91. Baur, R., "WM Steen, Laser Material Processing , Springer, Heidelberg (2003) ISBN 1-85233-698-6 (XV/408pp., 257, illust., EUR69. 95, $59.95, Softcover)," ***Optik***, 117 (1): 488-488 (2006).

92. Huang, Q. Hagstrom, J. Skoog, H. and Kullberg, G., "Effect of CO sub 2 Laser Parameter Variations on Sheet Metal Welding," ***International Journal for the Joining of Materials,*** 3 (1): 79-88 (1991).

93. Thomas, W. and Nicholas, E., "Friction stir welding for the transportation industries," ***Materials & Design,*** 18 (1): 269-273 (1997).

94. Amirthalingam ,M. Hermans, M. and Richardson, I., "Microstructural Development during Welding of Silicon-and Aluminum-Based Transformation-Induced Plasticity Steels—Inclusion and Elemental Partitioning Analysis," ***Metallurgical and Materials Transactions A,*** 40 (1): 901 (2009).

95. Amirthalingam, M., Hermans, M., Huizenga, R. Offerman, S. Sietsma, J. and Richardson, I., "In situ phase transformation studies on a transformation induced plasticity steel under simulated weld thermal cycles using synchrotron diffraction," ***In-situ Studies with Photons, Neutrons and Electrons Scattering, Springer,*** Berline,Germany, 133-148 (2010).

96. Eryürek, B., "Electrical resistance welding," ***Mech Eng Mag,*** 279 (1): 22-31 (1983).

97. Anık, S., "Welding technique handbook, processes and equipments," ***Kansu Printed, Turkey,*** 21-24 (1991).

98. Aslanlar, S., "The effect of nucleus size on mechanical properties in electrical resistance spot welding of sheets used in automotive industry," ***Materials & Design,*** 27 (1): 125-131 (2006).

99. RWMA, E., "Resistance Welding Manual," ***ed: Philadelphia, PA: RWMA,*** Philadelphia, USA, 30-32 (2003).

100. Bashenko, V. and Sosnin, N., "Optimization of the plasma arc welding process," ***Welding Journal,*** 67 (1): 233-237 (1988).

101. Kuo, M. and Chiang, J., "Weldability study of resistance spot welds and minimum weld button size methodology development for DP steel," ***SAE Technical Paper,*** 1(2): 148-191 (2004).

102. Zhou, M., Zhang, H. and Hu, S., "Relationships between quality and attributes of spot welds," ***Welding Journal-New York-,*** 82 (1): 72 (2003).

103. Donders, S. Brughmans, M. Hermans, L. Liefooghe, C., Van, H.,and Desmet, W., "The robustness of dynamic vehicle performance to spot weld failures," ***Finite Elements in Analysis and Design,*** 42 (1): 670-682 (2006).

104. Zhou, Y. Gorman, P. Tan, W. and Ely, K., "Weldability of thin sheet metals during small-scale resistance spot welding using an alternating-current power supply," ***Journal of Electronic Materials,*** 29 (1): 1090-1099 (2000).

105. Khan, M. I., "Spot Welding of Advanced High Strength Steels (AHSS)," ***University of Waterloo,*** Canada, 55-60 (2007).

106. Hofman, K. Soter, M., Orsette, C., Villaire, S. and Prokator, M., "AC or DC for resistance welding dual-phase 600?," ***Welding Journal,*** 84 (1): 46-48 (2005).

107. Tawade, G., Bhole, S., Lee, A. and Boudreau, G., Robust Schedules for Spot Welding Zinc Coated Advanced High Strength Automotive Steels," ***Society of Manufacturing Engineers,*** London, UK, 4-5 (2000).

108. Gedeon, S. and Eagar, T., "Resistance spot welding of galvanized steel: Part II. Mechanisms of spot weld nugget formation," ***Metallurgical Transactions B,*** 17 (1): 887-901 (1986).

109. Jung, G. "Spot Weldability of TRIP Steel with High Carbon, High Aluminium Content," ***Pohang University of Science and Technology, Pohang***, South Koria, 67-70 (2011).

110. Senkara, J. and Zhang, H. "Resistance Welding Fundamentals and Applications," ***ed: CRC Press Taylor & Francis Group,*** France, Paris, 23-27 (2006).

111. Browne, D., Chandler, H., Evans, J. James, P., Wen,J. and Newton, C., "Computer simulation of resistance spot welding in aluminum: Part II," ***Welding Journal-Including Welding Research Supplement,*** 74 (1): 417 (1995).

112. Thomson, H., Atkinson, R., Petticrew, M. and Kearns, A., "Do urban regeneration programmes improve public health and reduce health inequalities? A synthesis of the evidence from UK policy and practice (1980–2004)," ***Journal of Epidemiology & Community Health,*** 60 (1): 108-115 (2006).

113. Raut, M. and Achwal, V. "Optimization of spot welding process parameters for maximum tensile strength," ***International Journal of Mechanical Engineering and Robotics Research,*** 3 (1): 507-517 (2014).

114. Sun, X. and Dong, P., "Analysis of aluminum resistance spot welding processes using coupled finite element procedures," ***Welding Journal-New York-,*** 79: 215 (2000).

115. Sarwar, M., Ahmad, E., Qureshi, K. and Manzoor, T. "Influence of epitaxial ferrite on tensile properties of dual phase steel," ***Materials & Design,*** 28 (1): 335-340 (2007).

116. Dong, S. and Zhou, Y., "Effects of TiC composite coating on electrode degradation in microresistance welding of nickel-plated steel," ***Metallurgical and Materials Transactions A***, 34 (1): 1501-1511 (2003).

117. Yang, D., Brown, E. Matlock, D. and Krauss, G., "Ferrite recrystallization and austenite formation in cold-rolled intercritically annealed steel," ***Metallurgical Transactions A,*** 16 (1): 1385-1392 (1985).

118. Matlock, D. K., Krauss, G., Ramos, L. and Huppi, G. S., "A correlation of processing variables with deformation behavior of dual-phase steels," ***Structure and Properties of Dual-Phase Steels,*** 1 (1): 62-90 (1979).

119. Erdogan, M. "The effect of new ferrite content on the tensile fracture behaviour of dual phase steels," ***Journal of Materials Science,*** 37 (1): 3623-3630 (2002).

120. Pouranvari, M., Asgari, H., Mosavizadch, S., Marashi, P., and Goodarzi, M., "Effect of weld nugget size on overload failure mode of resistance spot welds," ***Science and Technology of Welding and Joining,*** 12 (1): 217-225 (2007).

121. Pouranvari, M. and Marashi, S., "Critical sheet thickness for weld nugget growth during resistance spot welding of three-steel sheets," ***Science and Technology of Welding and Joining,*** 16 (1): 162-165 (2011).

122. Sobhani, S., and M. Pouranvari. "Duplex Stainless Steel/Martensitic Steel Dissimilar Resistance Spot Welding: Microstructure-Properties Relationships." ***Welding Journal,*** 1(4): 1-16 (2019).

123. Kobayashi, Takaya, and Yasuko Mihara. "Numerical simulation of nugget formation in spot welding." I***n SIMULIA Community Conference,*** Japan, 1-8 (2014).

124. Anık, S., Ogur, A. and Aslanlar, S. "The effect of welding current on tensile-shear strength of galvanized chromate micro-alloyed steel sheets applied to electrical resistance spot welding," **In** ***Welding Technology 2nd National Congress,*** Ankara, Turkey, 12-17 (1999).

125. Anık, S. and Gulbahar, B. "The relationships between tensile-shear strength and weld nugget in 17% Cr-ferritic stainless steels," ***In Second National Welding Symposium, Proceedings,*** Istanbul, Turkey, 94-105 (1989).

126. M. Vural, "The effect of welding parameters on welding strength and behavior in spot welding of galvanised steel sheets and ferritic stainless steels," ***Ph. D. Thesis, Istanbul University,*** Istanbul, Turkey, 45-50 (1992).

127. Goodarzi, M., Marashi, S. and Pouranvari, M., "Dependence of overload performance on weld attributes for resistance spot welded galvanized low carbon steel," ***Journal of Materials Processing Technology,*** 209 (1): 4379-4384 (2009).

128. Hayat, F., Demir, B., Acarer, M. and Aslanar, S., "Effect of weld time and weld current on the mechanical properties of resistance spot welded IF (DIN EN 10130–1999) steel," ***Kovove Materialy,*** 47 (1): 11-17 (2009).

129. Winnicki, M., Małachowska, A., Korzeniowski, M. Jasiorski, M. and Baszczuk, A. "Aluminium to steel resistance spot welding with cold sprayed interlayer," ***Surface Engineering***, 34 (3): 235-242 (2018).

130. Olson, D., Lasseigne, A., Marya, M. and Mishra, B., "Weld features that differentiate weld and plate corrosion," ***Practical Failure Analysis,*** 3 (1): 43-57 (2003).

131. Porter, D. and Easterling, K., "Phase transformation in materials," ***Chapman & Hall, Boundary Row,*** London, 291-308 (1992).

132. Rodelas, J. M. *"Friction Stir Processing of Nickel-base Alloys*", ***The Ohio State University,*** Ohio, USA, 78-81 (2012).

133. Clarke, A., Speer, J., Miller, M., Hackenberg, D., Edmonds, D., "Carbon partitioning to austenite from martensite or bainite during the quench and partition (Q&P) process: A critical assessment," ***Acta Materialia,*** 56 (1):16-22 (2008).

134. Lee, J. L. Hon, M. H. and Cheng G. H., "The intermediate transformation of Mn-Mo-Nb steel during continuous cooling," ***Journal of Materials Science***, 22 (1): 2767-2777 (1987).

135. Gould, J., Khurana,S. and Li, T., "Predictions of microstructures when welding automotive advanced high-strength steels," ***Welding Journal-New York-,*** 85 (1): 111 (2006).

136. Aydin, H., "The mechanical properties of dissimilar resistance spot-welded DP600–DP1000 steel joints for automotive applications," ***Proceedings of the Institution of Mechanical Engineers, Part D: Journal of Automobile Engineering,*** 229 (1): 599-610 (2015).

137. Hernandez, B., Kuntz, V., Khan, M. and Zhou,Y., "Influence of microstructure and weld size on the mechanical behaviour of dissimilar AHSS resistance spot welds," ***Science and Technology of Welding and Joining,*** 13 (1): 769-776 (2008).

138. Marya, M., Wang, K. L., Hector, G. and Gayden, X., "Tensile-shear forces and fracture modes in single and multiple weld specimens in dual-phase steels," ***Journal of Manufacturing Science and Engineering,*** 128 (1): 287-298 (2006).

139. Zhao, D., Wang, Y., Zhang, L. and Zhang, P. "Effects of electrode force on microstructure and mechanical behavior of the resistance spot welded DP600 joint," ***Materials & Design,*** 50 (1): 72-77 (2013).

140. Marashi, P., Pouranvari, M., Amirabdollahian, S., Abedi, A. and Goodarzi, M., "Microstructure and failure behavior of dissimilar resistance spot welds between low carbon galvanized and austenitic stainless steels," ***Materials science and engineering: A,*** 480 (1): 175-180 (2008).

141. Pouranvari, M., Mousavizadeh, S., Marashi, S., Goodarzi, M. and Ghorbani, M., "Influence of fusion zone size and failure mode on mechanical performance of dissimilar resistance spot welds of AISI 1008 low carbon steel and DP600 advanced high strength steel," ***Materials & Design***, 32 (1): 1390-1398 (2011).

142. Ahmad, E., Manzoor, T. Hussain, N. and Qazi, N., "Effect of thermomechanical processing on hardenability and tensile fracture of dual-phase steel," ***Materials & Design,*** 29 (1): 450-457 (2008).

143. Dziedzic, M. and Turczyn, S. "Experimental and numerical investigation of strip rolling from dual phase steel," ***Archives of Civil and Mechanical Engineering,*** 10 (1): 21-30 (2010).

144. Xiong, Z., Kostryzhev A., Stanford, N. and Pereloma, E. V., "Microstructures and mechanical properties of dual phase steel produced by laboratory simulated strip casting," ***Materials & Design,*** 88 (1): 537-549 (2015).

145. Rathbun, R. W. Matlock, D. and Speer, J., "Fatigue behavior of spot welded high-strength sheet steels," ***Welding Journal***, 82 (1): 207-218 (2003).

146. Pouranvari, M. and Marashi, S., "Failure of resistance spot welds: tensile shear versus coach peel loading conditions," ***Ironmaking & Steelmaking,*** 39 (1): 104-111 (2012).

147. Zhang, H. and Senkara, J. "Resistance welding: fundamentals and applications", ***CRC press,*** Florida, USA, 45-51 (2011).

148. Pouranvari, M. and Marashi, S. "Failure mode transition in AISI 304 resistance spot welds," ***Weld. J,*** 91 (1): 303-309 (2012).

149. Wang, G. and Barkey, M. "Investigating the spot weld fatigue crack growth process using X-ray imaging," ***Welding Journal,*** 85 (1): 84-90 (2006).

150. Marya, M. and Gayden, X., "Development of requirements for resistance spot welding dual-phase (DP600) steels part 1—the causes of interfacial fracture," ***Development,*** 11 (1): 12 (2005).

151. Ma, C., Chen, D., Bhole, S., Boudreau, G., Lee, A. and Biro, E. "Microstructure and fracture characteristics of spot-welded DP600 steel," ***Materials Science and Engineering: A***, 485 (1): 334-346 (2008).

152. Shi, G. and Westgate, S. "Resistance spot welding of high strength steels," ***International Journal for the Joining of Materials,*** 16 (1): 9-14 (2004).

153. Zhang, H., Wei, A., Qiu, X. and Chen, J. "Microstructure and mechanical properties of resistance spot welded dissimilar thickness DP780/DP600 dual-phase steel joints," ***Materials & Design (1980-2015)***,54 (1): 443-449 (2014).

154. Sun, X. E., Stephens,V. and Khaleel, M. A., "Effects of fusion zone size and failure mode on peak load and energy absorption of advanced high strength steel spot welds under lap shear loading conditions," ***Engineering Failure Analysis,*** 15 b: 356-367 (2008).

155. David, S. and DebRoy, T., "Current issues and problems in welding science," ***Science***, 257: 497-502 (1992).

156. El-Sesy, I. and El-Baradie, Z., "Influence carbon and/or iron carbide on the structure and properties of dual-phase steels," ***Materials Letters,*** 57 (1): 580-585 (2002).

157. Rohni, S. N. A., "Properties of compressed banana fiber composite from agriculture waste using cold-setting adhesives," ***Faculty of Earth Sciences, University of Barcelona,*** Barcelona, Spain, 32-36 (2014).

158. Fadaei, A., Mahmoudi, A. and Borzuie, A., "Experimental study of the nugget diameter effect on tensile-shear strength in AISI 1008 spot welding specimens," ***J Mech Res Appl***, 4 (1): 1-7 (2012).

159. Ruge, J., Wösle, H., Ebert, K., Federn, K., Ehrlenspiel, K. H. P., "Konstruktionselemente," ***In Taschenbuch Für Den Maschinenbau, Ed: Springer***, London, UK, 346-505 (1981).

160. Hayat, F. and Sevim, İ. "The effect of welding parameters on fracture toughness of resistance spot-welded galvanized DP600 automotive steel sheets," ***The International Journal of Advanced Manufacturing Technology,*** 58 (1): 1043-1050 (2012).

161. Yunlian, Q., Ju, D., Quan, H. and Liying, Z. "Electron beam welding, laser beam welding and gas tungsten arc welding of titanium sheet," ***Materials Science and Engineering: A,*** 280 (1): 177-181 (2000).

162. Pradeep, M., Mahesh, N. and Hussain, R. "Process parameter optimization in resistance spot welding of dissimilar thickness materials," ***Delta,*** 3(3): 624 (2014).

163. Zhang, X. Q. G., Chen, L. and Zhang, Y. S. "Characteristics of electrode wear in resistance spot welding dual-phase steels," ***Materials & Design,*** 29 (1): 279-283 (2008).

164. Prashanthkumar, V. K., Venkataram, N. N., Mahesh, S., "Process Parameter Selection for Resistance Spot Welding through Thermal Analysis of 2mm CRCA Sheets," ***Procedia Materials Science,*** 5 (1): 369-378 (2014).

165. Taban, E. J., Gould, E., and Lippold, J. C., "Dissimilar friction welding of 6061-T6 aluminum and AISI 1018 steel: Properties and microstructural characterization," ***Materials & Design (1980-2015),*** 31(1): 2305-2311 (2010).

166. Kraus, A. D. and Bar-Cohen, A. "Thermal analysis and control of electronic equipment," ***Hemisphere Publishing Corp.,*** Washington, USA, 633 (1983).

167. Xia, Q. M., Pickett, D. J., Yang,. M., Zhang, Borghetti, J., "Impact of geometry on the performance of memristive nanodevices," ***Nanotechnology,*** 22 (1): 254 (2011).

168. Li, Q., Ito, K., Wu, Z., C. S. Lowry, and Loheide II,S. P., "COMSOL Multiphysics: A novel approach to ground water modeling," ***Groundwater,*** 47 (1): 480-487 (2009).

169. Patzák, B., Rypl, D. and Kruis, J. "MuPIF–A distributed multi-physics integration tool," ***Advances in Engineering Software,*** 60 (1): 89-97 (2013).

170. Kou, S., "Welding metallurgy," ***New Jersey State,*** New Jersey, USA, 431-446 (2003).

171. Isayev, A. and Terekhov, A., "Mechanical properties of resistance spot welded joints in zinc-plated TRIP steel," ***Welding International***, 28 (1): 324-328 (2014).

172. Safanama, D., Marashi, S. and Pouranvari, M. "Similar and dissimilar resistance spot welding of martensitic advanced high strength steel and low carbon steel: metallurgical characteristics and failure mode transition," ***Science and Technology of Welding and Joining,*** 17 (1): 288-294 (2012).

173. Nayak, S., Hernandez, V. B., Okita,Y. and Zhou, Y. "Microstructure–hardness relationship in the fusion zone of TRIP steel welds," ***Materials Science and Engineering: A,*** 551 (1): 73-81 (2012).

174. Kou ,S. *'Welding metallurgy*," ***John Wiley & Sons,*** Texas, USA, 78-81 (2003).

175. MI, K., Biro, E. and Zhou,Y. "Microstructure and mechanical properties of resistance spot welded advanced high strength steels," ***Materials Transactions,*** 49 (1): 1629-1637 (2008).

176. Association, J. S. and JIS, Z. "3140-1989 method of inspection for spot weld," ***Japanese Industrial Standard,*** Tokyo, Japan 45-46 (1989).

177. Standard, G. "Resistance spot welding," ed: DVS, USA, 12-15 (1986).

178. Chang, B., Li, M. and Zhou, Y. "Comparative study of small scale and 'large scale'resistance spot welding," ***Science and Technology of Welding and Joining,*** 6: 273-280 (2001).

179. Tsai, Chon L., Weng L. Dai, and David W. Dickinson. "Analysis and development of a real-time control methodology in resistance spot welding," ***SAE transactions,*** 1(2): 158-176 (1991).

180. Eisazadeh, H., Hamedi, M. and Halvaee, A. "New parametric study of nugget size in resistance spot welding process using finite element method," ***Materials & Design***, 31: 49-157 (2010).

181. Satpathy, M. P., Mohapatra, K. D., and Sahoo, S. K. "Ultrasonic spot welding of Al–Cu dissimilar metals: a study on parametric influence and thermo-mechanical simulation," ***International Journal of Modelling and Simulation,*** 38: 83-95 (2018).

RESUME

ABDULKARIM R. ALZAHOUGI was born in Azawia / Libya 1969 and he graduated first, elementary and high school education in this city, after that, he started undergraduate program in Tripoli In Civil Aviation high institute Department of Mechanical Engineering 1989. In 1994 he worked at centre of research. Then in 2003, he fulfilled the requirements for the Master degree of production Engineering (materials science) in Mechanical Technology at University of Belgrade. In 2007 he moved to another job as member of teaching in high institute. In 2016 he moved to Karabük University, Technology Faculty, Department of Manufacturing Engineering to study Ph.D. program.